JPRS L/10157

3 December 1981

Translation

RADIATING PROPERTIES OF SHOCK WAVES IN GASES

By

M.A. Tsikulin and Ye. G. Popov

FBIS FOREIGN BROADCAST INFORMATION SERVICE

NOTE

JPRS publications contain information primarily from foreign newspapers, periodicals and books, but also from news agency transmissions and broadcasts. Materials from foreign-language sources are translated; those from English-language sources are transcribed or reprinted, with the original phrasing and other characteristics retained.

Headlines, editorial reports, and material enclosed in brackets [] are supplied by JPRS. Processing indicators such as [Text] or [Excerpt] in the first line of each item, or following the last line of a brief, indicate how the original information was processed. Where no processing indicator is given, the information was summarized or extracted.

Unfamiliar names rendered phonetically or transliterated are enclosed in parentheses. Words or names preceded by a question mark and enclosed in parentheses were not clear in the original but have been supplied as appropriate in context. Other unattributed parenthetical notes within the body of an item originate with the source. Times within items are as given by source.

The contents of this publication in no way represent the policies, views or attitudes of the U.S. Government.

APPROVED FOR RELEASE: 2007/02/09: CIA-RDP82-00850R000400080011-7

JPRS L/10157

3 December 1981

RADIATING PROPERTIES OF SHOCK WAVES IN GASES

Moscow IZLUCHATEL'NYYE SVOYSTVA UDARNYKH VOLN V GAZAKH in Russian 1977

[Book by M.A. Tsikulin and Ye. G. Popov, Izdatel'stvo "Nauka," 173 pages]

CONTENTS

Annotation

This monograph contains experimental investigations of the radiating properties of large amplitude shock waves in gases. A review is given of methods for obtaining strong shock waves in rarified and dense gases and experimental results. Installations and the methods used to record the parameters of the shock waves are described. Explosion sources as a method for obtaining powerful radiation with a continuous spectrum were especially considered. Results are cited of studies of the intensity of the shock waves in the air and in the inert gas of various densities (at temperatures of up to 120,000°); their spectral investigation; measurement of the angular distribution of the wave front; and the shielding and other phenomena accompanying the radiation of strong shock waves. The possibilities of raising the efficiency of the explosion sources further are considered. Examples are cited of using the investigation results in astrophysics, physics of meteor phenomena, gas dynamics and plasma physics.

The book is intended, for specialists in the area of shock wave physics, plasma physics, astrophysics, and meteor physics, post-graduate students and students of the indicated specialties.

Foreword

The book cites results of the experimental investigations of the radiating properties of strong shock waves in dense gases which were carried out by the authors in the Earth Physics Institute /IFZ/ imeni O. Yu. Shmidt of the USSR Academy of Sciences during 1966-1969.

The experiments were organized primarily due to an increasing interest in the dynamics of radiating gas. Investigations in this area, related to many phenomena, for example, a strong explosion, the movement of cosmic bodies in the atmosphere, the effect of laser radiation on a substance, were moved forward considerably in recent years by the following Soviet scientists: Ya. B. Zel'dovich, Yu. P. Rayzer, N. G. Basov, O. N. Krokhin, L. M. Biberman, K. P. Stanyukovich, I. V. Nemchinov and others.

Various authors have established the basic possibility of using strong shock waves in gases as a powerful high temperature radiator. By creating shock waves in dense gases by means of condense explosive substance (VV), it is possible to obtain large radiation flows in small installations. Especially efficient in this respect are shock waves in heavy inert gases. The absence of expenditures for dissociation and the large atomic weight of the latter facilitates the achievement of high temperatures behind the shock front, and the transparency of the gas ahead of the front to hard ultraviolet leads to the radiation of considerably flows of energy by the wave.

The explosion of a VV charge in an atmosphere of heavy inert gas is used as a flash lamp in high speed photography /1-7/ . Recently, many investigators, in particular, Wanless /8/ proposed the use of such lamps for optical pumping of quanta oscillators. I. V. Nemchinov, M. A. Tsikulin and I. F. Zharikov / 9/ investigated by means of an explosion source, the effect of powerful ultraviolet radiation on various materials, their intensive evaporation and dispersion. A. N. Dromin and S. D. Savrov were able to detonate an explosive substance /10/ by a light pulse from such a source. Using an explosive source, A. A. Provalov and the coauthors /11/ observed a self-shielding phenomenon of the body surface from powerful radiation. The authors /12-14/ proposed a high-temperature radiator of the explosion type, suitable for photometry.

Radiation of shock waves was encountered in solving important practical problems related to strong explosions and the movement of cosmic bodies in the atmosphere. By setting up experiments with strong shock waves, it was possible to expand the investigation of optical properties of gases heated to a high temperature and investigating the effect of powerful radiation flows on a solid substance (ablation of solid bodies).

The shock wave remains an object of thorough experiments and theoretical investigations that provides valuable information on dissociation, ionization and other elementary processes in heated gases. Much attention is being devoted to luminescence, carrying various information about these processes. A detailed analysis of the volumetric gas radiation in numerous experiments in shock pipes can serve as an example of this. Strong shock waves in fairly dense gases, which are high-temperature surface radiators, may be obtained by explosive substances. Such shock waves present the possibility of studying experimentally the processes in dense plasma whose theoretic description causes many difficulties.

The carrying out of experimental investigations in the indicated direction requires a fairly high level of the measurement techniques of high-speed phenomena. The implementation of this work was made possible by the fact that the School for Investigating Explosion Processes, headed by academician M. A. Sadovskiy, achieved certain successes in understanding the essence of explosion phenomena, as well as in the development of the recording methods and apparatus. Optical and electronic devices developed at the IFZ for recording high-speed processers, used in our work, make it possible to study fully the complex physical process which is the propagation of a strong shock wave in gas.

A certain relationship between the investigations of explosion processes with such an especially astronomic problem as the movement of space bodies in the atmosphere of the earth, is due to one and the same object of the investigations--the shock wave, formed in the air when moving at supersonic speed. The well known papers by K. P. Stanyukovich / 15, 16/, V. A. Bronshten / 17, 18/ and others, as well as the paper by one of the authors / 19/ proves the common nature of these phenomena again. Therefore, the authors hope that the results of laboratory experiments on investigating the radiating properties of shock waves in gases, cited in this book, will find application in solving astronomic phenomena.

The work developed in several directions. The first, although an auxiliary but necessary direction, was in developing methods for obtaining strong shock waves. As a result, it was found possible to obtain shock waves with velocities of up to 80 km/sec and temperatures greater than 10^5°K in gases with normal density (at atmospheric pressure).

The second direction was studying the radiating properties of strong shock waves and their relationship to the front structure. Here, along with experimental results such as nonstationary shielding of the radiation front at certain conditions, theoretical results were also obtained, in particular, a deduction was made on the important role of the nonequilibrium processes ahead of the shock wave front.

On the basis of the results of the first two directions, optimal installations were developed to obtain powerful radiation flows with a continuous spectrum. Fairly high parameters were obtained: density of radiation flow at the target--15 to 20 Megawatt/cm^2; radiation time--20 to 30 microsec; the integral energy at the target reached 130 joules/cm^2 for a total irradiated surface of up to 100cm^2. Such radiators were used in the laboratory to ablate bodies under the influence of powerful radiating flows.

The description of the results of the work in the indicated directions makes up the content of the book. Some results of the work were reported in physics seminars of the Earth Physics Institute, the Problems of Mechanics Institute of the USSR Academy of Sciences and scientific conferences of the Moscow Physio-Technological Institute and published in scientific journals.

The Committee for Meteorites of the USSR Academy of Sciences showed great interest in the work. The authors were supported in their work by M. A. Sadovskiy, P. V. Kevlishvili, V. N. Rodionov, I. V. Nemchinov, N. M. Kuznetsov, Yu. P. Rayzer and are grateful to them.

The authors also express their gratitude to staff workers who helped in the work and participated in carrying out a number of experiments: Yu. Zatsepina, A. A. Provalova, I. E. Markovich, I. I. Divnova, Yu. N. Kiseleva, F. A. Sorokina and I. I. Zotova.

M. A. Tsikulin and Ye. G. Popov

The manuscript of the book was still unfinished when my teacher, noted specialist in the area of explosion physics, Mikhail Andreyevich Tsikulin, died. Staff workers of the laboratory headed by M. A. Tsikulin, gathered up the uncoordinated material of the manuscript and actively participated in completing the paper. However, we apparently were not able to avoid imperfections in several chapters of the book. In preparing the book for printing, V. A. Bronshten made a number of valuable comments and additions, and also took upon himself the cares related to issuing the book.

Ye. G. Popov

Table of Contents

2291
CSO:

CERTAIN PROBLEMS OF RADIATING GAS DYNAMICS

Moscow IZLUCHATEL'NYYE SVOYSTVA UDARNYKH VOLN V GAZAKH in Russian 1977 PP 7-16, 22-28

[Chapter 1 from the book "Radiating Properties of Shock Waves in Gases", by M. A. Tsikulin and Ye. G. Popov, Izdatel'stvo "Nauka", 173 pages]

[Text] The specific success achieved recently in the dynamics of a radiating gas is related to phenomena in which high energy concentration is reached and which leads to the state of a gas with very high temperature. Among these phenomena, besides detonation of an explosive charge in the gas, should be included nuclear explosions, the effect of a focussed laser beam and a powerful electric discharge.

The problems of producing a high-temperature ionized gas--a hot plasma--led to intensive research in this field. The number of papers published on plasma physics is very great and continues to grow. We will not consider here the problems related to a rarefied plasma (these problems are related mainly to the electrodynamics of a rarefied and dense conducting medium) and we will not pose the aim of providing a complete survey of the state of the dynamics of radiating gases. We shall note only the main aspects in the results and the existing difficulties and we shall consider the problems of motion of cosmic bodies in the atmosphere since this is related to shock wave formation.

1. Investigation of Strong Shock Waves in Gases

The state of a high-temperature gas is still achieved under terrestrial conditions only in the pulsed mode when the main moment is scattering of the initial formation at high velocity. Shock waves of considerable intensity occur with sufficiently high initial density of the gas in which scattering occurs and with sufficiently large dimensions of the device and the shock-compressed gas behind the front becomes the subject of investigation. Therefore, investigations of a high-temperature radiating gas are mainly investigations of strong shock waves in gases.

Because of a number of features, shock compression of a gas became one of the most important methods of achieving high temperatures. Heating in a shock wave occurs within a very short time comparable to the times of relaxation processes in the gas, which permits one to study the kinetics of these processes. During shock compression, one can achieve very high temperatures much greater than during adiabatic

compression to equilibrium pressure. And perhaps the most typical phenomenon that indicates high temperatures have been reached (on the order of 10,000° and above) is the glow of the gas in the shock wave. Detailed investigation of this glow was begun in the 1950s when laboratory methods of producing strong shock waves began to be employed. Methods of recording high-speed processes were improved adequately by that time. Without resorting to one or the other, the authors of earlier papers could still resolve some principle problems. As early as 1934 Muraour and Levy [20] pointed out that the glow observed during explosions is caused not so much by the thermal radiation of detonation products or their chemoluminescence as by the radiation of the ambient air shock-heated by scattered products. In 1943 Ya. B. Zel'dovich and O. I. Leypunskiy [21] demonstrated the capability of achieving high temperatures during shock compression of a gas with high atomic weight. Firing at a glowing flask filled with mercury vapors from a gun, they observed a bright flash during passage of a bullet through the vapors.

The front of investigations was expanded significantly with the appearance of shock tubes. In 1950 Ya. K. Gershanik, Ya. B. Zel'dovich and A. N. Rozlovskiy [22] employed an installation into which atmospheric air flowed into a tube containing the low-pressure mixture under investigations upon rapid removal of the plug. Instead of a plug, they subsequently began to use a diaphragm, after rupture of which a strongly compressed gas (hydrogen or helium) expanded and excited a shock wave in the gas under investigation. From the gas-dynamics viewpoint, the burst decays upon formation of a shock wave propagated toward the gas at lower pressure. A rarefaction wave propagates in the opposite direction. A diagram of the processes is given in Figure 1.

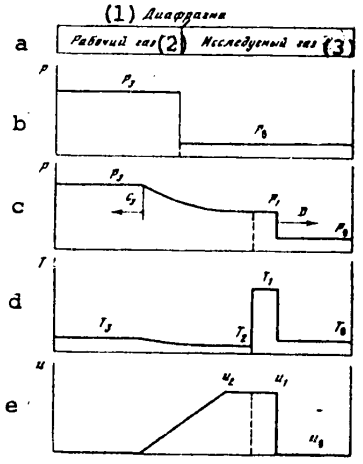

Figure 1. Operation of a Shock Tube: a--diagram of tube prior to operation; b--pressure profile before rupture of diaphragm; c-e--pressure profiles, temperatures and velocities of gas at some moment after rupture of diaphragm

[Key on following page]

[Key continued from preceding page]:

1. Diaphragm
2. Working gas
3. Gas to be investigated

The following is denoted here and further: p is pressure, D is the shock wave velocity, u is mass velocity, T is gas temperature and c is the speed of sound. The arrows indicate the direction of motion of the waves (the gas moves toward lower pressure). The dashed line denotes the contact burst--the boundary of the gases initially on both sides of the diaphragm. A relationship between the pressure behind the shock wave and the initial gas pressure in the high-pressure chamber is found from the condition of equal gas velocity on the contact burst. Adiabatic motion of the gas occurs on the rarefaction wave and the Riemann invariant $u + 2c/\gamma(\gamma - 1)$ is retained. Then from the condition $u_3 = 0$ we find

$$u_2 = \frac{2c_2}{\gamma_2 - 1}\left[1 - \left(\frac{p_3}{p_2}\right)^{\frac{\gamma_2 - 1}{2\gamma_2}}\right]. \tag{1.1}$$

The gas velocity behind the shock wave is

$$u_1 = c_0 \sqrt{\frac{2}{\gamma_1}} \frac{p_1/p_0 - 1}{\sqrt{(\gamma_1 + 1)\, p_1/p_0 + \gamma_1 - 1}}. \tag{1.2}$$

Having set u_2 and u_1 equal and having denoted the internal gas energy by $e = c^2/\gamma(\gamma - 1)$, we find the relationship of p_3 and p_1:

$$p_3 = p_1 \left\{1 - (p_1/p_0 - 1)\sqrt{\frac{[(\gamma_2 + 1)/2\gamma_2]\, e_0/e_2}{[(\gamma_1 + 1)/(\gamma_1 - 1)]\, p_1/p_0 - 1}}\right\}^{-\frac{2\gamma_2}{\gamma_2 - 1}}. \tag{1.3}$$

The ratio of densities on the shock burst is $\rho_1/\rho_0 = (\gamma_1 + 1)/(\gamma_1 - 1)$ for a strong shock wave and the temperature behind the shock front is then equal to

$$T_1 = T_0 \frac{\gamma_1 - 1}{\gamma_1 + 1} \frac{p_1}{p_0}. \tag{1.4}$$

The shock wave intensity p_1/p_0 and together with it the temperature behind the shock front T_1 may be very high with sufficiently high pressure drop on the diaphragm p_3/p_0. A significant parameter in this case is the ratio of internal gas energy in the high- and low-pressure chambers e_3/e_0. The higher this ratio, the higher the shock wave intensity and gas temperature. Having expressed the internal gas energy e by temperature T, the molecular weight μ and the adiabatic index γ, we find

$$\frac{e_3}{e_0} = \frac{\gamma_0 - 1}{\gamma_3 - 1} \frac{\mu_0 T_3}{\mu_3 T_0}. \tag{1.5}$$

The higher the gas temperature in the high-pressure chamber and the greater the molecular weight in the low-pressure chamber, the stronger the effect will be.

In 1953 Hollyer et al [23] first observed the glow in a shock tube filled with xenon. The glow occurred at the moment the shock wave was reflected from the open end of the tube and the glow spectrum changed from linear to continuous as the shock wave amplitude increased.

Petschek et al [24] later observed the glow of argon in a shock tube which also contained lines on a background of the continuous spectrum. Since then the volume of research performed in shock tubes has increased continuously.

However, one should note the essentially limited capabilities of a shock tube in achieving high temperatures. We find the finite intensity of a shock wave from formula (1.3) with infinitely large pressure drop on a diaphragm $p_3/p_0 \to \infty$. This is related to the fact that the gas behind the rarefaction wave cannot be cooled below absolute zero (gas condensation actually occurs much earlier). For the case of different gases (for example, $e_0 \ll e_3$), from formula (1.3) for $p_3/p_0 \to \infty$, we find the maximum values of pressure and temperature behind the shock front:

$$\frac{p_{1m}}{p_0} = \frac{\gamma_1 + 1}{\gamma_1 - 1} \frac{2\gamma_2}{\gamma_2 - 1} \frac{e_3}{e_0}, \tag{1.6}$$

$$\frac{T_{1m}}{T_0} = \frac{2\gamma_2}{\gamma_2 - 1} \frac{e_3}{e_0}. \tag{1.7}$$

Using the most advantageous combinations of gases, one can find a more than 100-fold temperature increase (Table 1).

Table 1

	He – Air	He–Xe	H_2–Xe
e_3/e_0	4.3	33	110
T_{1m}/T_0	23	165	770

When one uses the reflection of a shock wave from the closed end of a tube, one can increase the temperature additionally by a factor of $(3\gamma_1 - 1)/\gamma_1$, which is also twofold greater at $\gamma_1 = 1.2$. Thus, one can achieve an approximately 1,000-fold temperature increase in a shock tube; however, the real number is tens of times less due to gas ionization behind the shock front.

New capabilities were discovered with the appearance of electric discharge shock tubes. The shock wave is formed in these tubes as a result of rapid expansion of a gas heated by a powerful capacitor discharge and also by acceleration of the plasma formed by the magnetic field of the discharge. The working principle of the tube is shown in Figure 2. The bus along which current is fed to the discharge

gap is laid along the outer surface of the tube, inside which the discharge occurs. The plasma formed by the discharge, in addition to its own expansion, is ejected by the magnetic field of the discharge current since the conductors with opposite direction of current (in the bus and in the discharge) are repelled. Plasma scattering (at initial pressure of 0.7 mm Hg in the tube) at velocity up to 90 km/s was achieved in the first device of this type and in this case the temperature reached 120,000°K [25].

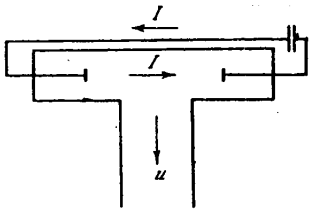

Figure 2. Diagram of Electric-Discharge Shock Tube

Modern electric-discharge tubes make it possible to produce shock waves with velocities greater than 100 km/s and gas temperature of more than 10^5 °K behind the front. Such high velocities and temperatures are achieved in strongly rarefied gases (the gas pressure in front of the wave does not exceed several mm Hg).

The dimensions of shock tubes and the density of the gas filling them are usually such that the heated zone is optically thin and radiates in all directions. Careful analysis of this radiation provided much valuable data on dissociation, ionization and other elementary processes in heated gases. A rich arsenal of procedures and means was worked out, that includes along with methods of astrophysics (analysis of the shape of spectral lines), new methods based on the use of electromagnetic radiation in different regions of the spectrum and beams of neutral and charged particles. A modern shock tube is a complex piece of equipment frequently created to investigate some single problem and outfitted with unique apparatus. The experimental material obtained in shock tubes is enormous. The number of published papers is counted in the thousands and there are many survey articles and books.

Shock waves in which the heated region with the optically dense became the subject of investigations very rarely. All the features of radiation are determined in this case by the narrow layer of gas adjacent to the wave front. It is for this reason that one can talk about the radiating properties of a strictly shock wave without relating them to the entire region of a shock-heated gas. These shock waves occur, for example, upon entry of large cosmic bodies into the atmosphere at high velocity and during nuclear explosions. Under laboratory conditions the shock waves that radiate in a similar manner can be created in gases at atmospheric pressure by means of powerful explosives. And although the specifics of experiments with explosives sustained the investigations, a number of interesting results has been obtained on this route during the past few years.

The glow of shock waves with velocities of approximately 8 km/s, which can be produced comparatively simply upon the emergence of an explosive detonation to a

boundary containing gas, has been studied in more detail. A bright glow was discovered in 1941 by Michel-Levy et al [26] upon the collision of two of these waves in argon. The relative glow intensity distribution measured by them through the spectrum was the same as that of a black body with temperature of 35,000°K. Later Stettbacher [27] made similar measurements for shock waves formed upon the discharge of a detonation from an explosive (tetranitromethane + toluene) into argon and air. The color temperature of the wave front was 27,000°K in experiments with argon and 10,500°K in experiments with air. Roth [28] very carefully measured the glow intensity distribution through the spectrum. The shock wave in his experiments was stimulated upon discharge of the detonation from an explosive (trotyl + + hexogen and then trotylhexogen) into argon. The color temperature of the front was 29,000 $\pm$ 1,000°K and was appreciably above the temperature of the shock-heated argon (24,000°K), calculated from shock relations. In 1965 Conger et al [7] attempted to compare the intensity of visible and hear ultraviolet radiation (λ = 230-330 nm) during explosive of a pentolite charge in argon. The color temperature of the front of 20,000°K, which was somewhat lower than the temperature of a shock-heated gas (23,500°K) obtained by calculation, corresponded to the intensity ratio.

The relative glow intensity distribution to the spectrum and the proximity of the color temperature of the front to the calculated temperature of the gas behind the front confirmed the opinion of investigators that the shock wave formed upon discharge of detonation from the explosive glows like a black body. However, total confidence in this appeared only after I. Sh. Model' [29] presented the results of measuring the absolute glow intensity in 1957. The shock wave in his experiments was stimulated upon discharge of the detonation from an explosive (trotyl + hexogen and later trotylhexogen) into air.* The absolute glow intensity measured behind a red light filter was like that of a black body with temperature of 10,000°K and this value coincided with the temperature of shock-heated air calculated from the wave velocity known from experiment. Recording the increase of glow intensity after discharge of the detonation from the explosive, I. Sh. Model' [29] and later Roth [28] managed to show that optically dense waves are formed in these experiments. All concepts toward this calculation were previously based on estimates of the absorption coefficient by the Kramers formula, the applicability of which to a non-hydrogen-like dense plasma raised doubts.

The data presented in papers [13, 14, 30-32] also indicate the similarity of a shock wave to absolutely black radiation.

The temperature and emissivity of a shock wave increase significantly with an increase of amplitude. Thus, if the density of the luminous flux from the front is equal to $1.6 \cdot 10^6$ W/cm^2 at shock wave velocity of 8 km/s in argon, it is then $1.6 \cdot 10^7$ W/cm^2 at velocity of 16 km/s. This explains the interest in the stronger shock waves than those which can be produced upon discharge of a detonation from powerful explosives to a boundary with a gas.

---

* We touch on the experiments with very strong shock waves, described by I. Sh. Model', somewhat later.

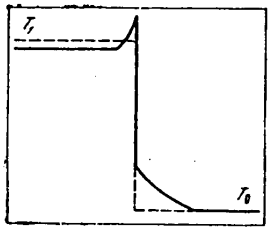

Figure 3. Temperature Profile of Strong Shock Wave With Regard to Radiation (dashed line--without regard to radiation)

Fundamental theoretical investigations of the role of radiation in strong shock waves were carried out by Ya. B. Zel'dovich and Yu. P. Rayzer. The results of investigations were published in 1957 in a cycle of articles [33-36] and were later included in a monograph [37]. It is shown that luminous heat transfer rearranges the structure of the front at high amplitudes (Figure 3). The gas in front of a strong shock wave is heated by powerful shortwave radiation from the front so much that it begins to absorb longwave (specifically, visible) radiation from the front and shields it. Therefore, the brightness temperature of the front, initially coinciding with the true gas temperature behind the front, lags behind it as the shock wave amplitude increases, passes through a maximum and decreases to a rather low value determined by the natural glow of the heated gas in front of the front. As an illustration, let us present the results of quantitative estimates of the phenomenon for a shock wave in air of normal density, made by Yu. P. Rayzer [35]. The dependence of the brightness temperature of the shock wave front in red light on the true temperature of the air behind the front is shown in Figure 4. The shielding effect is still small at gas temperature behind the front of T_1 = = 65,000°K and the brightness temperature T_{ya} is equal to gas temperature T_1. But even at T_1 = 90,000°K shielding of the front in red light is appreciable and T_{ya} = = 80,000°K. A further increase of amplitude intensifies the shielding of the front so much that it leads to a decrease of brightness temperature. Thus, T_{ya} = = 67,000°K at T_1 = 100,000°K and the brightness temperature decreases to a maximum value of T_{ya} = 17,000°K at even higher amplitudes, which almost does not vary until the wave amplitude increases strongly.

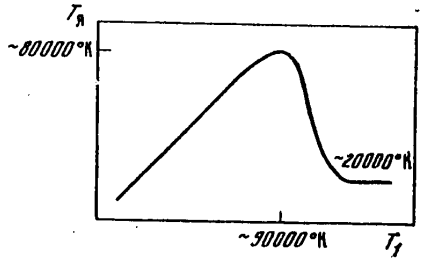

Figure 4. Dependence of Brightness Temperature of Front on True Temperature of Air Behind Front

The sharp difference of the brightness temperature of the front of a strong shock wave from the calculated temperature of the gas behind the front was observed by I. Sh. Model' [29]. Shock waves with velocity of 17 km/s were created by means of explosives in gases with high atomic weight (xenon, crypton and argon). Very high temperatures were achieved in this case--according to I. Sh. Model''s calculations, who took into account the multiple ionization and radiant cooling of a shock-heated gas, the temperature of xenon, crypton and argon were T = 110,000, 90,000 and 60,000°K, respectively. However, the brightness temperature of the front measured behind a red light filter was several times lower for all three gases and T_{ya} = 35,000-30,000°K. This divergence was not contained in the temperature measurement error ($\pm$ 15 percent) and was explained by shielding of the radiation by the heated gas in front of the front.

In the paper of I. Sh. Model' [29], the brightness temperature of the front was measured with the same value of shock wave amplitude. The variation of the brightness temperature of the front with an increase of shock wave amplitude could not be followed experimentally for a long time due to the absence of simple methods of producing rather strong shock waves. In 1964 A. Ye. Voytenko [38-40] proposed an effective method of producing strong shock waves by means of explosives and two years later A. Ye. Voytenko, I. Sh. Model' and I. S. Samodelov [41] observed the lag of the brightness temperature of the front behind the calculated temperature of the gas behind the front in experiments with xenon and air. The gas temperature behind the front reached T = 110,000°K at wave velocity of D = 43 km/s, while the brightness temperature of the front measured behind a red light filter comprised only T_{ya} = 72,000°K. The brightness temperature of the front in xenon reached its own maximum value of T_{ya} = 50,000°K (T = 120,000°K) at D = 18 km/s and decreased to a limiting value of T_{ya} = 22,000°K with a further increase of amplitude.

The radiating properties of strong shock waves in argon, xenon and air was studied by the authors jointly with Yu. A. Zatsepin [42]. The brightness temperature was measured immediately in several sections of the spectrum from the visible and ultraviolet regions. Not only the separation of the brightness temperature of the front from the calculated temperature of the gas behind the front but the variations in the intensity of radiation of the front at different angles indicated shielding of radiation at high amplitudes. The effect of shielding in the ultraviolet region was manifested more weakly than in the visible region. Experiments with argon to which several percent air was added led to an unexpected result and in this case the maximum brightness temperature did not exceed T_{ya} = 30,000°K and was much lower than in experiments with pure argon (T_{ya} = 90,000°K) or with air (T_{ya} = 75,000°K). However, unsteady shielding of the radiation of strong shock waves which led to a decrease of the brightness temperature of the front in time, discovered in experiments with inert gases, was of great interest.

Experimental investigations confirmed in only the most general features the theoretical concepts about shielding of radiation in strong shock waves. Shielding was observed in experiments at significantly lower shock wave amplitudes than followed from theoretical estimates. The possible reason for the differences--the absence of thermodynamic equilibrium in the gas before the front of a strong shock wave--was noted in [42]. To substantiate this hypothesis, one of the authors compared the times of relaxation processes in the heated layer in front of the front to the

time the gas was in the layer [43]. It turned out that some of the processes can remain incomplete. Consideration of this circumstance improved agreement with experiment.

Absorption of radiation by the narrow layer on the front where ionization of a shock-heated gas develops leads to additional decrease of the brightness temperature of the front. The authors of [13], studying the glow spectra of shock waves formed upon discharge of detonation from an explosive into inert gases, reached the same conclusion. The absorption lines of ions in the emission spectrum of shock waves were recorded and a decrease of the brightness temperature of the front was observed. These results could not be explained by radiant heating of the gas in front of the front, which was still too low in these experiments.

The unsteady nature of shielding of the radiation of strong shock waves in inert gases is not contained within the framework of existing theoretical concepts. The characteristic features of the phenomenon found in experiments indicate the development of a much wider shielding layer in front of the shock wave front than was assumed. It is appropriate to note in this regard that a significant electron concentration far in front of the shock wave front (the so-called "precursor") was observed repeatedly in experiments in shock tubes. There are indications that electron diffusion from a shock-heated gas to the region in front of the front plays a specific role in formation of the "precursor." The argon temperature before the front (presumably due to energy transfer by these electrons) reached 8,000°K in [44]. However, most investigators link the formation of the "precursor" to excitation of the atoms of gas before the front by radiation in the resonance lines and their subsequent photoionization. L. M. Biberman and B. A. Veklenko [45] showed that a layer of excited atoms forms in front of the shock wave front due to absorption of resonance photons in the lens of the lines and subsequent acts of re-radiation similar to diffusion. This process was considered in [46] with regard to photoionization of excited atoms. There is no unified opinion on the causes of "precursor" formation. Further investigations will show whether the phenomena touched on above are related to unsteady shielding of the radiation of strong shock waves.

§2. Problems of moving large cosmic bodies in the atmosphere

In the light of the progress made in the dynamics of a radiating gas, great significance is being attached to the studies of the movement of large cosmic bodies in the atmosphere during which powerful shock waves are formed, and the temperature of the gas behind the front reaches high values so that radiation acquires an important role in this physical process. In particular, the broad class of meteor phenomena in the earth's atmosphere belongs here. Of the great variety of aspects of studying meteor phenomena, among which it is possible to name astronomical, cosmogonic, chemical and other studies [47], let us mention the problems pertaining to meteor physics, the problems of the movement of bodies in the atmosphere, in rarefied and dense gases. On approaching the earth, cosmic bodies experience acceleration as a result of the earth's attraction; bodies with zero velocity accelerate to 11 km/sec -- this is the lower limit. The upper limit is defined from the addition of the orbital velocity of the earth (30 km/sec)

and the maximum possible heliocentric velocity of meteor bodies which is equal to 42 km/sec for nonhyperbolic orbits. Thus, the extra-atmospheric velocity falls within the limits of 11-72 km/sec.

At such velocities, meteor bodies experience strong interaction with the air in the atmosphere: in the upper layers, in the molecular flux mode, and in the lower layers, in the continuous flow mode with the formation of a powerful shock wave. In the molecular flux mode at altitudes of 80-120 km where the free path length of the molecules is much greater than the dimensions of the meteor bodies, interaction with the air takes place just as with individual molecules. This interaction leads to loss of mass of the meteor by evaporation under the effect of the impact of the air molecules and to the excitation of the atoms of the evaporated material which determines the radiation of meteors.

In the continuous flux mode, behind the front of the shock wave formed ahead of large cosmic bodies, the gas has a temperature from tens to hundreds or thousands of degrees, and radiant energy fluxes developed to values on the order of 10^9 watts/cm^3. These processes determine both the loss of mass (ablation) of the meteor body and its radiation. The study of the radiative properties of such shock waves, the radiant energy transport and the effect of powerful radiation fluxes on matter is of great scientific interest.

At the present time there has been significant improvement of the physical theory of meteors -- small cosmic bodies entering the earth's atmosphere and completely burning up in its upper layers. Meteors are recorded by their glow; the method of radar tracking of meteor trails was developed only recently [48]. The greater part of the available data on the cosmic bodies in the atmosphere pertains to meteors, the movement of which is not accompanied by the formation of a shock wave. This sampling of observation data is explained by the comparatively

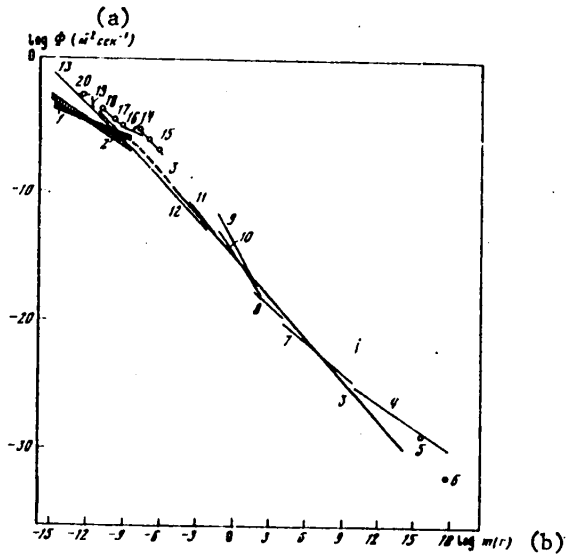

Figure 5. Distribution of meteor bodies by mass
1, 2 -- microcraters on the moon, 3 -- craters on the moon, 4 -- asteroids, 5 -- Apollo group (Whipple), 6 -- comets (Whipple), 7 -- meteorites (Braun), 8 -- meteorites (Hawkins), 9 -- meteors (Millman, Bohrland), 10 -- meteors (Hawkins, Apton), 11 -- meteors (Lindblad), 12 -- meteors (Watson), 13 -- cosmic dust (Weinberg), 14 -- zodiacal light (Alsasser), 15 -- "Pegasus," 16 --"Explorer," 17 -- "Mariner," 18 -- "Pioneer," 19 -- "Lunar Orbiter," 20 -- OGO-III

Key:
a. $m^{-2}sec^{-1}$)
b. m(g)

high frequency of meteors and the presence of regular meteor flow. The graph in Figure 5 presents comparative data on the frequency of meteor phenomena of different scales -- from cosmic dust with a particle mass of 10^{-15} g to asteroids. The logarithm of the mass is plotted on the x-axis in grams, and the logarithm of the meteor body flow per square meter per second is plotted on the y-axis.

Let us present the basic principles of the physical theory of meteors [49].

From the law of conservation of momentum we have

$$m\frac{dv}{dt} = -\Gamma S\rho v^2, \tag{1.8}$$

where m and v are the mass and the velocity of the meteor body, ρ is the air density, S is the cross sectional area of the meteor body, Γ is the drag.

Expressing the cross sectional area S in terms of the mass m, the density of the meteor body δ and the shape factor A, we obtain the first equation of the physical theory of meteors -- the braking equation

$$\frac{dv}{dt} = -\Gamma A \delta^{-1/3} m^{-1/3} \rho v^2. \tag{1.9}$$

One of the basic principles in the physical theory of meteors is the principle that energy transmitted to a meteor body by air molecules colliding with it is predominantly spent on evaporation of it:

$$Q \frac{dm}{dt} = -\frac{1}{2} \Lambda S \rho v^3, \tag{1.10}$$

where Q is the energy of evaporation of one g of meteoric matter, Λ is the heat transfer coefficient (the fraction of the kinetic energy of the air molecules colliding with the meteor body spent on evaporation). The heat transfer coefficient Λ turns out to be a comparatively large value on the order of 0.5.

From (1.8) and (1.10) we obtain the second basic equation -- the mass loss equation

$$\frac{dm}{dt} = \sigma m v \frac{dv}{dt}, \tag{1.11}$$

where $\sigma = \Lambda/2\Gamma Q$ depends weakly on the velocity so that when the mass of a meteor body decreases significantly, the velocity loss is very small. The basic equations also include the glow equation

$$I = -\frac{1}{2} \tau \left(\frac{dm}{dt}\right) v^2 \tag{1.12}$$

and the ionization equation

$$\alpha = -\frac{\beta}{\mu v} \left(\frac{dm}{dt}\right), \tag{1.13}$$

where I is the radiation of the meteor per unit time, τ is the fraction of the kinetic energy of the meteor atoms converted to light energy (luminosity), α is the linear electron density of the meteor trail, β is the number of free electrons generated by one evaporating atom of the meteor body (the ionization factor), μ is the average mass of an atom of the meteor body.

Combining equations (1.11) and (1.12), it is possible to express the value of σ in terms of measured values of the brightness of the meteor I and its velocity v:

$$\sigma = -I \Big/ \left(\int_{t}^{t_1} I\,dt\right) v \frac{dv}{dt}. \tag{1.14}$$

By processing actual data obtained by camera recordings, in reference [50], reliable confirmation was found for the fact that the value of σ varies little with variation of the velocity and mass of the meteor.

The primary recording technique and source of information about meteor phenomena remains recording the glow of the meteor in the atmosphere. Therefore the importance of the radiative properties of meteor bodies is unquestioned.

The visually noted brightness of a meteor trail is related to the radiation intensity of the meteor I [51] and it is denoted by the absolute stellar magnitude

$$M = 24{,}6 - 2{,}5 \lg I, \tag{1.15}$$

and it is also related to the illumination E on the earth's surface created by the meteor radiation and expressed by the visible stellar magnitude m [52]:

$$E = 2{,}1 \cdot 10^{-6} \cdot 2{,}512^{-m} \text{ lux}. \tag{1.16}$$

The stellar magnitude is related to the initial mass and velocity of the meteor body. A meteor of zero stellar magnitude corresponds to a velocity of 40 km/sec and an initial mass of about 1 g.

A great deal of actual data have been accumulated on the radiation of meteors. The application of night photographic patrolling using special cameras for automatic recording of meteors equipped with obturators for measuring the velocity and diffraction gratings for recording the glow spectrum of the meteors offers the possibility of simultaneously measuring the brightness of the meteors I, their velocity v and the spectral characteristics.

The recorded spectra of meteors (their number in 1971 exceeded 1300 [53]) basically are of a linear nature with luminescence of the lines of the atoms making up the meteor body. This indicates that basically the meteor radiation is recorded in the molecular flux mode where the atoms of the meteor body excited by impacts with the molecules of the air emit. Meteor physics is still experiencing a number of difficulties with its improvement. A survey of the physical theory of meteors indicates that many values entering into the equations are insufficiently precisely known and subject to significant refinement; therefore it is necessary to exercise caution with regard to the conclusions of the theory. For example, the estimation of the density of meteor bodies from velocity data based on optical measurements diverges strongly from the actual measured value as it turned out for the Prshibram meteorite [54] (by the estimate based on trajectory measurements 0.4 g/cm^3, actually according to the specimens found 3.6 g/cm^3) and for the Lost City meteorite [55]: according to the optical measurement data 0.1 g/cm^3, and actually for the bronzite chondrite which this meteorite turned out to be, the density is 3.8 g/cm^3. The exact determination of the constants τ and β in the glow and ionization equations (1.12) and (1.13) has great significance. This offers the possibiiity of a quantitative comparison of the results of optical and radar measurements which recently have been accumulated very rapidly. Whereas the meteor problem has not been fully resolved theoretically, in any case there is a large amount of factual data for the solution of this problem.

Another situation is observed for the phenomenon of the movement of quite large cosmic bodies in the atmosphere. First of all, here we note the extraordinary shortage of factual data from recording the glow of large bolides although this phenomenon is not so rare, as is clear from the graph in Figure 5. Many processes pertaining to this phenomenon have not even been isolated for detailed study as a result of the complexity and absence of the data.

With the formation of a powerful shock wave in front of the moving cosmic body, many physical processes occur, among which it is possible to isolate the following as independent: ionization of the gas behind the shock wave, the radiation of the powerful shock wave, radiant energy transported in the heated gas behind the front (comparable to or exceeding the hydrodynamic transport, the effect of radiation on the matter of the cosmic body and destruction of it under the effect of radiation (ablation). All of these processes also determine the laws of movement of a large meteor body in the atmosphere, the variation of its mass and velocity.

The progress recently made in plasma physics, in the dynamics of the high-temperature gas and in adjacent fields have determined the well-known progress in the mentioned problems of the movement of cosmic bodies in the earth's atmosphere.

A large number of papers have been written on the ionization of a gas behind a shock wave and the optical properties of the ionized gas, including as applied to meteor physics [17-19, 56-100]. This problem is the best developed.

Intensive studies of the problem of the effect of radiation on matter have been started [9-11, 101-120]. Here it is especially necessary to note the large number of papers on the effect of laser radiation on matter appearing in connection with the rapid development of laser engineering [101-120]. Nevertheless, the study of the effect of radiation with a continuous spectrum is of the

greatest interest for the problem of the ablation of cosmic bodies in the atmosphere.

In spite of the development of such research on the general physics level the studies of the ablation of bodies in the situation of flow of a continuous gas around them have been made at random. It is necessary to note that a detailed investigation of the specific process of the ablation of a cosmic body under the conditions of radiant energy transport in a dense gas flow behind the shock wave front can give a result which will be difficult to reconcile with the results for small meteoroids by selecting the value of the coefficients in the basic equations. In this respect, as was pointed out earlier [17, 19], the experiments have great significance. It is possible to set up experiments on the modern level of the development of engineering reproducing the actual meteor flight conditions and processes occurring on interaction of them with the air. The flight of meteors in the upper layers of the atmosphere at a velocity of 16 km/sec has been reproduced by shaped-charge firing of metal balls from a rocket at high altitude [121]. The glow spectrum of a meteor with a velocity to 56 km/sec has been reproduced by the effect of an electron beam on a specimen [122]. Under laboratory conditions it is possible to accelerate metal particles to a velocity of 40 km/sec [123, 124] using an explosive charge. An interesting study of the ablation of solid states simulating meteor bodies was performed using a plasmotron producing a plasma flux at a temperature of 10000°K [125].

New possibilities for studying the effect of powerful radiation fluxes on meteor bodies are being opened up in connection with the use of explosive high-temperature sources of light, the emitter in which is a powerful shock wave in a gas. By this method it is possible to obtain a light source with a temperature of more than 100,000°K, producing a radiation flux for the investigated specimen

with a density on the order of 100 Mwatts/cm^2. Under the effect of such a powerful radiation flux the material of the specimen evaporates, and further effect of the radiation occurs in the presence of a layer of vapor over the surface of the specimen, which reproduces the ablation conditions of a meteor body behind the powerful shock wave. This method is being developed by the authors of [9, 11] in connection with studying the radiative properties of powerful shock waves in gases.

What has been stated with respect to the ablation of large cosmic bodies can also be applied to their movement in the earth's atmosphere, to the law of variation of their mass and velocity. It is necessary to expect that variation of the specific process of the interaction of a meteor body with the air flow from small meteor bodies to large meteorite-forming bolides will have its impact on the basic equations, the values of the coefficients in them, and their dependence on the velocity. This is noted when processing the results for a large bolide [126] when the value of the coefficient σ in the equation (1.11) quickly decreases with a decrease in the velocity from $\sigma=9\cdot10^{-13}$ at v=20 km/sec to $\sigma=2\cdot10^{-13}$ for v=7 km/sec. Accordingly, it is necessary to note the result obtained in reference [127] from estimating the intensity of the ablation of a meteor body in the radiant thermal conductivity mode in the gas and in the vapor behind the shock wave front where the mass loss turns out to be proportional to the velocity of the meteor body which, as was demonstrated [17], does not differ from the solution of equation (1.10) with constant coefficient Λ. In reference [127] an effort was made to estimate the nature of the variation of Λ and its influence on the ablation.

In equation (1.12) which describes the glow of meteors, it is proposed that the radiation energy is proportional to the kinetic energy of the lost mass of the meteor body inasmuch as the emitter is the atoms of the meteor body excited by the air molecule impacts. When a large meteor body is moving in the

atmosphere, the emitter is the shock wave that is formed; in this case the radiation process is accompanied by the formation of a shielding layer ahead of the wave front and other effects.

Thus, the problem of the radiation of a large meteorite-forming bolide is more complicated than the radiation of small meteroids. The results of the experimental study of the radiative properties of shock waves in gases presented in the given book will promote the statement of this problem.

3. Problems of Experimental Investigation

The deficiency of experimental data on the radiating properties of a gas in optically dense layers and in strong shock waves in dense gases was noted in previous sections during survey of some problems of the dynamics of a radiating gas related both specifically to the radiating properties of shock waves and to applied problems.

An optically dense shock wave rarely became the subject of investigation. This situation is explained by the specifics of experiments with explosives except these waves have not yet been produced in them. The glow of shock waves with velocities of approximately 8 km/s, which can be produced comparatively simply upon discharge of a detonation to a boundary with a gas, was studied in more detail. However, the contradictory results obtained [7, 28] require further experiments. The glow of shock waves with velocities above 10 km/s was studied in only two papers [29, 41]. The main purpose of these investigations was achieved--to detect the self-shielding of strong shock waves predicted by theory under

laboratory experiment conditions. However, if the spectral composition of visible radiation was studied during discharge of detonation and if the first measurements were made in quartz ultraviolet, then one would have to make a judgment about the radiating properties of stronger shock waves only from measurements in red light. The angular distribution of the radiation of the front was not investigated in a single one of the papers known to us, although the idea of a shock wave as a radiator remains incomplete without it. With regard to the theoretical aspect of the problem, the influence of a number of effects on the radiating properties of shock waves has still not been studied. Thus, the estimates of the optical thickness of the layer on the front in which gas ionization develops, which we made, shows that the layer can appreciably affect the nature of radiation of the shock wave. One can also show the absence of thermodynamic equilibrium in the heated layer before the front, which should be taken into account when calculating the brightness temperature of strong shock waves.

Familiarity with papers whose main results were discussed above and estimates of the influence of some effects on the radiating properties of waves determine the need to set up systematic experiments. We posed the following specific tasks:

--to estimate the influence of the shielding effect of strong shock waves on their radiating capability on the basis of measurements of brightness temperature in different regions of the spectrum and with different initial gas pressures;

--to compile a more complete concept of the spectral composition of the radiation of shock waves by measurements in the ultraviolet, visible and infrared regions of the spectrum and to obtain data on the angular distribution of radiation;

--to calculate the brightness temperature of shock waves in some gases and to compare the results of experiment and calculation on the basis of existing theoretical concepts.

Based on the results of experimental investigation of the radiating properties of waves, it was suggested that one turn to problems related to the use of a shock wave as a light source. Almost all the papers published on this problem are devoted to generation of lamp flashes for high-speed photography. The authors recently suggested that an amplitude-stable strong shock wave created by specially shaped explosive charges be used as a high-temperature brightness standard [12-14]. I. V. Nemchinov earlier pointed out the possibility of using explosive sources for experimental investigation of the effect of powerful ultraviolet radiation on a solid. The authors designed a source suitable for these purposes in which the radiator was a strong shock wave in argon. A glowing region occurred above the targets exposed to a radiation source and the piezosensor installed below the target recorded the mechanical pulse [9, 11]. Further investigations in this direction were concentrated on solving the problem of generation of an explosive source with radiant flux density of 10^7 W/cm^2 and above for experimental study of optical and mechanical phenomena that accompany the effect of powerful radiation with continuous spectrum on a solid.

PRODUCING STRONG SHOCK WAVES IN GASES

Moscow IZLUCHATEL'NYYE SVOYSTVA UDARNYKH VOLN V GAZAKH in Russian 1977 pp 24-36

[Chapter 2 from the book "Radiating Properties of Shock Waves in Gases", by M. A. Tsikulin and Ye. G. Popov, Izdatel'stvo "Nauka", 173 pages]

[Text] Experimental investigations of surface-radiating shock waves are closely related to the method of producing them in dense gases. Explosives are used to produce these waves in the papers known to us. If one takes into account that the pressure behind the front of strong shock waves in dense gases can reach 10^4-10^5 atmospheres, the use of explosives is the simplest and still the most practically unique solution.

Production of strong shock waves by means of the focussed admission of pulsed lasers may be promising to study these waves in gases. Experiments are described in the literature [128-130] in which a process similar to a strong explosion occurred after gas absorption of this emission and the velocity of the shock wave was initially equal to approximately 100 km/s.

1. Exciting Shock Waves when Detonation Exits into the Gas

This method of producing shock waves is the simplest and most thoroughly studied. L. D. Landau and K. P. Stanyukovich [15] calculated the motion of disintegrating detonation products [15]; references to experimental papers can be found in the survey of Ya. B. Zel'dovich and Yu. P. Rayzer [36] and in the survey of Lochte-Holtgreven [131]. Yu. N. Ryabinin, I. I. Tamm and M. A. Tsikulin [19, 132] studied the similarity of shock waves from explosive charges in the near zone.

A number of simplifications that raise doubts of the accuracy of the results is usually made when determining the parameters of a shock wave by calculation. Therefore, when the question of the parameters of a shock wave created by a specific device arises, experimental methods of determining them are preferable.

A plane shock wave in a cuvette with the gas under investigation was created in our experiments by the device shown in Figure 6. The velocity of the shock wave was determined by photoscanning achieved by means of the SFR-2 device in the slit photochronograph version.

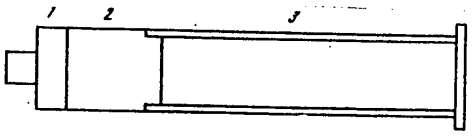

Figure 6. Device for Producing Shock Waves: 1--supplementary charge (lens) that produces a plane detonation front; 2--charge 50 mm in diameter and 60 mm long cast from TG 40/60 (mixture of 40 percent trotyl and 60 percent hexogen); 3--glass cuvette 200 mm long with quartz window

The highest velocity of a shock wave measured during the first moment after discharge of the detonation comprised the following in different gases (in km/s):

He	Ne	Air	Ar	Kr	Xe
11.4	10.4	9.8	9.4	8.7	8.3

The density and effective index of the adiabatic curve of the gas are contained in solution of the problem of scattering of detonation products to the gas. Since the adiabatic curve of the gas is approximately identical at high temperatures for different gases, the velocity of the shock wave should depend only on density. This dependence is approximated by the straight line in the coordinate axes selected in Figure 7.

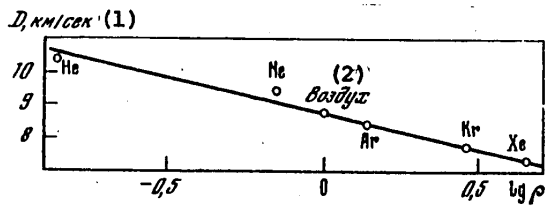

Figure 7. Dependence of Shock Wave Velocity D During Discharge of Detonation from TG 40/60 on Gas Density ρ Related to Air Density

Key:
1. km/s
2. Air

Along with the good recurrence of the results with this method of shock wave production, we note the weak influence of charge size on the value of velocity near its surface. Thus, a decrease of the diameter and length of the charge by one-half in experiments with argon and air did not lead to an appreciable decrease of velocity. The stronger attenuation of the shock wave along the length of the cuvette observed in this case agrees with the conclusions on the similarity of shock waves from explosive charges [19, 132]. This influence of charge size, naturally from the theoretical viewpoint, permits one to compare the results to the measurements of other authors.

Lochte-Holtgreven [131] gives a velocity of 9.5 km/s of a shock wave in air upon discharge of a detonation from TG 50/50. If the linear dependence of shock wave velocity on the velocity of explosive detonation observed in [132] is used, the given value is equal to 9.8 km/s upon recalculation for TG 40/60 and coincides with our measured values.

Christian and Yarger [133] achieved a lower velocity of 8.7 km/s than in our paper upon discharge of a detonation from TG 40/60 into argon. The difference is easily explained by the fact that a plate of inert material was located between the explosive and the gas in [133]. Anderholm [30] presents a value of D = 9.3 km/s close to our value. Roth [28] presents a velocity of 8.3 km/s upon discharge of a detonation from TG 40/60 into argon; this value does not agree by the temperature measured by him (a velocity of D = 9.5 km/s corresponds to this temperature) and it does not agree with our value of D = 9.4 km/s.

Unlike the other experiments described above, Roth [28] did not observe attenuation of the shock waves in argon near the charge. It is appropriate to note in this regard that attenuation of a shock wave in argon near the charge was also not observed in our first experiments with the devices shown in Figure 6. The reason for the confusion was bending of the front near the cuvette walls toward the motion of the shock wave.* Having separated the wall from the charge, this bending could be prevented and attenuation of the shock wave could be observed by measuring the velocity of the plane section of the front. Apparently the divergence of the measured value of shock compression $\rho_1/\rho_0 = 7.9$ with the calculated value of 9.3 and to the measurements of other authors ($\rho_1/\rho_0 = 9.4$) [133] is also related in [28] to bending of the front near the wall.

Unfortunately, measurements of shock wave velocity in xenon and other gases, which would permit better judgment of the results obtained here and which would permit a check of the function in Figure 7 that generalizes similar measurements, are not described in the literature.

Although methods of producing stronger shock waves have been developed recently, the possibility of achieving a temperature up to 30,000-40,000°K behind the front supports the interest in these types of experiments during discharge of detonation from powerful explosives into heavy inert gases.

2. Producing Shock Waves by Detonating Charges With a Cumulative Channel

Shaped charges were and remain the subject of numerous investigations. Koski et al, N. N. Novikov, Novak and others produced jets with velocities of 60-100 km/s [134-137] when metal shells were squeezed by explosion of these charges. However, such high velocities are achieved only in a strongly rarefied gas. Thus, if the jet moves in it at velocity of 60 km/s during initial argon pressure of 10^{-3} mm Hg, an increase of pressure to 100 mm Hg reduces the velocity to 8 km/s [136]. Cylindrical shaped charges described below are more effective to produce strong shock waves in a dense gas. The jet in the channel of these charges is formed during collapse of detonation products (gas cumulation) rather than by collapse of the

*This problem is considered in more detail in Chapter, Section 4.

metal shell. Shock waves with velocities of approximately 16 km/s can be produced in gases with initial pressure of 760 mm Hg by using these charges.

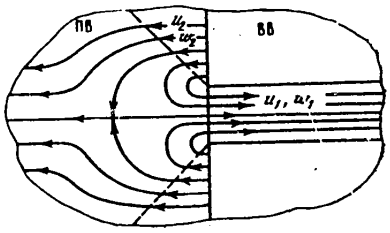

Figure 8. Flow Pattern During Detonation of Shaped Charge. PV--explosion products

Let us consider the gas dynamic flow pattern and let us estimate the velocities of the jet and the shock wave. The flow pattern in the coordinate system where the detonation front is quiescent (Figure 8) is steady. It is assumed that the external dimensions of the charge are rather high and can be disregarded.

For steady flow along the streamlines, the Bernoulli integral is retained

$$w + \frac{u^2}{2} = \text{const}. \tag{2.1}$$

On streamlines beginning with the detonation front,

$$w_1 + \frac{u_1^2}{2} = w_2 + \frac{u_2^2}{2}, \tag{2.2}$$

where w_2 and u_2 are the enthalpy and velocity of products behind the detonation front and w_1 and u_1 are the same values in the jet. Equality (2.2) is also fulfilled on a special streamline passing along the axis of symmetry with unlimited external dimensions. The equation of state of the explosion products $p = A\rho^n$, together with relations on the detonation burst, yields

$$u_2' = u_2 + V = V/(n+1), \tag{2.3}$$

$$w_2 = \frac{n}{n-1} p_2/\rho_2, \tag{2.4}$$

$$p_2 = \rho_{BB} V^2/(n+1), \tag{2.5}$$

$$\rho_2 = \frac{n+1}{n} \rho_{BB}, \tag{2.6}$$

where u_2' is the velocity of the products behind the burst in a fixed coordinate system, V is the rate of detonation of the explosive and ρ_{VV} is its density. During flow into a vacuum $w_1 = 0$; during flow into a gas

$$w_1 = \frac{n}{n-1} p_1/\rho_1 = \frac{n}{n-1}\left(\frac{p_2}{p_1}\right)^{1/n} \frac{p_1}{\rho_2}, \quad (2.7)$$

and pressure p_1 is found from relations on the contact burst between the jet of the explosion products and the gas shock-compressed by it. If U is the flow velocity in a fixed coordinate system (it is the velocity of the piston creating the strong shock wave), then

$$p_1 = p_{\text{уд.в}} = \frac{\gamma+1}{2}\rho_0 U^2, \quad (2.8)$$

where γ is the effective index of the adiabatic curve of a shock-heated gas and ρ_0 is the initial gas density. After the derived expressions are substituted into equality (2.2), the following equation is found for dimensionless flow velocity $x = U/V$:

$$\frac{n^2}{n^2-1} = (x-1)^2 + \frac{n^2}{n^2-1}\left(\frac{2}{\gamma+1}\right)^{1/n} [(\gamma+1)\rho_0/\rho_{\text{вв}}]^{\frac{n-1}{n}} x^{\frac{2n-2}{n}}. \quad (2.9)$$

One can note immediately that the flow velocity is linearly related to the rate of detonation V. During flow into a strongly rarefied gas $\rho_0 \to 0$ and

$$U = \left(1 + \frac{n}{\sqrt{n^2-1}}\right) V; \quad (2.10)$$

if one assumes that n = 3, then U = 2.06 V. Let us compare (2.10) to the known expression for the velocity of products after the detonation wave has been discharged into a vacuum:

$$U_p = \frac{3n-1}{n^2-1} V; \quad (2.11)$$

if n = 3, then U_p = V. Higher scattering rates $U_p \approx 1.5$ V have been observed experimentally. The divergence is caused by the fact that the explosion products are easily described by a power equation of state with index n = 3 at densities of $\rho \sim \rho_{VV}$, whereas the index decreases to n = 1.3-1.4 upon expansion into a gas at $\rho_0 \ll \rho_{VV}$ [138]. The process of product expansion can be fully described by introducing the effective value of n = 2. Thus, we find U_p = 1.67 V for this value of n, which is close to the experimentally observed velocities. It is obvious that the value n = 2 will better describe the expansion of products upon detonation of a shaped charge. The flow velocity is U = 2.15 V for n = 2 and $\rho_0 \to 0$. Thus, the uncertainty in selection of the value of n hardly affects the flow rate in the channel.

Let us present the results of calculating the flow rate U and the shock wave D found after substitution of ρ_{VV} = 1.69 g/cm^3 and V = 7.8 km/s (TG 40/60), normal gas density ρ_0 and index γ of an ionized gas into equation (2.9) (see Appendix).

		Air	Ar	Xe	$\rho_0 \to 0$
U, km/s	n = 2	16.4	16.4	16.1	16.8
	n = 3	15.9	15.9	15.7	16.1
D, km/s	n = 2	18.3	18.4	18.5	—
	n = 3	17.7	17.8	18.0	—

Let us emphasize again that, as follows from these data, the problem of the value of index n plays no significant role. On the other hand, the flow velocity is weakly dependent on gas density and is almost equal to the flow velocity to a vacuum.

The considered problem (Figure 9) has one typical dimension--the diameter* of the shaped channel d. The solution obviously correctly describes detonation of a charge of limited dimensions if the length of the charge channel $l \gg d$ and outer diameter $\varnothing \gg d$. It is also obvious that it is sufficient to require that $l \gg d$ for the existence of steady flow. However, the Bernoulli integral on a special streamline passing along the axis of symmetry is not expressed in this case by the same relations on a detonation burst. It is qualitatively clear that the discharge from the size reduces the flow velocity at $\varnothing \sim d$ and the flow velocity will asymptotically approach the values calculated above at $\varnothing/d \to \infty$.

More than 100 experiments were conducted in which the effect of charge configuration and of different explosives on the flow velocity and the shock wave in a gas was studied.

After initiation the detonation wave emerges to the bottom of the charge channel (see Figure 9) and excites the shock wave in the gas. An advancing detonation front of the jet is formed as a result of subsequent collapse of products in the channel (Figures 10 and 11). The flow velocity increases and accordingly the shock wave velocity increases. Covering a path of approximately 8-10 diameters of the channel d, the shock wave gains maximum velocity and maintains it during subsequent motion in the channel. A photochronogram of a shock wave and jet in a glass tube attached to the charge is shown in Figure 11 (a truncated charge with $l = 5d$ was used in the experiment, which made it possible to observe the acceleration of the jet and the shock wave to maximum velocity in the tube). The value of the maximum velocity depends on the ratio of diameters $\varnothing/d$. The shock wave velocity increases with an increase of ratio.

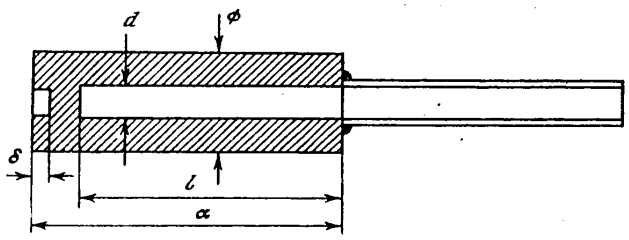

Figure 9. Shaped Charge: l--length of charge; δ--depression for detonator

The adherence to geometric similarity in motion of the shock wave was checked in experiments with charges whose channel diameter d varied from 3 to 18 mm. It

*Axial symmetry is not used in solving the problem. It is easy to show that the results are valid for the case of plane symmetry and generally for a channel with arbitrary cylindrical surface.

turned out that similarity is disturbed with thin channel walls (Ø - d ≤ 10 mm for TG 40/60). The velocity of the shock waves decreased in these cases. Deviation from similarity can be explained by the proximity of the wall thickness to the critical diameter of explosive detonation. Experiments with charges of cast trotyl for which deviation from similarity was checked more intensively, indicate this. Figure 12 reflects the noted characteristics where the dependence of steady shock wave velocity in air on the ratio of diameters Ø/d of a charge of TG 40/60 are plotted from experimental results.

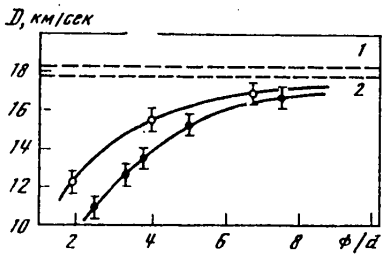

Figure 12. Dependence of Shock Wave Velocity on Ratio of Diameters Ø/d: dark circles--d = 8 mm; light circles--d = 15 mm; 1 and 2--calculated values of velocity at Ø/d → ∞ for n = 2 and n = 3, respectively

The velocities of shock waves and the detonation rates of charges of different cast explosives were also measured in the experiments. Both velocity and the rate of detonation was measured in a separate experiment, for which the charge and glass tube attached to it were placed in the visual field of the photochronograph. The results of the measurements are presented in Figure 13.

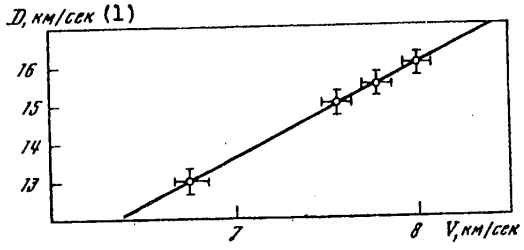

Figure 13. Dependence of Shock Wave Velocity in Air on Rate of Charge Detonation

Key:
1. km/s

The effect of initial gas pressure (or rather of density) on the shock wave velocity in the channel can be judged from the following values measured in experiments with argon (charge dimensions were d = 25 mm, l = 180 mm and Ø/d = 2.4):

p_0, mm Hg	760	300	200	100	50
D, km/s	11.0	12.2	12.8	13.3	14.5

Formation of the jet surpassing the detonation front was observed in several experiments with charges having the plane of symmetry (two parallel explosive plates).

Comparing the results outlined in this section, one can state that there is good agreement of approximate theory with experiment. Analysis of flow and an estimate of flow and shock wave velocity do not take friction into account. It is obvious that lengthening of the jet and column of a shock-heated gas leads in the final analysis to intensive slowing of them in the channel as the charge detonates. Contact with jet products and the shock-heated gas may cause breakdown or detonation of the explosive. In some experiments the length of the channel reached 30 d (40 d with attached tube), but a reduction of shock wave and flow velocity was not observed. Friction and interaction with the explosive in the channel still apparently play no significant role at $l/d \leq 30$ (according to [139], these effects are manifested at $l/d \geq 100$).

Using a lens with delay of the detonation front near the axis to initiate a shaped charge, shock waves with velocities up to 20 km/s were produced in air and argon. Velocity was increased from 15 to 19 km/s when conical constricting nozzles were installed at the channel output.

Shaped charges are used extensively in this paper during investigation of the radiating properties of strong shock waves. The stability of shock wave amplitude in experiments with these charges gave the authors the idea of using it as the radiator in a high-temperature explosive brightness standard.

3. Producing Strong Shock Waves by Compressing Gas Under Conditions of Acute-Angled Geometry

A. Ye. Voytenko [38-40] developed this method of producing shock waves. The capabilities of the method characterize shock wave velocities of 43 km/s in air and 37 km/s in xenon measured in [41] (the initial gas pressure was atmospheric). Velocity comprised 90 km/s in [38] during flow of shock-compressed hydrogen into air rarefied to 10^{-1} to 10^{-2} mm Hg; a plasma with temperature of approximately 200,000°K can be produced during shock deceleration of a hydrogen jet.

This method is used in the present paper with several nonessential changes during investigation of the radiating properties of strong shock waves ($D > 20$ km/s). The shock wave velocity reached 80 km/s and the temperature behind the front was $T = 120{,}000$°K in experiments with helium of normal density. A plasma with temperature of 300,000°K and particle density of $1.7 \cdot 10^{21}$ cm^{-3}, higher than in [38], can be produced in the reflected wave. Further improvement of the method that permits production of as high-temperature dense plasma as desired under laboratory conditions is of undoubted interest for the problem of thermonuclear fusion.

A device to produce strong shock waves is shown in Figure 14. The lens 1 initiates a plane detonation wave in charge 2 of hexogen pressed to density of

1.74 g/cm^3. Plate 3 accelerated by the explosion products squeezes the gas in chamber 4. The mass velocity of the gas is close to the phase velocity of the point where the plate joins the chamber and exceeds several times the flight velocity of the plate. The heated compressed gas is expelled into the tube 5 and generates a strong shock wave.

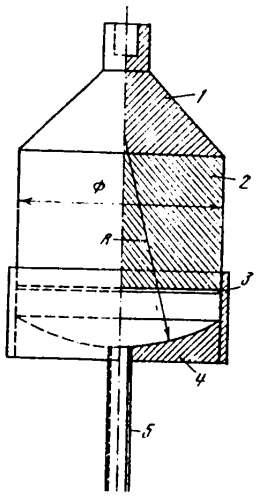

Figure 14. Device to Produce Strong Shock Waves in Gases: 1--lens; 2--charge 84 mm in diameter and weighing 500 grams; 3--duralium plate 1 mm thick; 4--duralium chamber with radius of curvature of R = 84 mm (δ = 10 mm); 5--glass tube 10 mm in diameter and 200 mm long.

According to [38-40], an increase of the radius of curvature R of chamber 4 increases the shock wave velocity, but the shock wave velocity decreases at R > Ø (presumably due to friction and heat dissipation). In our experiments chamber 4 had optimum radius of R = Ø in this regard. To reduce friction and radiant heat dissipation, chamber 4 and plate 3 were polished to a mirror finish. In [41], chamber 4 was filled with hydrogen and was separated by a thin diaphragm from tube 5 containing the gas to be investigated. In our experiments with the chamber filled with helium, no appreciable increase of shock wave amplitude in the gas under investigation was observed; therefore, in most cases both the chamber and tube were filled with the gas to be investigated (a diaphragm was not installed). Plate 3 was glued to the charge 2, by which the air inclusions between the plate and charge were removed, which could lead to ruptures of the plate during explosion. Because of this it was possible to use thinner plates than in [41], without the danger of their breakdown. A linear dependence of shock wave velocity on plate velocity was observed in [40]. The use of a more powerful explosive and thinner plates in our experiments than in [38-41] and also the closer contact between the charge and plate favored acceleration of the plate to high velocities. The plate velocity was measured and was equal to 6 km/s in one of the experiments.

4. Other Methods of Producing Strong Shock Waves

The methods suggested below were tested in the search for more effective methods of producing strong shock waves. Although these methods were not used in investigation of the radiating properties of shock waves, the results are of definite interest.

If a detonating rod is placed in a channel (Figure 15), a piston moving at the rate of detonation is formed under certain conditions of scattering products by closing the channel walls. Obviously, $p_2 \geq p_1$, where p_2 is the pressure in the expanding products and p_1 is the gas pressure in the shock wave, is required. Expressing pressure p_1 by piston velocity V and assuming that n = 3 in the power equation of state of products with one-half decrease of density behind the detonation explosion and n = 1.3 with a further decrease of density [138], the condition $p_2 \geq p_1$ can be reduced to the following:

$$0{,}05_{\text{ВВ}}\,(S_0/S)^{1.3} \geqslant \frac{\gamma+1}{2}\rho_0, \tag{2.12}$$

where S_0 and S are the cross-sectional areas of the rod and channel. We find $S/S_0 \leq 18$ for $\rho_0 = 1.3\cdot10^{-3}$ g/cm^3, $\gamma = 1.2$ (air), V = 7.8 km/s and $\rho_{VV} = 1.69$ g/cm^3 (TG 40/60).

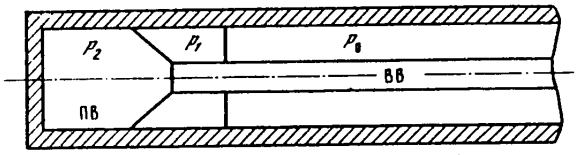

Figure 15. Production of Shock Wave Upon Detonation of a Rod in a Channel

In the experiments a TG 40/60 rod 300 mm long was placed in a steel tube 50 mm in diameter and with wall thickness of 5 mm. Filling the cross section of the tube with shock-heated air and argon was observed at $S/S_0 \leq 16$, which is in good agreement with the given estimate. This filling was not observed at $S/S_0 > 16$--the shock-heated gas slipped between the tube walls and explosion products.

The problem of detonation of a rod in a channel has much in common with that of detonation of a shaped charge. Specifically, one can show that the explosion products will overtake the detonation front at $p_2 > p_1$ and their velocity will approach the calculated values in Section 2 at $S/S_0 \to 1$. In experiments with $S/S_0 = 4$, the shock wave velocity in air comprised 9.5 km/s. Mass gas velocity of 8.6 km/s in the wave, which exceeds the rate of detonation of TG 40/60, corresponds to it. This excess may be an indirect confirmation of the formation of a jet overtaking the detonation front. However, the possibility of an increase of the rate of detonation of the explosive cannot be excluded. A similar explanation is suggested in several papers on investigation of the "channel effect"--the effect of a shock-heated gas on an explosive in similar experiments [140].

Experiments were conducted to intensify shock waves during motion in a constricted conical channel (Figure 16). The channel, cut in a strong steel ingot, usually did not break down under the effects of the explosion. A shock wave with concave, approximately spherical front was created by a charge of cast TG 50/50 weighing 500 grams with delay of the detonation wave in the center. The effect of angle β at the vertex of the cone on amplification was studied (see Figure 16, a). It is clear that the wave will be attenuated at small value of β rather than amplified (as occurs in a tube with parallel walls). Shock wave velocity in the attached tube comprised D = 9 km/s in experiments with argon and air at β = 22° and D = = 12 km/s at β = 26 and β = 30°. To evaluate the capabilities of the method, a transparent plexiglass cone was attached to a steel truncated cone (see Figure 16, b). In experiments with air, the shock wave was decelerated sharply (to D = = 5 km/s) without travelling 0.4 cm to the vertex of the cone and having velocity of D = 26 km/s. The wave was decelerated over a distance of approximately 5 cm from the vertex in argon, having velocity of D = 12 km/s.

From the gas-dynamics viewpoint, the motion in the cone is equivalent to a converging spherical shock wave. The problem of convergence of the shock wave to the center has an automodel solution $R \sim |t|^{\alpha}$, where R is the radius of curvature of the front, α = 0.715 for the index of the adiabatic curve γ = 1.4 and $\alpha \to 1$ at $\gamma \to 1$ [15]. Analysis of photochronograms of a shock wave in a cone with air showed that motion is close to automodel at R < 6 cm and up to deceleration (R = = 0.4 cm) with automodel index $\alpha = 0.75 \pm 0.05$.

An explanation for premature deceleration of the shock wave in experiments (not at the vertex of the cone) should apparently be sought in the instability of the converging spherical shock wave. This instability could be manifested due to the asphericity of the shock wave created by an explosive charge or due to subsequent distortion of the shape of the wave front when it interacts with the channel wall. The latter is the most probable since the shock waves were created by identical explosive charges both in argon and in air. At the same time curvature of the front caused by heating of the channel walls and by radiation of the shock wave adjacent to them could be observed directly in experiments with argon. We shall dwell on these experiments somewhat later (Chapter 4, Section 4). We note here that addition of a slight air impurity to the argon, which intensively absorbs the ultraviolet radiation of the shock wave, led to the fact that the wave was decelerated later than in pure argon 2-3 cm from the vertex of the cone at D = 14-15 km/s.

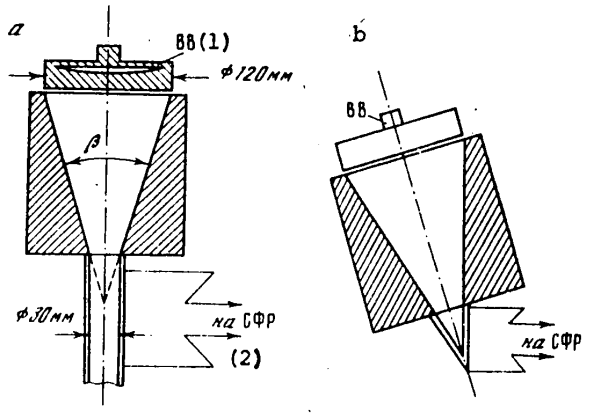

Figure 16. Amplification of Shock Wave in Cone. SFR--high speed photorecorder

METHOD FOR MEASURING THE INTENSITY TEMPERATURE AND OTHER VALUES

Moscow IZLUCHATEL'NYYE SVOYSTVA UDARNYKH VOLN V GAZAKH in Russian 1977 pp 37-61

[Chapter 3 from the book "Radiating Properties of Shock Waves in Gases", by M. A. Tsikulin and Ye. G. Popov, Izdatel'stvo "Nauka", 173 pages]

[Text] The parameters that characterize the radiating properties of strong shock waves in gases and namely the radiant flux density in various regions of the spectrum and accordingly the brightness temperature in these regions were measured with time resolution using modern optical and electronic equipment to record high-speed phenomena. The photographic method was used in the visible and near ultraviolet regions and the photoelectric method, which also duplicated measurements in the visible regions, was used in the infrared region.

1. Basic Concepts of the Radiation Theory

The radiating properties of strong shock waves in gases, like other self-luminous objects, are analyzed by comparison to the radiation of an absolutely black body. Since the radiation intensity of a black body is dependent only on temperature, it is possible to characterize the brightness of radiators by the corresponding temperature of an absolutely black body or brightness temperature.

Let us present in more detail, following [37], the main concepts of the physical theory of radiation.

The following three main values are introduced by means of the photon distribution function by frequencies ν in space r and by the directions of propagation of radiant energy near the solid angle vector Ω.

The spectral intensity of radiation I_ν is the amount of radiant energy in the spectral range $d\nu$ passing within one second through an area of 1 cm^2 placed at point r perpendicular to the direction of propagation lying in the element of solid angle $d\Omega$ near vector Ω:

$$I_\nu = h\nu cf(\nu, r, \Omega), \tag{3.1}$$

where $h\nu$ is the photon energy and c is the speed of propagation. The dimensionality of this value is erg/cm^2·steradian. After integration by frequencies, we find the radiant flux density per unit of solid angle--erg/cm^2·s·steradian.

The spectral radiation density U_ν is the amount of radiant energy in spectral range $d\nu$ in 1 cm^3 of space:

$$U_\nu = \frac{h\nu}{c} \int_{(4\pi)} f d\Omega = \frac{1}{c} \int_{(4\pi)} I_\nu d\Omega. \tag{3.2}$$

The dimensionality is erg·s/cm^3. After integration with respect to frequencies, we find the energy density--erg/cm^3.

The spectral flux S_ν is the amount of radiant energy in spectral range $d\nu$ passing within 1 second through an area of 1 cm^2 in all directions:

$$S_\nu = h\nu c \int_{(4\pi)} f \cos\theta \, d\Omega = \int_{(4\pi)} I_\nu \cos\theta \, d\Omega. \tag{3.3}$$

The dimensionality is erg/cm^2. After integration with respect to frequencies, we find the energy flux density--erg/cm^2·s.

With isotropic distribution of radiation when f and I_ν are not dependent on direction Ω, the radiation density is equal to

$$U_\nu = 4\pi h\nu f = \frac{4\pi}{c} I_\nu, \tag{3.4}$$

and there is no flux: $S_\nu = 0$ since an identical number of photons is transported in both directions.

For a medium in a state of thermodynamic equilibrium at constant temperature T, the radiation field is also equilibrium, i.e., the number of photons emitted by matter during 1 second in 1 cm^3 in a given frequency range $d\nu$ and in a given direction Ω is exactly equal to the number of absorbed photons. The field of equilibrium radiation is isotropic, i.e., it is not dependent on the direction and on the specific properties of the medium, being a universal function of temperature and frequency.

The function of the spectral equilibrium radiation density $U_{\nu p}$ introduced by Planck, has the form

$$U_{\nu p} = \frac{8\pi h\nu^3}{c^3} \frac{1}{e^{h\nu/kT} - 1}; \tag{3.5}$$

hence

$$I_{\nu p} = \frac{2h\nu^3}{c^2} \frac{1}{e^{h\nu/kT} - 1}. \tag{3.6}$$

These formulas k = $1.38 \cdot 10^{-16}$ erg/deg is a Boltzman constant and c is the speed of light.

We find the value of unidirectional flux, i.e., the amount of radiant energy passing in one direction through a unit area by integrating $I_{\nu p}$ with respect to a hemisphere:

$$S_{\nu p} = \int\limits_{(2\pi)} I_{\nu p} \cos\theta \, d\Omega. \tag{3.7}$$

Substituting $I_{\nu p}$ here and bearing in mind that

$$d\Omega = \frac{R^2 \sin\theta \, d\theta \, d\varphi}{R^2} = \sin\theta \, d\theta \, d\varphi, \tag{3.8}$$

we find

$$S_{\nu p} = 2\pi \int\limits_0^{\pi} I_{\nu p} \cos\theta \sin\theta \, d\theta = \pi I_{\nu p}, \tag{3.9}$$

$$S_{\nu p} = \frac{2\pi h \nu^3}{c^2} \frac{1}{e^{h\nu/kT} - 1}. \tag{3.10}$$

The integral unidirectional flux with respect to the spectrum is

$$S_p = \int\limits_0^{\infty} S_{\nu p} \, d\nu = \sigma T^4, \tag{3.11}$$

where $\sigma = \frac{2\pi^5 k^4}{15 h^3 c^2} = 5{,}67 \cdot 10^{-5}$ эрг/см^2·сек·град^4 is a Stefan-Boltzman constant.

There is a very general confirmation for the ration of the absorbing and radiating capability of bodies. Assume that a cavity filled with equilibrium radiation is identified in an arbitrary body with constant temperature T, sufficiently long so that radiation does not penetrate it fully but was absorbed. A radiation flux $S_{\nu p}$, part of which is reflected and part of which is absorbed by the body, impinges on the surface of the body from the cavity. Let the reflectivity of the body be R_ν and let the absorptivity be $A_\nu = 1 - R_\nu$. The amount of radiation absorbed in the body is $S_{\nu r} \cdot A_\nu$. Due to equilibrium, the same amount of energy is radiated by the body into the cavity $J_\nu = S_{\nu p} \cdot A_\nu$. The values of A_ν, R_ν and J_ν are the characteristics of the body, but the ratio J_ν / A_ν, i.e., the ratio of the radiating capacity of the body to its absorptivity is not dependent on the property of the body and is a universal function of frequency and temperature:

$$J_\nu / A_\nu = S_{\nu p}. \tag{3.12}$$

This statement is called Kirchhoff's law.

A body which fully absorbs the radiation impinging on it, i.e., for which $A_\nu = 1$, $R_\nu = 0$ and $J_\nu = S_{\nu p}$, is called an absolutely black body.

Let us consider a sufficiently long body with constant temperature T and with refractive index equal to unity in which radiation is in equilibrium with the matter and let us mentally cut it into two parts and let us take away one part. The unidirectional radiation flux through a plane from the direction of the body is then $S_{\nu p}$. Thus, a plane space filled with matter with constant temperature T radiates from the surface like an absolutely black body with temperature T.

Let us calculate the luminous flux Φ per unit area $d\sigma$ with radiating area $d\Sigma$ located at distance R (Figure 17):

$$d\Phi = I \frac{\cos\theta_1 \cdot \cos\theta_2}{R^2} d\Sigma, \tag{3.13}$$

where I is the equilibrium radiation intensity from the surface of the radiating body. Expressing $d\Sigma$ by R and angles θ_1 and θ_2, one can in each specific case calculate Φ at a given point of space. For example, if area Σ is the circular layer in a disk, one can easily calculate the radiation flux Φ on the axis through area σ parallel to the disk. From Figure 18, $\theta_1 = \theta_2$ and θ and

$$d\Sigma = 2\pi R^2 \operatorname{tg}\theta\, d\theta, \tag{3.14}$$

Hence,

$$\Phi = 2\pi I \int_0^{\theta_0} \sin\theta \cos\theta\, d\theta = \pi I \sin^2\theta_0 \tag{3.15}$$

or

$$\Phi = S_{\nu p} \sin^2\theta_0. \tag{3.16}$$

In similar fashion, we have for a radiating sphere (Figure 19)

$$d\Sigma = 2\pi R \sin\theta_2 \frac{R d\theta_1}{\cos\theta_1}, \tag{3.17}$$

$$\Phi = 2\pi I \int_0^{\theta_0} \sin\theta_2 \cos\theta_2\, d\theta_2 = \pi I \sin^2\theta_0, \tag{3.18}$$

$$\Phi = S_{\nu p} \sin^2\theta_0. \tag{3.19}$$

Measuring Φ and then determining the value of $S_{\nu p}$ from geometric concepts, we can clearly determine the temperature of the radiating body.

These measurements are usually made with out making absolute measurements of radiation flux, but by comparing it to the flux from a standard source. We shall return later to this problem.

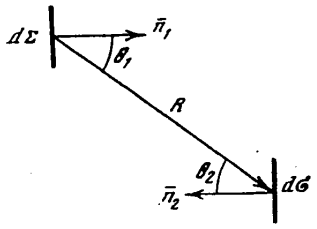

Figure 17. Calculation of Radiation Flux Density

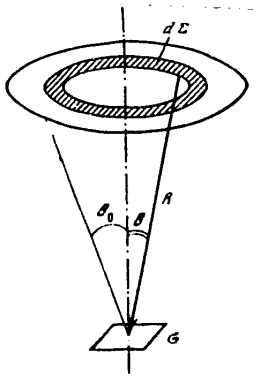

Figure 18. Calculation of the Flux Density From a Disk-Radiator

Thus, the flux is determined at some distance for flat disk and spherical radiators by the square of the sine of half of the angle at which this light source is visible since specific differences of shape of the light source are unimportant. Therefore, both the sphere and generally any source of circular radiation are visible as a flat disk to us. This property is the consequence of Lambert's law or the law of cosines which says that the radiation flux through a surface is proportional to the cosine of the angle between the direction of propagation of the radiation and the normal to the surface.

The condition of "blackness" of a given body is total absorption of the radiation impinging on it, for which the dimensions of the body should exceed many-fold the length of radiation travel, i.e., the optical thickness of the body should be great.

Let us consider the equation of radiation transfer in a medium.

An amount of radiation $I_\nu d\sigma dt$ flows in an elementary cylinder (Figure 20) with area of the base $d\sigma$ and height ds whose axis coincides with the direction of the luminous flux during time dt to the base located at a point with coordinate s while $(I_\nu + dI_\nu)d\sigma dt$ flows from the base located at a point with coordinate s + ds. The increment of beam intensity consists of the local increment during the passage of path ds by the light and of the increment upon transition from coordinate s to coordinate s + ds at a given moment of time:

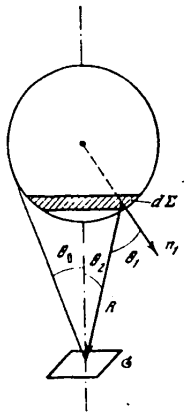

Figure 19. Calculation of Flux Density from a Spherical Radiator

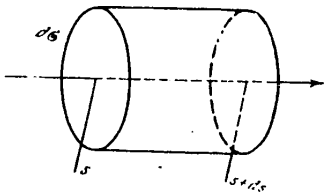

Figure 20. Deriving the Equation of Radiation Transfer

$$dI_\nu = \frac{\partial I_\nu}{\partial t}\frac{ds}{c} + \frac{\partial I_\nu}{\partial s}ds. \tag{3.20}$$

Beam intensity varies due to emission and absorption of light in the given elementary cylinder. The amount of radiation emitted in the cylinder during time dt_ν is equal to

$$j_\nu\left(1 + \frac{c^2}{2h\nu^3}I_\nu\right)d\sigma dt, \tag{3.21}$$

where j_ν is the emissive capacity of matter. The second term in parentheses takes into account the so-called stimulated or induced emission (the probability of stimulated emission of a photon of given frequency and given direction is proportional to the radiation intensity of the same frequency and the same direction existing at a given point of space). An amount of radiation $\varkappa_\nu I_\nu d\sigma dtds$, where $\varkappa_\nu$ is the absorption coefficient, is absorbed in the cylinder during the same time. Compiling the balance and dividing the derived expression by the product of differentials $d\sigma dtds$, we find the equation

$$\frac{1}{c}\frac{\partial I_\nu}{\partial t} + \frac{\partial I_\nu}{\partial s} = j_\nu\left(1 + \frac{c^2}{2h\nu^3}I_\nu\right) - \varkappa_\nu I_\nu. \tag{3.22}$$

The ratio of the emissive and absorption capability of the body, according to Kirchhoff's law, is a universal function of frequency and temperature in a state of equilibrium

$$\frac{j_\nu}{\varkappa_\nu} = \frac{I_{\nu p}}{1 + \frac{c^2}{2h\nu^3} I_{\nu p}}, \tag{3.23}$$

where radiation intensity I_ν is substituted for the equilibrium value $I_{\nu p}$ (3.6), hence

$$j_\nu = \varkappa_\nu I_{\nu p} (1 - e^{-h\nu/kT}). \tag{3.24}$$

Let us remove the parentheses in the right side of equation (3.22) and let us replace j_ν in the second term for the derived expression into which we substitute the expression for $I_{\nu p}$. The right side of equation (3.22) then assumes the form

$$j_\nu - \varkappa_\nu (1 - e^{-h\nu/kT}) I_\nu. \tag{3.25}$$

Hence, it is obvious that stimulated emission can be interpreted as a decrease of absorption: part of the photons seems to be absorbed and emitted again at the same point with the same frequency and in the same direction. These acts of "reradiation" can formally be disregarded if one assumes that the absorption coefficient has a somewhat smaller value:

$$\varkappa'_\nu = \varkappa_\nu (1 - e^{-h\nu/kT}). \tag{3.26}$$

In this interpretation Kirchhoff's law acquires the following form:

$$j_\nu = \varkappa'_\nu I_{\nu p}, \tag{3.27}$$

and then the transfer equation is written in the following form:

$$\frac{1}{c}\frac{\partial I_\nu}{\partial t} + \frac{\partial I_\nu}{\partial s} = \varkappa'_\nu (I_{\nu p} - I_\nu). \tag{3.28}$$

Noting that the differential expression in the left side is a final product of intensity along the path of propagation, we rewrite the equation in the form

$$\frac{dI_\nu}{ds} + \varkappa'_\nu I_\nu = \varkappa'_\nu I_{\nu p}. \tag{3.29}$$

Equation (3.29) has the solution

$$I_\nu = \int_{s_0}^{s} I_{\nu p} \exp\left[-\int_{s'}^{s} \varkappa'_\nu \, ds''\right] \varkappa'_\nu \, ds' + \text{const}. \tag{3.30}$$

Let us consider examples. Let a body with constant temperature T occupy an infinite half-space s > 0 and is limited by a plane surface. The intensity near the surface is then equal to

$$I_\nu = \int_0^\infty I_{\nu p} e^{-\tau_\nu}\, d\tau_\nu = I_{\nu p}, \tag{3.31}$$

i.e., it is equal to the radiation intensity of an absolutely black body with temperature T (in this formula $\tau_\nu = \int_0^s \varkappa'_\nu\, ds$ is optical thickness).

Let us consider the radiation of a plane layer of finite thickness Δ. For radiation intensity we have

$$I_\nu(\theta) = \int_0^{\Delta/\cos\theta} I_{\nu p} e^{-\tau_\nu/\cos\theta} \frac{d\tau_\nu}{\cos\theta} = I_{\nu p}(1 - e^{-\tau_\nu/\cos\theta}); \tag{3.32}$$

here τ_ν is the optical thickness in a direction perpendicular to the surface. For an optically thin layer $\tau_\nu << 1$ we find

$$I_\nu = I_{\nu p}\tau_\nu/\cos\theta \tag{3.33}$$

--the brightness of this radiating body increases with deviation of the observation angle from the normal.

Thus, an optically thin layer radiates differently at different angles, i.e., not according to Lambert's law. One of the methods of experimental checking of the "blackness" of a body is based on this effect: if the radiating body is of different brightness at different angles to the surface it does not radiate like a black body.

Not only the radiation intensity at a given angle to the surface is of interest, but the radiation flux from the surface of the body, i.e., the radiation flux emerging in all directions--the so-called spectral surface brightness, is also of interest.

For the radiation flux we have (see (3.7))

$$S_\nu = \int_{(2\pi)} I_\nu \cos\theta\, d\Omega. \tag{3.34}$$

Substituting the expressions for I_ν and $d\Omega$, we find

$$S_\nu = 2\pi \int_0^{\pi/2} \cos\theta \sin\theta\, d\theta \int_0^\infty I_{\nu p} e^{-\tau_\nu/\cos\theta} \frac{d\tau_\nu}{\cos\theta}, \tag{3.35}$$

or

$$S_\nu = 2\pi \int_0^\infty I_{\nu p}\, d\tau_\nu \int_0^1 e^{-\tau_\nu/\cos\theta}\, d(\cos\theta). \tag{3.36}$$

Having substituted $1/\cos\theta = w$, we have

$$\int_0^1 e^{-\tau_\nu/\cos\theta}\, d(\cos\theta) = \int_1^\infty e^{-\tau_\nu w}\, \frac{dw}{w^2} = E_2(\tau_\nu), \tag{3.37}$$

where $E_n(z) = \int_1^\infty e^{-zw}\, \frac{dw}{w^n}$ is the integral exponents. Instead of (3.36) we now find

$$S_\nu = 2 \int_0^{\tau_\nu} S_{\nu p} E_2(\tau_\nu)\, d\tau_\nu. \tag{3.38}$$

For a semi-infinite body $\int_0^\infty E_2(z)\, dz = 1/2$ и $S_\nu = S_{\nu p}$. For a layer of finite thickness τ_ν we have

$$S_\nu = 2S_{\nu_p} \int_0^{\tau_\nu} E_2(\tau_\nu)\, d\tau_\nu = S_{\nu_p}[1 - 2E_3(\tau_\nu)]. \tag{3.39}$$

The values of $1 - 2\, E_3(\tau_\nu)$ at given values of τ_ν are given in Table 2.

Table 2.

τ_ν	$1-2\,E_3(\tau_\nu)$	τ_ν	$1-2\,E_3(\tau_\nu)$	τ_ν	$1-2\,E_3(\tau_\nu)$
0	0	0,6	0.616	2,0	0,938
0,05	0,096	0,8	0,712	2,5	0,968
0,2	0,300	1,0	0,782	3,0	0,988
0,4	0,476	1,5	0,888		

The following effective parameters can be determined for a radiator different from an absolutely black body:

--the spectral brightness temperature for a given wavelength, setting the given spectral flux S_ν equal to the corresonding value for an absolutely black body:

$$S_\nu = S_{\nu p}(T_R); \tag{3.40}$$

--the integral brightness temperature for a complete flux from a given radiator S, setting this value equal to the complete flux from a "black" radiator:

$$S = \sigma T_{\text{в}}^4. \tag{3.41}$$

The integral brightness temperature averages all the specific characteristics of the radiator. Therefore, it is more convenient in most cases to use the spectral brightness temperature. We shall subsequently use only this concept and will omit the word "spectral" and the subscript .

The brightness temperature for an optically thick body is usually dependent on frequency. This is related to the fact that the layer radiating from the outside near this body is one with thickness 2-3 lengths of radiation travel. But the edge of the body is not heated uniformly and the temperature decreases toward the surface due to radiation losses. Due to the dependence of the absorption coefficient on frequency, the travel distances of different photons are different since different photons emerge to the outside from different depth where the temperatures are different.

For example, the total absorption coefficient for water-hydrogen-like atoms, which includes free-bound and inhibited absorption by electrons in the atom, is given by the Unsold-Kramers formula for small photons less than ionization potential $h\nu << I$

$$\varkappa_\nu = \frac{16\pi^2}{3\sqrt{3}} \frac{e^6 Z^2 kTN}{h^4 c\nu^3} e^{-\frac{I-h\nu}{kT}} = 0{,}96 \cdot 10^{-7} \frac{NZ^2}{I^2} \frac{e^{-(x_1-x)}}{x^3} c\text{м}^{-1}, \tag{3.42}$$

where Z is the nuclear charge, N is particle concentration and $x = h\nu/kT$ and $x_1 = I/kT$.

We then find the radiation paths $l_3 > l_2 > l_1$ and according to this $T_3 > T_2 > T_1$ near the edge of a radiating body where temperature decreases toward the surface for frequencies $\nu_3 > \nu_2 > \nu_1$, i.e., "blue" photons are hotter than "red" photons. If one is given the flux distribution in the frequency function (S_ν) for an absolutely black body at a specific integral brightness temperature, the observed flux distribution by frequencies is shifted toward the blue direction.

We considered the condition of the "blackness" of the body and established that the optical thickness of the body should be great for this. The absorption coefficient of matter is equal to the absorption cross section per particle multiplied by particle concentration. The absorption coefficient corresponding to resonance absorption in the spectral lines whose absorption cross section is very high emerges to the forefront with low particle concentration.

In classical theory the model of a radiating atom is an elastically bound electron which oscillates near a position of equilibrium--a harmonic oscillator. Since the oscillating electron moves in accelerated fashion, it emits light.

If the energy losses during the period are low, the rate of radiation is calculated by the formula

$$C = \frac{2}{3} \frac{e^2}{c^3} w^2, \tag{3.43}$$

where w is acceleration. Since for an oscillator $w = 4\pi^2\nu_0^2 r$, then from (3.43) we find the equation of energy loss

$$\frac{dW}{dt} = -S = -\frac{32\pi^4 e^2}{3c^3}\nu_0^4 r^2 = -\frac{8\pi^2 e^2 \nu_0^2}{3mc^3}W, \tag{3.44}$$

where $W = 4\pi^2 m\nu^2 r^2$ is the oscillator energy. The value

$$\gamma = \frac{8\pi^2 e^2 \nu_0^2}{3mc^3} \tag{3.45}$$

is called the attenuation constant and is an inverse value of time during which the oscillator energy decreases by a factor of e.

Considering the problem of stimulated oscillation of an oscillator with attenuation in the light wave field and calculating the work of the field, i.e., its energy absorption, we find the effective absorption cross section of the oscillator

$$\sigma_\nu = \frac{e^2\gamma}{4\pi mc}\frac{1}{(\nu-\nu_0)^2 + \left(\frac{\gamma}{4\pi}\right)^2}; \tag{3.46}$$

hence, the maximum absorption cross section in the center of a line with wavelength λ is:

$$\sigma_\nu = \frac{3}{2\pi}\lambda^2.$$

This is a very high value. For example, for λ = 650 nm at $N = 10^{18}$ cm^{-3}, the absorption coefficient comprises

$$\varkappa_\nu = \sigma_\nu N = 2\cdot 10^9 \ см^{-1} \tag{3.47}$$

and the radiation path is $l_\nu = 5\cdot 10^{-10}$ cm, whereas the radiation path comprises a value on the order of a meter for the braking mechanism or by the Unsold-Kramers formula with the same particle concentration and with low temperature of approximately 10^4°K.

Thus, conditions of the "blackness" of radiation are achieved primarily in the centers of spectral lines. And since the radiation of a body cannot be greater than that of an absolutely black body, the intensity of the spectral line when the condition of "blackness" is reached "pushes against" the curve for a black body at given temperature (Figure 21). A characteristic feature of the spectral line that reaches saturation is a flat section at the apex of intensity. The temperature--the same brightness temperature, but already determined by the spectral line, is also determined by the intensity of these saturated spectral lines.

If the intensity of the spectral line does not reach saturation, the matter becomes considerably more complicated. In quantum theory the spectral line intensity of

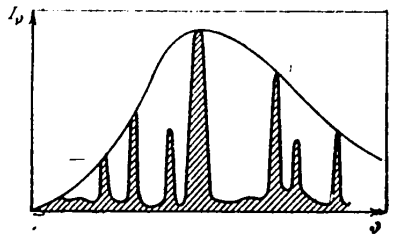

Figure 21. Radiation Spectrum of Body Opaque in Center of Some Lines

frequency $_{mn}$ of transition from state n to state m, i.e., the energy emitted in the line of 1 cm^3 within 1 second is equal to the product of the number of emitting atoms N_n by the value of the photon $h\nu_{mn}$ and by the probability of transition A_{mn}:

$$I_{mn} = N_n \cdot h\nu_{mn} \cdot A_{mn}. \tag{3.48}$$

The probability of transition A_{mn} is an internal property and is not dependent on external conditions with respect to the atom--on temperature, particle concentration and so on.

According to Kirchhoff's law or the principle of detailed equilibrium, one can establish the relationship between the probabilities of emission and absorption for a given transition. Making the analogy with classical concepts about the atom as a set of oscillators, the absorption or radiating capacity of the atom in a given line is usually characterized by the number of classical oscillators with natural frequency $_{mn}$ which would produce the same effect as the atom being considered. This number f is called the oscillator force--this is an average value calculated for one degree of freedom of the electron. The total force is three times higher according to the fact that the electron in the atom has three degrees of freedom. Everything is usually expressed through the absorption force f_{pogl}, bearing in mind the relation

$$f_{nm\ изл} = \frac{g_m}{g_n} f_{mn\ погл}, \tag{3.49}$$

where g is the statistical weight of state. The following determination occurs for the value f_{izl}: $3\ f_{nm.izl} = A_{nm}/\gamma$--the ratio of the probability of transition $n \to m$ to the classical attenuation constant γ. For a classical oscillator $A_{nm} = \gamma$ and $f_{nm} = 1/3$. We then have

$$I_{nm} = \frac{3\gamma g_m}{g_n} h\nu_{nm} f_{nm} N_n. \tag{3.50}$$

Bearing in mind that $N_n = \frac{g_n}{g_1} N_1 \exp\left(-\frac{E_n - E_1}{kT}\right)$, where subscript 1 denotes the ground state and substituting the value of γ into (3.50), we find

$$I_{nm} = \frac{8\pi^2 he^2 \nu_{nm}^3 g_m}{mc^3 g_1} f_{nm} N_1 \exp\left(-\frac{E_n - E_1}{kT}\right). \tag{3.51}$$

Knowing the constants for the given levels of the atom and measuring the intensities of the corresponding lines, one can determine the temperature and particle concentration of the radiating body. The values of oscillator forces which are unknown for far from all atoms cause the greatest difficulties. This value is difficult to calculate precisely and is usually determined experimentally.

In conclusion let us dwell on the units of measurement of light values. Clarity is necessary in this problem when discussing the different aspects of the radiating properties of shock waves in gases.

Since radiation is essentially a phenomenon of radiant energy transfer, it is natural that these values are measured in energy units. We shall also proceed in this manner when discussing the results.

Determination of the main values of radiation theory with the following dimensions was also presented above: spectral intensity I_ν--erg/cm^2·steradian, spectral density U_ν--erg·s/cm^3 and spectral flux S_ν--erg/cm^2.

The following determination of energy flux F in a beam of light with the spectral distribution β_λ occurs in illumination engineering:

$$F = K\int \beta_\lambda V_\lambda d_\lambda, \tag{3.52}$$

where β_λ is essentially spectral flux S_ν integrated by the source area, K is a coefficient and V_λ is the so-called visibility curve corresponding to the averaged spectral sensitivity of the human eye. The unit of value of F is the lumen.

Further, the ratio of the value of flux inside a small solid angle near a given direction of radiation has luminous intensity

$$I = \frac{dF}{d\Omega}. \tag{3.53}$$

If the source radiates uniformly in all directions, then $4\pi I = F$. The unit of luminous force is the candle--the luminous force of a source yielding a luminous flux of one lumen inside a solid angle equal to one steradian.

The illumination at a given point is the flux per unit area:

$$E = dF/dS; \tag{3.54}$$

and is calculated in units of lumens/m^2 (lux) or lumens/cm^2 (phots).

The luminosity of a light source is the ratio of the total luminous flux of the light source to its area:

$$R = dF/dS \tag{3.55}$$

with units similar to the units of illumination: radlux and radphot.

The brightness of a light source is the ratio of the luminous force in a direction perpendicular to its surface to the size of the surface:

$$B = \frac{1}{\cos\theta}\frac{dI}{dS}. \tag{3.56}$$

The unit of brightness is the stilb or candle/cm^2. The unit nit or candle/m^2 equal to 10^{-4} stilb is also used. It is obvious from determination of the brightness of a source B, luminous force I and luminous flux F that it is the brightness of the source B that is the analog of radiation intensity I_ν with the difference that brightness B is averaged by the light sensitivity of the human eye--the visibility curve. The visibility curve V_λ is given in Figure 22 in the form of the relative sensitivity of the eye averaged for many individuals with normal vision. The highest sensitivity, i.e., the highest color sensation, was detected for wavelength of 555 nm and is taken as the unit.

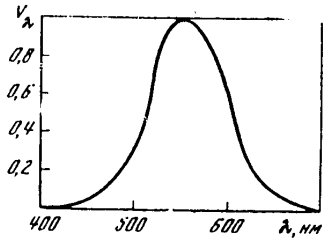

Figure 22. Visibility Curve

Introducing the visibility curve in relative form, one must absolutely determine the value of coefficient K in formula (3.52). The experimentally determined value of K, measured from comparison of luminous flux F and spectral distribution β_λ, was equal to 683 lumens/watt according to the latest measurements.

2. Measuring the Intensity Temperature by Photography

The main element in the photographic method of recording luminous radiation parameters is the light-sensitivity of the photoemulsion. After being developed, as a result of the effect of radiation(exposure), the photoemulsion reveals darkening which can be analyzed by its capability to retard radiation. The measure of opaqueness--the optical density or density of darkening Δ--is the common logarithm of the ratio of incident flux F_0 to the passing flux F_1 during translucence of the developed film:

$$\Delta = \lg\frac{F_0}{F_1}.$$

The dependence of darkening density Δ on the logarithm of radiant energy density (exposure) lgΦt, acting on the photoemulsion, is expressionby the characteristic curve (see Figure 23 in which the typical regions are noted). The normal work of the photoemulsion as a measuring element is accomplished on the condition that the darkening density does not go beyond the bounds of the linear section. One resorts

to different exposure times t to remain within the limits of this section upon comparison of objects differing strongly in brightness from each other (10-30-fold or more). In this case one relies on the so-called law of intersubstitution. The latter means that all things being equal, darkening density is dependent only on the product $H = \Phi t$ rather than on each value separately. However, if there is a large difference of exposure times, deviations from this law are observed. The dependence of the exposure logarithm lgH, which yields the same darkening density $\Delta = \text{const}$ (isoopacity), on absolute exposure time is given in the graph of Figure 24. It is typical that no deviations from the law of intersubstitution are noted in the range of 10^{-5} to 10^{-8} second [141, 142].

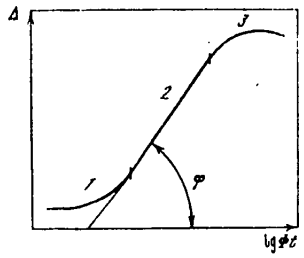

Figure 23. Characteristic Curve of Photoemulsion: 1--fog and zone of underexposures; 2--zone of linear exposures; 3--zone of overexposures and solarization; $tg\phi = \gamma$--contrast coefficient

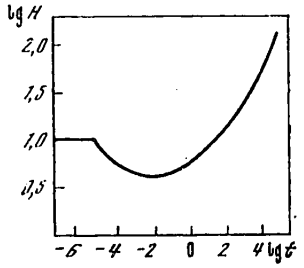

Figure 24. Isoopacity of High-Contrast Panchromatic Film (according to [141, 142])

The quality of photoemulsions has recently reached a high level in many respects. For example, the spectral sensitivity of photoemulsions extends from 120 nm in the far ultraviolet to 1,100-1,200 nm in the infrared region of the spectrum. The absolute sensitivity of some photoemulsions exceeds by tens and hundreds of times the sensitivity, for example, of ordinary aerial photographic film, which permits objects to be recorded with comparatively low brightness temperature (on the order of 10,000°K with exposure time of 10^{-7} to 10^{-8} second). The resolution of the photoemulsion reaches several hundred lines per millimeter, which still makes this measuring element incomparable to any other light sensitive element. Taking this into account, the photographic method must be noted as one of the most effective methods of investigating radiation processes.

I. Sh. Model' [29] used photographic photometry methods to study the brightness of shock waves; he had already described the details and advantages of this method. The brightness of a shock wave was recorded during its work by means of a two-lens slit photochronograph. The sun, whose brightness temperature was measured by a pyrometer at the moment of filming, was used as the comparison standard. The standard was photographed twice at different rotational frequency of the photochronograph mirror, which corresponded to different exposure times. The results of these filmings were used to construct a linear section of the characteristic curve of the photoemulsion. A shock wave, being a brighter object, was photographed at higher mirror rotational frequency than the standard. The law of intersubstitution was applied when plotting the characteristic curve and when determining the brightness temperature. The accuracy of measuring a temperature of 30,000-35,000°K is estimated at $\pm$ 15 percent.

This method was improved in [32, 41, 42]. An SFR device more improved than the photochronograph described by I. Sh. Model' was used to record brightness (the error related to the inaccuracy of determining the mirror rotational frequency was actually eliminated by this). Although an IFK-50 xenon lamp (brightness temperature of 6,300 $\pm$ 200°K in red light) is a more convenient comparison standard than the sun [41], the disadvantages related to the great difference of the brightness of the standard and the shock wave were retained. These disadvantages were eliminated in [42, 32], where an EV-39 flash lamp with brightness temperature of 41,000°K was used as the comparison standard.

I. Sh. Model' [29] noted one of the advantages of the photographic method--the possibility of simultaneous recording of the brightness and velocity of a shock wave. It is even possible to record simultaneously the brightness of the front at two different angles by measuring its velocity and checking the optical thickness of a shock-heated gas [32]. The specifics of explosive experiments, specifically the laboriousness of experiments to produce strong shock waves (D > 20 km/s) forces one to be limited to minimum statistics and to extract as much information as possible from each experiment. Therefore, the noted advantages of the photographic method predetermined its widespread use in the experiments described here. We developed the method jointly with Yu. A. Zatsepin.

Brightness temperature is determined from photometric comparison of darkening densities produced on a photoemulsion during slit scanning of a shock wave and brightness standard on the SFR-2 device. The ultraviolet (λ_{ef} = 330 nm), violet (λ_{ef} = 432 nm), blue (λ_{ef} = 442 nm) and yellow (λ_{ef} = 560 nm) sections of the spectrum were separated by light filters. The transmission curves of the light filters used in the experiments, measured on the SF-4 spectrophotometer, are presented in Figure 25. The effective length λ_{ef} is determined with regard to the spectral sensitivity of the photoemulsions.

The lenses of the SFR-2 device are replaced with quartz lenses, which were specially designed by N. M. Sitsinskaya for λ_{ef} = 330 nm and were manufactured at the OKB IFZ [Special Design Office of Institute of Physics of the Earth imeni O. Yu. Schmidt], during measurements in the ultraviolet region of the spectrum. The device was adjusted and focussed on the object by means of a fluorescent screen placed on the focal arc of the photochronograph. A mercury lamp is used for illumination.

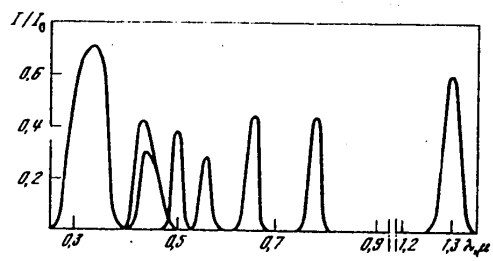

Figure 25. Transmission Curves of Light Filters Used

The brightness standard is an EV-39 pulsed light source that radiates like a black body with temperature of 41,000°K over a wide spectral range of 200-600 nm [143]. The proximity of the brightness temperature of the standard to the measured temperature reduces the error of the method and permits one to avoid the procedures that compensate for the large difference in brightness of the standard and shock wave. The standard and shock wave are photographed at identical error rotational frequency. Because of the short (180 microseconds) luminous pulse of the EV-39 source, one can do away with shutters that cut off one rotation of the photochronograph mirro (the same is true of filming the shock wave).

The darkening marks are imprinted when filming the standard to plot the characteristic curve of the photoemulsion in each experiment. A graduated attenuator is placed on the focal arc of the SFR device for this purpose. Synchronization of the position of the rotating mirror with the EV-39 flash lamp is selected such that the photoemulsion is exposed behind the graduated attenuator during the entire period of the flash when its brightness remains unchanged. The standard and darkening marks photographed in this manner are presented in Figure 26. If the temperatures to be measured are expected to be higher than the standard temperature, the darkening marks are imprinted first by the same method and at the same mirror rotational frequency, but with completely open lens diaphragm of the SFR device (so that the range of darkening densities of the marks always encompasses the darkening densities from the standard and shock wave). The identity of the conditions for filming the marks, standard and shock wave permits one to avoid relying on the law of intersubstitution when determining the brightness temperature.

When filming the EV-39 source, the SFR device is adjusted so that its slit cuts out a strip in the center 0.5 mm wide from the discharge opening of the source. Thus, the radiation of the central spot of a discharge 1 mm in diameter, for which brightness temperature of 41,000°K is guaranteed, is separated during time scanning from the radiation of the peripheral regions of the discharge with lower temperature. To increase the image size of the radiator of the EV-39 source on the negative (and thus facilitate densitometry of it), the latter is photographed from the closest possible distance l_1 equal to 2 meters for the SFR-2 device. It was required that the visual field of the photochronograph encompass no less than 15 cm for simultaneous recording of the brightness and velocity of the shock wave. A distance of l_2 = 5 meters satisfied this condition. The difference in distances is taken into account by multiplying the ratio of radiation intensity of the shock wave and the standard, measured by the darkenings, by the value , where

f = 21 cm is the focal distance of the inlet objective of the SFR-2 device. This correcting factor is close to 1 at $f << l_1$ and l_2 and is equal to 0.873 in the experiments. The distances l_1 and l_2 are measured with accuracy of $\pm$ 1 cm, to which corresponds the negligibly small contribution of intensity $\pm$ 0.1 percent to the measurement error. The identity of the conditions for filming the standard and shock wave is adhered to in the remainder. Specifically, establishing the width of the slit and diaphragm of the photochronograph objective during adjustment to the standard is not violated during subsequent filming of the shock wave. The effect of photochemical processing on the measurement results is eliminated by the fact that the standard, the darkening marks and the explosive experiment are photographed on the same segment of the photographic film and are subsequently processed together.

The greatest error of the method includes the natural inhomogeneity of darkening of the negative. To estimate this error, a uniformly illuminated screen was photographed with the photochronograph mirror rotating. The fluctuations of darkening density on the negatives obtained by this method and recorded by the MF-4 microphotometer were random in nature and did not exceed $\pm$ 0.015. These fluctuations obviously included the errors introduced by the SFR-2 device, for example, the lack of parallelism of the slit blades, the nonuniform scanning through the focal arc, the possible dependence of the reflection coefficient of the rotating mirror on the angle of incidence of radiation and so on (incidentally, the effect of the latter two factors was eliminated in the experiments by the fact that the standard, the darkening marks and the shock wave were always imprinted at the same location of the focal arc). The error in measuring the radiation intensity, introduced by the fluctuations of density, was determined by the characteristic curve of the photoemulsion and did not exceed $\pm$ 2 percent. The accuracy of relative measurements of intensities hardly differing from each other is set equal to this value. When estimating the accuracy of relative measurements of strongly different intensities, the error introduced when plotting the characteristic curve by a step attenuator is taken into account. A 10-step attenuator that yields a sufficient number of gradations of darkening densities for correct plotting of the characteristic curve is used in the experiments. As shown by measurement of the transmission of the attenuator fields on the MF-4 microphotometer, the error is determined to a significant degree by the nonuniformity of transmission within the field,* comprising $\pm$ 2 percent. Taking the foregoing into account, the maximum error of relative measurements of radiation intensity is estimated at $\pm$ 4 percent.

During absolute measurements, the EV-39 source adds an error of $\pm$ 7 percent in the range of λ = 300-550 nm and $\pm$ 10 percent in the range of λ = 200-300 nm [143]. The error in absolute measurements from the EV-39 is taken at $\pm$ 12 percent in the section of λ = 550-600 nm, while the brightness temperature of the source is 38,000°K [144]. The accuracy of absolute measurements of brightness temperature, corresponding to the errors given above in measuring radiation intensity, is given in Table 3.

*Light filters used in the experiments were placed in front of the photoelement of the microphotometer to take into account the weak spectral dependence of the transmission coefficient of the fields. The transmission coefficient of the fields in the ultraviolet part of the spectrum is taken from the certificate of the step attenuator and the correctness of the taken values is confirmed by the coincidence of the certificate data to measurements in the visible region.

Table 3. Accuracy of Measuring Brightness Temperature T/T, percent

$T \cdot 10^{-4}$° K	1	2	3	4	6	8	10
$\lambda = 560$ нм	5	8	9	9	10	11	12
$\lambda = 432$ нм	3	5	6	7	8	9	10
$\lambda = 330$ нм	3	4	5	6	7	8	9

The velocity and brightness temperatures of the shock wave front, corresponding to the radiation normal to the front and to radiation at an angle of 45° to the front, are measured simultaneously in each experiment and the optical thickness of the shock-heated gas is checked. Part of the measurements were made simultaneously in the ultraviolet and yellow regions of the spectrum. Setting up the experiment in this manner made it possible to make use of the comparatively high accuracy of relative measurements and to compare the results obtained in a separate experiment.

It is shown in Figure 27, a and b how the brightness temperature of shock waves was measured simultaneously at different angles. The shock wave in a glass cuvette 1, filled with the gas to be investigated, is excited after rupture of diaphragm 2 and is recorded through the n window 3 (in version b after reflection from the mirror 4) by a photochronograph in the form of the longitudinal scanning 1 in Figure 28. The brightness temperature corresponding to radiation normal to the front is determined from this scanning. The radiation emerging at an angle of 45° to the front is reflected from the mirror 4 (directly in version b without reflection) and is recorded by the photochronograph in the form of the inclined scanning 2 in Figure 28. The brightness temperature corresonding to radiation at an angle of 45° to the front is determined from this scanning.

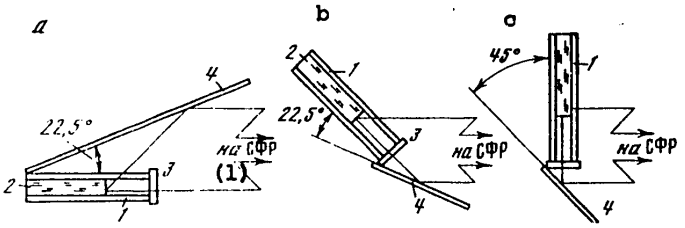

Figure 27. Diagrams of Simultaneous Recording of Brightness and Velocity of Front: 1--cuvette; 2--diaphragm; 3--window; 4--mirror

Key:
1. To SFR

Since the thickness of the gas layer radiating at angle of 45° impinges linearly upon approach to the wall of the cuvette, the optical thickness of a shock-heated gas can be estimated by the variation of the darkening density of the inclined scan from one of its edges to the other.

The inclined scan 2 in Figure 28 fixes the position of the shock wave front in time and permits one to measure (by its slope) the velocity of the front. The error in measuring the velocity did not exceed $\pm$ 3 percent in the experiments.

One detail in Figure 28 merits attention. The brightness section of the front disappears in time, being forced out by the less bright section adjacent to the cuvette walls. It will be shown later (in Section 4 of Chapter 4) that this section of lesser brightness corresponds to sharp bending of the front near the cuvette wall. It is interesting to note here that it is obvious from the sloping scan in Figure 28 that the velocity of the bright section is lower than that of the section adjacent to the walls (by 4-5 km/s in the given case). The possibility of distinguishing the velocities of individual sections of the front was useful for correct interpretation of the experimental results. The diagrams of simultaneous recording of the brightness and velocity of the front shown in Figure 27, a and b almost repeat the diagram described in [29, 41] and shown in Figure 27, c. However, the existing differences lead to the fact that it becomes impossible in version c to measure the velocities of the individual sections of the front, to measure the brightness temperature of the front at an angle and to check theoptical thickness of the shock-heated gas.

The reflection coefficients of mirror 4 (see Figure 27) and the transmission of the cuvette wall at the corresonding angles are measured on the SF-4 spectrophotometer and are taken into account when determining the brightness temperature. The error in measuring them is low ($\pm$ 0.5 percent) and is essentially not reflected in the accuracy of absolute measurements of intensity and brightness temperature. The accuracy of relative measurements of radiation intensities of the front at different angles, related to discharge of hardly differing intensities, is estimated at $\pm$ 3 percent with regard to this error.

The simultaneous measurements in the ultraviolet and yellow regions of the spectrum were made for a number of experiments by using two synchronously operating SFR-2 devices and the diverging light beam of a semitransparent mirror.

A stable shock wave in air with known brightness temperature is photographed along with the EV-39 source in some experiments to check the correctness of the results (described in Section 1, Chapter 6).

3. Method of Spectral Investigation of Radiation

Measurements of the brightness temperature in some regions of the spectrum separated by light filters do not provide a full idea of the spectral composition of the radiation of shock waves. These experiments were supplemented in [28, 30, 31] by spectral investigation of radiation in the visible region, which is qualitative in nature and is limited in [31] by an attempt to estimate roughly the color temperature of the shock wave from the spectral sensitivity of the photoemulsion. At the same time combining spectral methods with photometry methods makes it possible to extract the most detailed data (qualitative and quantitative) on the radiation of shock waves from the spectrophotochronograms. We used this method in [13, 32] to study the spectral brightness of shock waves in the ultraviolet and visible regions.

The time-resolved spectra of ultraviolet and visible radiation (λ = 220-700 nm) of shock waves are recorded by the SP-111 transmission spectrophotochronograph [145]. The SFR-2 photochronograph with SP-77 and SP-78 spectral attachments is also used for this purpose in the visible region [146]. To record large details in the spectrum, one can have low scattering and to record small details, for example, narrow

lines, one can have high scattering. Therefore, several versions of spectral recording are used in the experiments.

1. The SFR-2 device with SP-77 prism attachment; the reverse scattering is 100-200 A/mm, resolution is approximately 10 Å and a section of λ = 390-700 nm is encompassed.

2. The SFR-2 device with the Uran-10 aperture-ratio input lens and SP-78 attachment; reverse scattering is 42 A/mm, resolution is 4 Å and a section of $\Delta\lambda$ = 100 nm is encompassed during one procedure.

3. The SP-111 device with interchangeable diffraction grating of 200 lines/mm; reverse scattering is 42 A/mm, resolution is 4 Å and a section of $\Delta\lambda$ = 200 nm is encompassed during one procedure.

4. The SP-111 device with grating of 600 lines/mm; reverse scattering is 14 Å/mm, resolution is 1.4 A, a section of $\Delta\lambda$ = 70 nm is ecompassed during one procedure.

5. The SP-111 device with grating of 1,200 lines/mm; reverse scattering is 7 Å/mm, resolution is 0.7 Å and a section of $\Delta\lambda$ = 35 mm is encompassed during one procedure.

The time resolution in versions 1-5 is equal to 10^{-7} second.

When investigating the radiation of shock waves in inert gases, version 3 is used whose spectral resolution was adequate to detect and study the lines in the spectrum. Experiments with shock waves in air were conducted using all the enumerated versions.

A Q-12 quartz spectrograph and STE-1 spectrograph that provide resolution of 0.1 Å were also used in attempts to detect the narrow lines in the radiation spectrum of a shock wave in air. The shock wave amplitude within 15 microseconds in these experiments, although it lengthened the exposure of the photographic emulsion, remained constant after which the glow of the shock wave was cut off (see Section 1, Chapter 6 for cutoff).

The sufficiently high contrast of the panchrome-type 15 aerial photographic film used to record the spectra is enhanced by developing in D-19 contrast-effective developer. The developing time (approximately 10 minutes), corresponding to the maximum contrast of the negative, is selected experimentally. Because of these measures, one can confidently record the lines whose intensity differs by one percent or more from the adjacent continuum (the darkening inhomogeneities of the negative noted in Section 2 are random and smoothly variable with respect to the recorded lines and do not prevent detection of them on the spectrophotochronograms).

Spectral brightness temperature is determined from photometric comparison of the spectrophotochronograms of the shock wave and the EV-39 brightness standard. The darkening marks are imprinted simultaneously with filming of the standard, for which the step attenuators with known spectral transmission of the fields are placed on the focal arcs of the SFR-2 and SP-111 devices. G. P. Ilyushin and

V. G. Klokov synchronized the SP-111 device, due to which the process of filming the standard with the marks and shock wave was similar to that described in Section 2. The shock wave and the EV-39 source were photographed at identical distances.

The spectrum of a mercury lamp used subsequently to tie in the spectrophotochronograms and identification of the lines is imprinted immediately prior to the explosive experiment or filming the EV-39 source with the mirror of the SP-111 device rotating. The linearity of dispersion of the device made it possible not to complicate the experiment by imprinting a more detailed comparison spectrum. The weak continuum of the track did not remain on the spectrophotochronograms in the radiation spectrum of the mercury lamp.

In the remainder, the method of measuring the spectral brightness temperature repeats the method of measuring the brightness temperature, described in Section 2, in individual regions of the spectrum separated by light filters. The accuracy of absolute and relative measurements is the same as for the method in Section 2.

The EV-39 source with darkening marks, a stable shock wave in air with known brightness temperature (as a control) and the shock waves in each of the gases to be investigated were photographed under identical conditions in experiments with inert gases. The results of filming are processed together. This makes it possible to use the higher accuracy of relative measurements when comparing the spectral brightness of shock waves in each of the gases to each other.

Since the possibility of measuring the velocity of a shock wave in the experiments is lost when working with spectral devices, either charges and devices that yield a shock wave easily reproducible by velocity are used or the spectral method is used jointly with the method described in Section 2. In the first case the velocity of the shock wave is measured in preliminary experiments and in the second a synchronously operating spectral device and photochronograph, the light beam to which is separated by a semitransparent mirror, are used. Radiation normal to the front is studied in experiments by spectral methods.

An end window is installed on the cuvette in experiments with inert gases. The cuvette is evacuated to 10^{-3} mm Hg and is filled with a gas to the necessary pressure. The cuvette is also filled with argon and helium by prolonged pumping (approximately 5 min) interrupted by an explosion. A cover with a slit through which the gas escapes is installed instead of an end window in this case and the radiation of the shock wave is investigated. The content of the impurities in the argon crypton and xenon used does not exceed 0.01 percent and the impurity is 0.005 percent in helium and neon. An exception is an impurity of 1 percent xenon in crypton.

In order to disregard the transmission of the end window, the latter is introduced into the light beam when filming the brightness standard.

The density of the radiation flux from the front is estimated in experiments with inert gases at approximately 10^6-10^7 W/cm^2 and in experiments with helium up to $3 \cdot 10^8$ W/cm^2. Absorbing such powerful radiation, the walls and end window of the cuvette may lose their initial transparency. The end window located normally to

the radiation is under more severe conditions in this regard. To attenuate the effect of radiation on the window, long cuvettes (ratio of length to diameter is equal to 10-20) are used. Strong shock waves are attenuated in these cuvettes as they approach the window. Estimates showed that the density of the radiation flux on the walls and window of the cuvette and the length of its effect do not exceed those values in experiments which explosive sources produce (described in Section 2, Chapter 6). Special experiments were set up in which quartz, silicate and plexiglass plates were exposed to an explosive source. The shock wave was observed through the plates by means of a photochronograph. The transmission coefficient of the plates and the time variation of the transmission was determined from comparison of the darkening densities on the negative due to radiation of the shock wave travelling past the plate and through it. The transmission coefficient of quartz and silicate glass did not vary, while that of plexiglass decreased by 30-50 percent by the end of exposure to the source (within 20 microseconds). Therefore, windows of silicate glass were used in the experiments when investigating the visible radiation of a shock wave and windows of quartz were used when investigating ultraviolet radiation.

4. Measuring the Intensity Temperature by Photoelectric Radiation Receivers

The photographic method is inapplicable when investigating the radiation of shock waves in the infrared region of the spectrum. Although there are photoemulsions suitable for the near infrared region, it is difficult to record the radiation of a shock wave in time due to their low sensitivity. This disadvantage of the photographic method is compensated for by the photoelectric measurements described below. The feasibility of these measurements, including measurements of visible radiation, also includes the fact that it is possible to compare the results to the results of measurements by the photographic method. The fact of coincidence of one and the other gives reliability to each of the methods used.

Radiation in spectral sections with λ_{ef} = 500, 660, 660 and 778 nm and $\Delta\lambda$ = 10 mm, separated by light filters (see Figure 25), is recorded by an FEU-22 photomultiplier (range of sensitivity λ = 4,200 nm and maximum sensitivity at λ = 700 nm). Radiation in the infrared section at λ_{ef} = 1,300 nm and $\Delta\lambda$ = 40 nm is recorded by an FD-GI germanium-indium photodiode (range of sensitivity = 500-1,800 nm and maximum sensitivity at λ = 1,500 nm).

The signals from the FEU-22 and FD-GI are transmitted to OK-33 and OK-17M oscillographs and are photographed.

The brightness standard is an SIlO-300 light-measuring lamp. The brightness temperature of the tungsten strip of the lamp is measured in the spectral section of λ_{ef} = 660 nm by means of the EOP-51 precision optical pyrometer and is equal to 2,600 $\pm$ 10°K. The brightness temperature of the strip of the remaining spectral sections is determined from the results of these measurements and the tabular values of spectral darkness of the incandescent tungsten.

A diagram of photoelectric measurements is shown in Figure 29. The lamp strip or the shock wave 1 are projected by objective 2 so that their image completely fills the opening in the screen 4. The large difference of brightness of the shock wave and strip (reaching approximately 10^5 for λ_{ef} = 500 nm) is compensated for by

installation of a diaphragm 3. The diameter of the diaphragm opening 3 is selected so that the brightness of the images of the shock wave and strip of the lamp coincide; the electronic apparatus records only the coincidence of signal amplitudes in this case. The brightness temperature is then determined from the results of measuring the diameter of the diaphragm opening on the comparator.

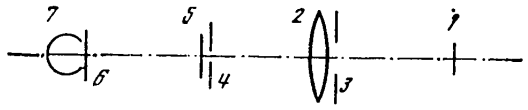

Figure 29. Diagram of Photoelectric Measurements: 1--shock wave front or standard; 2--objective; 3--diaphragm; 4--screen with opening; 5--ground glass; 6--light filter; 7--photomultiplier

The differences in the angular distribution of radiation introduced by the diaphragm are corrected by the ground glass 5, after which the light impinges on the photocathode through the light filter 6. Scattering of radiation by the ground glass was checked in the following manner. The diaphragm 3 was placed (within the objective) in its own plane when the lamp was switched on; the current of the FEU-22 was measured simultaneously by a milliameter. The readings of the millameter did not change when the diaphragm was moved, which indicated the effectiveness of scatter-scattering.

The light signal from the strip lamp is simulated by a rotating disk with openings (not shown in Figure 29) and is photographed from the oscillograph screen.

For the infrared region of λ_{ef} = 1,300 nm, the difference of brightness of the shock wave and lamp strip is not as high in the experiments (no more than 256 times it); therefore, the same diaphragm is used in measurements and calibration. The image of the strip or shock wave is projected through the light filter directly onto the inlet pupil of the photodiode and completely fills it (there is no screen 4 and ground glass 5). The signal from the lamp is measured on the load resistor of the photodiode by a millivoltmeter and is compared to the signal from the shock wave recorded by the oscillograph. The linearity of the photodiode is first checked and slight nonlinearity of the oscillograph is taken into account.

The accuracy of photoelectric measurements is estimated with regard to the error of measuring the temperature of the strip by a pyrometer, the error upon comparison of the signals on the oscillograms, the error of measurements with a millivoltmeter and milliameter, the error in measuring the diaphragm diameter on the comparator and the inaccuracy of tabular values of the darkness of tungsten. This analysis provides accuracy of absolute measurements of intensity of $\pm$ 10 percent for λ_{ef} = = 600, 778 and 1,300 nm and $\pm$ 12 percent for λ_{ef} = 500 and 560 nm.

Charges that produce a shock wave easily reproducible in amplitude and whose velocity is measured in preliminary experiments are used during photoelectric measurements.

RADIATION PROPERTIES OF SHOCK WAVES DETERMINED BY RESULTS OF THE EXPERIMENT

Moscow IZLUCHATEL'NYYE SVOYSTVA UDARNYKH VOLN V GAZAKH in Russian 1977 pp 62-94

[Chapter 4 from the book "Radiating Properties of Shock Waves in Gases", by M. A. Tsikulin and Ye. G. Popov, Izdatel'stvo "Nauka", 173 pages]

[Text] Propagation of a strong shock wave in a gas was accompanied by intensive glow. Despite the brevity of the process, this glow was always observed visually in the form of a blindingly bright flash at the moment of explosion. The gas which was under atmospheric pressure and at room temperature underwent approximately tenfold compression in the shock wave and was heated to 10^4-10^5°K depending on the wave amplitude. The heated gas radiated like an opaque body from the surface due to the high density and significant ionization. And this is the main difference from experiments in shock tubes where the gas density and temperature are such that the heated region is optically thin and radiates in all directions.

Data of the classical (the Unsold-Kramers formula) or of the quantum-mechanics (Biberman-Norman formula) theory of radiation absorption, for example, indicate the great optical thickness of the heated gas in experiments. According to quantum-mechanics theory, the paths of the visible and near ultraviolet radiation in a shock-heated gas are on the order of 10^{-1} to 10^{-3} cm and the value of 10^{-1} cm corresponds to the lowest temperatures measured in experiments. The dimensions of the heated zone are at least an order higher. Unfortunately, it is difficult to judge the extent to which existing theories of radiation absorption are applicable to a very dense plasma behind a strong shock wave front. Therefore, proof of the opaqueness of a shock-heated gas, obtained directly from experiments, is of great value. For example, the nature of variation of radiation intensity from the front of shock waves formed upon discharge of detonation from the explosive to a boundary with a gas indicates this. The fact is that the radiation intensity increases in proportion to the thickness of the layer immediately after discharge of the detonation while the layer of shock-heated gas is still optically thin. However, the increase of radiation intensity stops when the thickness of the layer increases so much that it becomes opaque as the shock wave propagates. In experiments the increase of radiation intensity occupied a rather short time so that one almost always dealt with optically dense shock waves. Confirmation of the opaqueness of a heated gas over a wide range of shock wave amplitudes was achieved when radiation emerging at an angle of 45° to the plane of the front was recorded. The thickness of the gas radiating at an angle of 45° decreases linearly as it approaches the

wall of the cuvette along which the shock wave is propagating. Therefore, the optical thickness of the gas can be estimated by the variation of radiation intensity near the wall. This problem was analyzed in detail when describing the method of measurement.

No appreciable decrease of radiation intensity near the cuvette wall was observed in experiments with strong shock waves, i.e., the gas behind the front radiated like an opaque body. Taking the resolution on photochronograms into account, it was also possible to estimate from above the paths of radiation in a shock-heated gas. The latter were known to be less than 10^{-1} cm. Radiation intensity at an angle of 45° decreased near the cuvette wall only at comparatively low shock wave velocities (for most gases at velocities of D = 5-8 km/s). To ensure opaqueness of the gas behind the front, large-dimension cuvettes with diameter of not more than 10-15 mm were used at these velocities and cuvettes of 25 and even 50 mm in diameter were used in experiments with strong shock waves. Thus, it was possible to significantly increase the dimensions of the heated zone and to make it optically dense. And even so the heated zone became optically thin at still lower velocities and radiated in all directions; in this case the radiation intensity from the front both at an angle of 45° and at normal angle decreased sharply so much that the instruments could no longer record it. The lowest of the velocities at which radiation intensity was still measured defines those cases for each of the gases when the shock wave was optically dense and cases when it became optically thin.

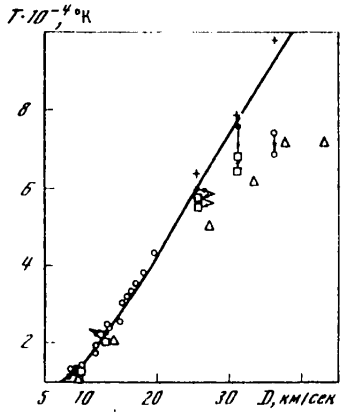

Figure 30. Brightness Temperature of Shock Waves in Air: dark circles--λ = 330 nm; light circles--λ = 432 nm; light squares--λ = 560 nm; light triangles--λ = 650 nm; +--temperature of shock-heated gas restored by values of brightness temperature at different angles

The main results of the investigations are the measured values of brightness temperature and the velocities of the shock wave front. The brightness temperature of the front was measured over a wide range of shock wave amplitudes by using light filters that separate narrow sections of the spectrum from the visible

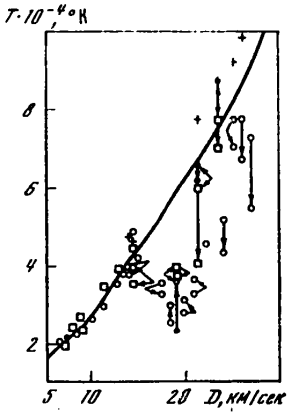

Figure 31. Brightness Temperature of Shock Waves in Argon: dark circles--λ = 330 nm; light circles--λ = 432 nm; light squares--λ = 560 nm; +--temperature of shock-heated gas restored from values of brightness temperature of front at different angles

region and the quartz ultraviolet. The velocity and brightness temperatures of the front corresponding to the intensity of radiation normal to the front and to radiation intensity emerging at an angle of 45° to the plane of the front were measured simultaneously in each experiment. The measurements were made immediately in two different sections of the spectrum in some experiments. Setting up the experiment in this manner made it possible to use the comparatively high accuracy of relative measurements and to compare the results obtained in individual experiments to each other (it was not always possible to compare the results of different experiments in detail due to the instability of radiation of high-amplitude shock waves). The values of brightness temperature measured simultaneously in two different sections of the spectrum or at different angles to the plane of the front are joined by arrows in Figures 30-38, where the results are presented. The arrow from a point corresponding to the radiation normal to the front indicates the point corresponding to radiation at an angle of 45° to the front if they did not coincide within the relative measurement error (unlike the values for different sections of the spectrum when the arrows indicate both points immediately). The absolute measurement error in Figures 30-38, even without saturated parts, is not denoted. Its value can easily be presented from Table 3, reduced upon description of the measurement method.

The radiation of shock waves for several fixed amplitudes was subjected to especially thorough investigation. The time-resolved radiation spectra of shock waves were recorded by using a spectrochronophotograph. The brightness temperature distribution of the front within a broad spectral interval encompassing the quartz ultraviolet, visible and infrared regions, was measured by the intensity of radiation normal to the front. The results of these measurements are presented in Figures 39 and 40.

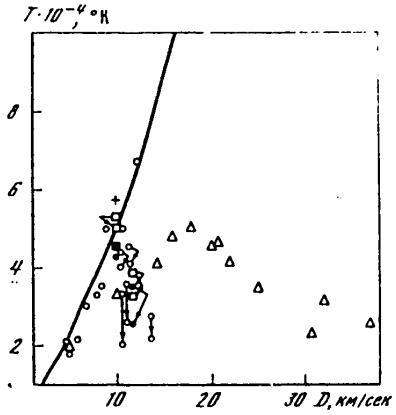

Figure 32. Brightness Temperature of Shock Waves in Xenon: dark circles--λ = 330 nm; light circles--λ = 432 nm and 442 nm; light squares--λ = 560 nm; light triangles--λ = 650 nm; +--temperature of shock-heated xenon restored from values of brightness temperature at different angles

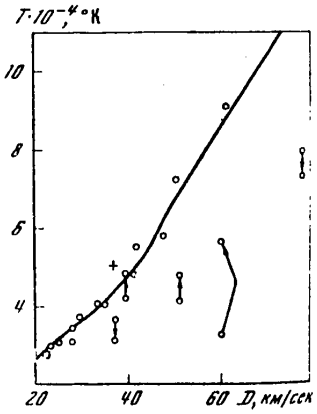

Figure 33. Brightness Temperature of Shock Waves in Helium: light circles--λ = 432 nm; light squares--λ = 560 nm; +--temperature of shock-heated helium restored from values of $T_{уд}$ at different angles

Comparison of the brightness temperature of the front to the gas temperature behind the front evokes special interest when investigating the radiation of optically dense shock waves. The gas temperature behind the front, calculated from the shock wave velocity known from experiment, is presented in Figures 30-40. Detailed description and the results of calculations are given in the Appendix.

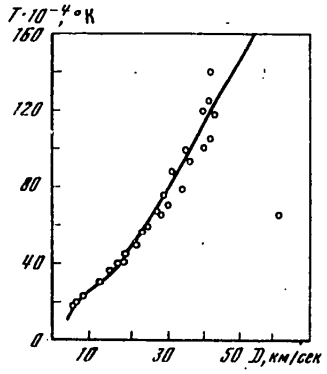

Figure 34. Brightness Temperature of Shock Waves in Neon (λ = 432 nm); the points are taken from [169] for D > 12 km/s

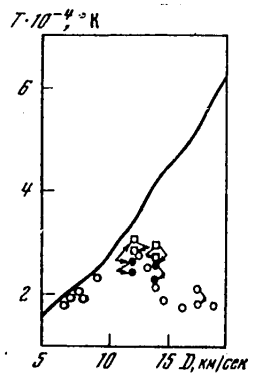

Figure 35. Brightness Temperature of Shock Waves in Argon With Air Impurity: dark circles--λ = 330 nm; light circles--λ = 442 nm; light squares--λ = 560 nm; curve--calculated temperature behind front for pure argon

The radiating properties of shock waves in air and in inert gases differ appreciably. A number of features were discovered in experiments with inert gases that forced one to re-evaluate the capabilities of a shock wave as a radiator. The transient nature of radiation by strong shock waves and the presence of absorption lines in the spectrum could not be explained on the basis of existing theoretical concepts. On the one hand, it was required to determine and to scrupulously describe the experimental results, being limited in this case only to some of the more obvious conclusions. On the other hand, one had to reconsider some what the theory of radiation of strong shock waves when interpreting the results (see the next chapter).

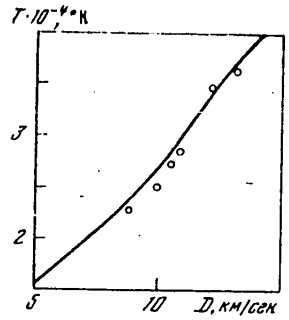

Figure 36. Brightness Temperature of Shock Waves in Argon at Pressure of p_0 = 300 mm Hg, λ = 432 nm

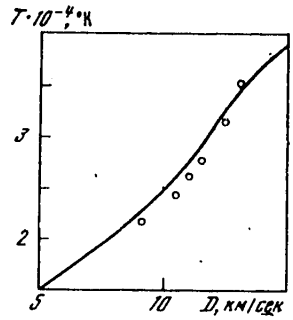

Figure 37. Brightness Temperature of Shock Waves in Argon at Pressure of p_0 = 100 mm Hg, λ = 432 nm

1. Intensity of Strong Shock Waves in Air

The values of brightness temperature and velocities of the shock wave front in air measured in experiments are presented in Figures 30 and 39. In Figure 30, the results of our measurements are supplemented by values of brightness temperature of the front in red light measured by A. Ye. Voytenko, I. Sh. Model' and I. S. Samodelov [41]. The theoretical dependence of the temperature of shock-heated ionized air on wave velocity, calculated by N. M. Kuznetsov [147], is presented in the same figure for comparison.

If the shock wave velocity did not exceed 20 km/s, the brightness temperature of the wave front was identical in different sections of the spectrum (Figure 39). The values of brightness temperature corresponding to the intensity of radiation normal to the front and to radiation intensity at an angle of 45° to the plane of the front also coincided with each other. All the measured values of brightness temperature at velocities of D = 820 km/s are applicable within error to the theoretical curve for the gas temperature behind the front.

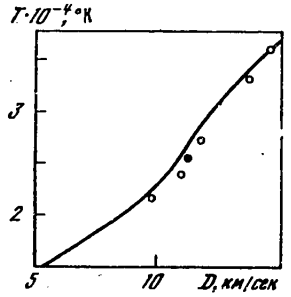

Figure 38. Brightness Temperature of Shock Waves in Argon at Pressure of p_0 = 50 mm Hg, λ = 432 nm

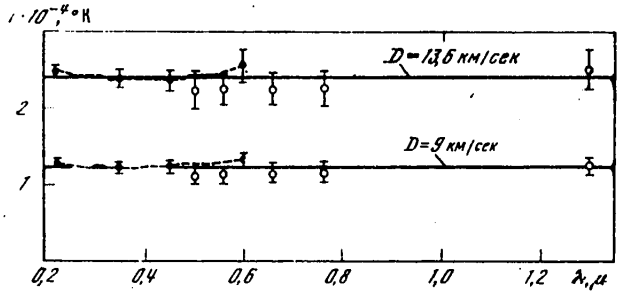

Figure 39. Distribution by Brightness Temperature Spectrum of Shock Waves in Air: dark circles--from spectrophotochronograms; light circles--photoelectric measurements; straight lines--gas temperature behind front

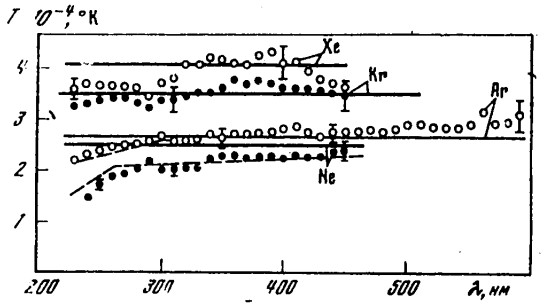

Figure 40. Spectral Distribution of Brightness Temperature of Shock Waves in Inert Gases: light and dark circles--from spectrophotochronograms; straight lines--calculated temperature of gas at first moment of detonation; dashed line--calculated temperature behind front at moment maximum brightness is reached

However, at high velocities, beginning at D = 25 km/s and above, the brightness temperature of the wave front for the visible sections of the spectrum was always appreciably below the calculated temperature of the gas behind the front. The deviation of the indicated temperatures exceeds 20,000°K for the highest velocities presented in Figure 30. The total error which the measurements and calculations introduced is at least one-third less. In one of the experiments whose results are not presented in Figure 30, A. Ye. Voytenko and colleagues [41] managed to produce a shock wave in air with velocity of D = 55 km/s. The calculated gas temperature behind the front is equal to 160,000°K at this velocity, but the brightness temperature of the front measured in experiment was only 25,000°K. Judging by everything, the maximum brightness temperature of the front of shock waves in air is reached for the visible region of the spectrum at velocities of D = 35-45 km/s and is equal to 70,000-80,000°K.

Thus, the brightness temperature of the front initially coincides with the calculated temperature of the gas behind the front with an increase of the shock wave amplitude, then lags behind it, passes through a maximum and decreases to a rather low value. An explanation of this phenomenon is given in the papers of Ya. B. Zel'dovich and Yu. P. Rayzer [33-37]. The narrow layer of air adjacent to the strong shock wave front is ionized by powerful shortwave radiation and, losing transparency, shields the front. The brightness temperature of the front becomes lower than the gas temperature behind the front and the shielding effect is intensified so much so that the brightness temperature passing through a maximum decreases to a limiting value determined by the natural glow of the shielding layer as the shock wave amplitude increases. Theoretical estimates of the maximum and limiting brightness temperature of a shock wave in air, based on these concepts, are in satisfactory agreement with experimental data. This problem will be considered in detail in the next chapter.

A difference between brightness temperatures corresponding to normal radiation and radiation at an angle of 45°, appeared at high shock wave velocities together with a lag of brightness temperature of the front behind the calculated gas temperature behind the front. Therefore, the points belonging to visible sections of the spectrum in Figure 30 seem to split at high velocities (with the exception of values for the red section λ = 650 nm from [41], which were measured only by the intensity of radiation normal to the front). The difference is small, but it was recorded confidently due to the high accuracy of the relative measurements. And, which it is important to note, the brightness temperature of the front corresponding to radiation intensity at an angle of 45° was always below the brightness temperature corresponding to the intensity of radiation normal to the front.

This difference of the indicated brightness temperatures may be experimental proof of the existence of a low-temperature layer that shields the radiation of the high-temperature zone of gas behind the front regardless of the dependence on comparison to the calculated gas temperature behind the front. Moreover, the optical thickness of the shielding layer can be determined from experiment if one disregards its natural glow in the case of weak shielding. The optical thickness of the shielding layer τ is then related to the intensity of radiation normal to the front I_1 and to the radiation intensity at an angle of 45° to the front I_2 in the following manner:

$$I_1 = I_0 e^{-\tau}, \quad I_2 = I_0 e^{-\sqrt{2}\tau}, \tag{4.1}$$

where I_0 is the radiation intensity from the heated gas behind the front. Hence,

$$\tau = \frac{1}{\sqrt{2}-1} \ln \frac{I_1}{I_2}, \quad I_0 = I_1 \left(\frac{I_1}{I_2}\right)^{1/(\sqrt{2}-1)}. \tag{4.2}$$

The intensity I_0 determined in this manner permits one to find from intensities I_1 and I_2 known from experiment the true gas temperature behind the front under conditions of shielding (the true temperature is equal to brightness temperature in the absence of shielding, the criterion of which may be coincidence of the measured values I_1 and I_2). Some of the values of gas temperature behind the front obtained in this manner are presented in Figures 30-38 and coincide within the limits of error to the theoretically calculated values.*

No difference of the brightness temperature of the front at different angles nor a leg of it behind the calculated temperature of shock-heated air was observed in the ultraviolet region of the spectrum. Judging from experimental data (see Figure 30), shielding of radiation in this region of the spectrum should be expected at higher shock wave velocities than in the visible region.

The results indicate the greater transparency of the shielding layer to ultraviolet radiation and agree in this case to theoretical data on the nature of the spectral dependence of radiation absorption by ionized gases. Thus, according to the Unsold-Kramers formula, the absorption coefficient of radiation with wavelength of λ = 330 nm is approximately one-half that of radiation with wavelength λ = 560 nm. The results of experiment of quantum-mechanics theory [91], which takes into account the hydrogen dissimilarity of absorption by nitrogen and oxygen, is explained even better--the considered coefficients here differ approximately fivefold. For example, shielding is appreciable at D = 31 km/s in yellow light (λ = 560 nm) (Figure 30) and the optical thickness of the shielding layer is estimated from experiment (τ = 0.15) whereas τ = 0.03 in the ultraviolet region (λ = = 330 nm) due to the difference of absorption coefficients and the lag of brightness temperature comprises only approximately 2,000°K, i.e., there should essentially be no shielding. In red light where the absorption coefficient is approximately 1.5-fold greater, a value of τ = 0.22 is found and the brightness temperature for radiation normal to the front is T_{ya} = 61,000°K and agreement with measurement results is obvious here.

*In time the following question arises: can one follow with optical means the gas temperature in strong shock waves, for example, during powerful explosions. It was assumed that this could not be done due to shielding of radiation by the heated layer before the front. The results presented here indicate that if the radiation intensity from the front is measured at two different angles, then the gas temperature behind the front can be determined up to amplitudes when the natural radiation of the heated layer becomes significant.

2. Intensity of Strong Shock Waves in Inert Gases

The experimentally measured values of the brightness temperature and the velocity of the shock waves in inert gases are presented in Figures 31-38, 40. The theoretical relations for the temperature of shock-heated ionized gases as a function of the wave velocity calculated by the authors are presented also for comparison.

As has already been noted earlier, the least of the velocities for which the measurements were performed were limited by the necessity of insuring quite large optical thickness of the shock-heated gas. The maximum velocities, as a rule, were limited by the possibilities of the devices used to obtain the shock waves. In low-density gases, for example, in helium, it was possible to achieve higher velocities than in heavy gases such as argon or xenon. For these regions, the velocity range of the shock waves encompassed by the experiments was different for each of the gases (in argon, for example, this was 8-26 km/sec, and in helium, 20-80 km/sec). However, in spite of these and certain other differences, the qualitative nature of the radiation by shock waves in inert gases was identical.

Just as in the experiments with air, if the shock wave velocity in inert gases did not exceed a defined value, the brightness temperatures of the wave front coincided in the different sections of the spectrum and at different angles.

Comparison of the brightness temperature of the front with the calculated gas temperature behind the front also occurred in this case. The shock waves in xenon, for which the brightness temperature of the front in the visible part of the spectrum was systematically below the calculated value of the shock-heated xenon already at low velocities of D=5 to 9 km/sec, constituted an exception. Thus, in a defined range of velocities the nature of the radiation by the shock waves was the same as for an absolutely black body, or it approached it (the experiments with xenon). At high shock wave velocities the brightness temperatures corresponding to radiation from different segments of the spectrum and at different angles to the plane of the front ceased to compare with each other and turned out to be below the calculated gas temperature behind the front.

However, in contrast to the experiments with air, when studying the shock waves in inert gases, a decrease in the brightness of the wave front was observed with time. This was manifested especially clearly in the experiments where the shock wave front did not change, whereas the brightness temperature of the front dropped noticeably in a few microseconds. For example, in one of the experiments with xenon with a constant velocity of the shock wave of D=12 km/sec, the brightness temperature of the front in blue light dropped from 67,000 to 22,000°K in 2 microseconds (the radiation intensity from the front decreased by 5.5 times). A simultaneous decrease in brightness over the entire area of the front was rarely observed. More frequently two or three spots not having clear boundaries appeared on the glowing front. The brightness temperature of the spot was reduced significantly in a few microseconds, and the spots themselves increased in size and encompassed the entire front. The large dispersion of the values of the brightness temperature at velocities of D>14 km/sec in argon, D>10 km/sec in xenon, D>25 km/sec in neon and D>35 km/sec in helium is connected with this nonsteady

radiation of the shock waves. The drop in brightness of the front with time was also noted at lower velocities. Thus, in a series of specially stated experiments[1] the shock wave in argon at a velocity of D=12 km/sec was created in a tube 84 mm in diameter; here the brightness temperature of the wave in blue light drop dropped from 33,000 to 28,000°K in 25 microseconds (the radiation intensity decreased by 35%). A reduction in the intensity of the visible radiation from the front for a still lower velocity of D=8.3 km/sec was reported by Roth [28]. In his experiments the shock wave was created in a tube 10×10 cm in cross section with exit of the detonation from TG 40/60 to the argon; a noticeable decrease in intensity by approximately 20% was observed in the first three microseconds after exit of the detonation, and in the glow spectrum of the shock wave, absorption lines appeared after 3 microseconds. The appearance of the weak absorption lines 1 microsecond after exit of the detonation into the argon was also observed by the authors of [13]. However, the nonsteady nature of the radiation from the front at such low velocities was manifested primarily in the form of these weak absorption lines. The reduction in radiation intensity recorded by Roth is more naturally related to the damping of the shock wave. Taylor and Kane [31], who observed a decrease in radiation intensity in analogous experiments, hold to the same opinion.[2] Somehow or other at low velocity the nonstationarity of the radiation was weakly manifested. It was only noted in experiments where the area of the shock wave front was completely large. It is possible to propose that with an increase in the front area the effect becomes more intense. Under the

[1]We are talking about experiments with explosion sources of light which will be described in Chapter VI.

[2]A possible reason why Roth did not detect the damping of the shock wave is discussed in §1 of Chapter II and §4 of Chapter IV.

condition of our experiment, as a result of the restriction on the weight of the explosive charge, this proposition could not be checked by further increase in the area of the front. However, experiments were run in which the diameter of the couvettes was decreased from 15 to 8 mm. The nonsteady reduction in brightness of the powerful shock waves in narrow couvettes was insignificant, and nonuniformities of the brightness with respect to area of the front did not occur.[1] The maximum brightness temperatures under the conditions of a reduction in brightness of the front with time were obtained in the same experiment, where the shock wave velocity increased sharply, for example, after rupture of a thin diaphragm separating the couvette into two parts. Here the highest temperatures were measured after a reduction in brightness came for the individual sections of the front.

The nonsteady nature of radiation by powerful shock waves and, in particular, the dependence of the brightness not only on the velocity, but also on the acceleration of the front are, in the opinion of the authors, caused by a delay in

---

[1]It is possible to use the influence of the couvette dimensions on the nature of the radiation by powerful shock waves to explain the divergences in Figure 32 where the results of A. Ye. Voytenko, I. Sh. Model' and I. S. Samodelov [41] are presented along with our results. The diameter of the couvettes in reference [41] judging by the moving image camera recording of the experiment presented there was 5 mm, so that the nonsteady reduction in brightness and the dispersion of the experimental points caused by this were less (according to [41], the mean square divergence of the points reached $\pm$15%). In addition, the values of the brightness temperature in red light carried over from [41] to Figures 30, 32 are average. In order to reflect the nonsteady nature of the radiation by powerful shock waves in inert gases, the results of our measurements in Figures 30-38 were intentionally not averaged. Accordingly, let us note that previously I. Sh. Model' [29] measured the following values of the brightness temperature of the front in red light: T_b=30,000°K for D=17.6 km/sec in Ar, T_b=34,000°K for D=17.2 km/sec in Kr and T_b=35,000°K for D=16.9 km/sec in Xe. I. Sh. Model', et al. [41] explain the divergence of the last value from their later data in that under the effect of the shock wave emission, the windows made of organic glass used in reference [29] lost their transparency. However, the noted divergence can be explained also by the nonsteady state nature of the radiation of the shock waves.

the formation of the shielding layer. Let us note the time of formation of the layer beginning with the existing ideas about the shielding of radiation in powerful shock waves. Ionizing radiation heats up the gas in a narrow layer in front of the shock front in the time $t \sim \ell/D$, where ℓ is the length of path of the radiation, D is the velocity of the front. In inert gases of normal density $\ell \approx 10^{-3}$ cm [148]. Setting D=10 km/sec, we obtain $\tau \approx 10^{-9}$ sec. This is $\sim 10^3$ times less than the delay observed in the experiments. However, consideration has still not been given to the fact that the intensity of the ionizing radiation reaches its maximum value some time after excitation of the shock wave when the layer of shock-heated gas becomes optically dense for this radiation. The buildup time of the intensity is characterized by the ratio ℓ/D, where now ℓ is the length of path of the ionizing radiation in the shock-heated gas reduced to the gas density ahead of the front. For estimation of the length of path ℓ, data on the ionization composition of the shock-heated gas presented in the appendix were used. The photoionization cross sections of the atoms were taken from reference [148], and the photoionization cross sections of the ions were assumed to be hydrogen-like. As applied to the experimental conditions, the ratio ℓ/D turned out to be within the limits of 10^{-9} to 10^{-7} sec. Thus, the time of formation of the shielding layer ahead of the front is better dictated by the time of formation of a region that is optically dense for the ionizing radiation behind the front. Nevertheless, this time is too small to explain the delay observed in the experiments. It is possible to go beyond the scope of the developed ideas and propose that for some reason a broad shielding layer was set up in the experiments $\ell \sim 1$ cm wide. Then the characteristic setup time $\ell/D \sim 10^{-6}$ sec agrees with the experimental data.

In contrast to the experiments with air, in inert gases the intensity distribution of the radiation from the front at different angles had a different

nature at large amplitudes. The amount the intensity of the radiation normal to the front exceeds the intensity of the radiation at an angle of 45° was retained only for the first moment after excitation of the powerful shock wave. After 2-5 microseconds the intensity of the radiation normal to the front, decreasing with time, became lower than the radiation intensity at an angle of 45°, for which a slower decrease with time was observed. This type of nonstationarity was manifested especially strongly in the experiments with helium (see Figure 33) and also in the experiments with argon at reduced pressures (see Figures 36-38). Thus, in one of the experiments with helium 0.5 microsecond after excitation of the shock wave, the velocity D=78 km/sec, the brightness temperature of the front T_b=78,000°K for normal radiation and T_b=73,000°K for radiation at an angle of 45° were measured, and 2 microseconds after, the brightness temperature of the front for normal radiation dropped to T_b=32,000°K and became lower than the brightness temperature T_b=56,000°K for radiation at an angle of 45° (after 2 microseconds the velocity was D=60 km/sec).

The diagram of the recording of the shock wave radiation presented in Figure 27 gives the simplest interpretation of the result obtained -- the shielding layer which is narrow at the first point in time after excitation of the shock wave broadened in 2 microseconds to several diameters of the couvette (that is, to $\ell \sim 1$ cm), and the radiation at an angle to the front did not intersect the entire shielding layer. It is even more correct to talk about a plug of semitransparent gas occurring in the couvette ahead of the shock wave front instead of a layer of gas.

Decreasing with time, the brightness temperature for the segment λ=330 nm became lower than the simultaneously measured temperature for the section λ=560 nm (see Figures 31-33). This obviously means that the absorption coefficient of the

radiation by the gas in the shielding layer for the section λ=560 nm was less than for the section λ=330 nm. However, from the theory it follows that this spectral dependence of the absorption coefficient occurs only at comparatively low temperatures, below 15,000°K in Ar and below 10,000°K in Xe.[1] However, at such low temperatures, only a layer on the order of 1 cm thick can noticeably shield the radiation.

In some experiments with xenon at velocities of D>10 km/sec it was possible to observe an increase in the brightness of the front in 1 microsecond with approximation of it to the end window of the couvette. This result also indicates that ahead of the shock wave front at a distance on the order of 1 cm there was a plug of semitransparent gas shielding the radiation from the front. No buildup of brightness of the front was observed in the narrow couvettes 8 mm in diameter before its arrival at the end window. Obviously, in narrow couvettes the conditions for the formation of such a plug ahead of the front were worse, which also appears to be entirely natural. In order to avoid confusion, let us note that in the experiments with other inert gases the end window either was not installed (argon, helium) or the observations were disturbed (argon at reduced pressures) by the instability of the plane front which will be discussed in §4.

Thus, in order to give a noncontradictory explanation to the above-enumerated characteristics of the radiation of powerful shock waves in inert gases, it remains to confirm the previous proposition that a shielding layer on the order of 1 cm thick is observed ahead of the shock wave front in a time on the order of 1 microsecond. Again we emphasize that the formation of such a wide layer cannot

---

[1] Analyzing the spectral dependence of the absorption coefficient, we considered the corrections for the nonhydrogen nature of the absorption calculated in reference [92].

be explained on the basis of the existing ideas of shielding the radiation of powerful shock waves by a layer arising as a result of photoionization of the cold gas ahead of the front by short-wave emission. Without touching on the possible nature of this layer, let us consider the results of measuring the brightness temperature of shock waves in the front with an admixture of air.

In the first experiments the couvette was filled with argon not by purging, but by forcing out the lighter air. It was assumed that the air admixture, unavoidable in this filling approach has no influence on the shock wave brightness. The values of the brightness temperature measured in these experiments are presented in Figure 35. A comparison with the results of Figure 31 for pure argon (filling by purging) indicates the significant influence of the admixture -- the brightness temperature of the front of the powerful shock waves in argon with air admixture turned out to be appreciably lower. In order to see that the air admixture is at fault in this divergence, three experiments were performed in which the volumetric concentration of the air was checked and amounted to 5%. The data from these experiments sell well within the results presented in Figure 35. All of the above-noted peculiarities of the radiation of powerful shock waves indicating the formation of a broad shielding layer ahead of the front were manifested in argon with air impurity. In particular, with approach of a powerful shock wave to the end window of the couvette the brightness temperature of the front increased in 1-0.5 microsecond, reaching the same values achieved in pure argon by the time of arrival at the window (these values are not presented in Figure 35). Arranging the couvette parallel to the slit of the moving image camera (the radiation recording time is presented in Figure 27, c), it was possible directly to observe the formation of the weakly glowing plug ahead of the front extending a distance of more than 1 cm. For a long time this glow ahead of the front was

connected with reflection of the couvette walls. Subsequently, it was noted that the glow is not manifested immediately, but 1-2 microseconds after excitation of the shock wave (in contrast to reflection which was also observed, but arose immediately). Similar glow was also observed in experiments with pure inert gases, but, being weaker, it was not so clearly isolated against the background of the reflection.

In the conclusion of this section let us note that the efforts to convert to strict quantitative studies of nonsteady phenomena in powerful shock waves have run into a number of difficulties. First of all these include the highly unstable nature of the phenomena themselves when apparently in identical experiments nonsteady changes in intensity have been quantitatively distinguished. It is convenient to investigate these phenomena in experiments where the shock wave velocity does not change noticeably for at least 10 microseconds, but such waves cannot be obtained with a velocity of D>15 km/sec. Great difficulties have also arisen from the instability of the plane front during movement of the powerful shock waves in the couvettes. This phenomenon is the subject of §4 of the given chapter, and here we shall only note that as a result of the disappearance of the plane front 5-10 microseconds after excitation of the shock wave frequently it has not been possible to establish what values the brightness temperature will drop to as it decreases with time.

3. Results of Spectral Investigation of Radiation

From the results of the studies presented in §1, 2 of this chapter, it is possible to draw the conclusion that shock waves with velocities of D=8 to 20 km/sec in the air, D=7 to 14 km/sec in argon, D=7 to 25 km/sec in neon, and D=20 to 35 km/sec in helium radiated just as an absolutely black body in the experiments. This is indicated by the comparison of the brightness temperatures in the various sections of the spectrum and at different angles to the plane of the front among

each other and with the calculated gas temperature behind the front. For the same reasons it is necessary to consider the radiation of shock waves with the velocities of D=4 to 10 km/sec in xenon similar to absolutely black; in the given case the brightness temperature of the front in visible light was somewhat below the calculated temperature of the shock-heated xenon, which indicates the radiation shielding. These conclusions were more precisely defined during spectral studies of the radiation of shock waves, the results of which are presented below.

Figure 41. Moving image camera photograph of shock wave radiation in the air obtained using the SFR-2 camera with SP-77 attachment (λ=390-700 nm)
1 -- detonation exit to the bottom of the channel, 2 -- stable shock wave in the channel, 3 -- drift of the shock-heated gas out of the tube

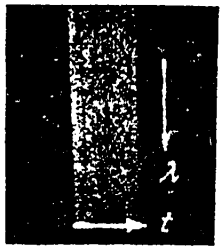

Figure 42. Moving image camera photograph of the radiation of a shock wave in the air with a velocity of D=14 km/sec obtained using the SP-111 (λ =220 to 400 nm)

Figure 43. Moving image camera photograph of the radiation of a shock wave in the air at a velocity of D=14 km/sec obtained on the STE-1 camera
The top line is blue light, the botton line is yellow light, in the upper right hand and lower lefthand corners are the ultraviolet (λ>390 nm) and red (λ<700 nm) ends of the spectrum

A study was made of the radiation spectrum of shock waves in the air with velocities of D=9 to 14 km/sec. The spectrum was recorded in the range of λ=220 to 700 nm with resolution in time. Several impressions from the moving image camera photographs are presented in Figures 41-43. The radiation spectrum turned out to be continuous. In spite of the most careful examination of the moving image camera photographs, no lines could be detected on them. Let us note that the procedure used made it possible to record quite powerful lines, the intensity of which differed by 1% or more from the adjacent continuum.

The maximum resolution achieved on the moving image camera SP-111 with diffraction grating of 1200 lines/mm was 0.7Å. At the same time, experiments have been performed in which the investigated radiation of the shock wave was specially cut out, and the recording was made by the STE-1 or Q-12 spectrograph with resolution of 0.1Å. The impression from the spectrogram taken in this way is presented in Figure 43. However, even on these spectrophotograms with resolution of 0.1Å the lines were absent.

In accordance with [149], we estimated the possible width of the lines under experimental conditions. Different mechanisms lead to broadening of the lines to $\Delta\lambda$~0.1 to 100Å. The least line width is limited by doppler broadening of $\Delta\lambda$~0.1Å.

Apparently the absence of the lines in the spectrum is caused by the nature of the shock wave emission and not by the possibilities of the procedure. This nature of the emission, which is extraordinary for a gas heated to high temperatures, makes the shock wave similar to incandescent bodies.

As is demonstrated in §1, in order to determine the absence or presence of shielding of the radiation in shock waves there is no necessity for performing the tedious calculations of the parameters of a multiply ionized gas beyond the front or to take absolute measurements of the brightness temperature of the front -- it is sufficient to compare the intensity of the radiation from the front at different angles. The absence (presence) of lines in the radiation spectrum of the shock wave can also serve as proof of the absence (presence) of shielding. Actually, inasmuch as the absorption coefficient in many of the lines is much greater than in the adjacent continuum, even weak shielding of the radiation leads to the appearance of absorption lines in the spectrum. The procedure used for recording the lines permits the statement that the shielding of the radiation in the lines and (the more so in the continuum) did not exceed 1%.

The spectral moving image camera recordings offer the possibility not only of more precise determination of the qualitative representation of the radiation by shock waves, but also the simplest means of measuring the brightness temperature of the front inside a wide segment λ=220 to 600 nm. If we consider that in addition to this the brightness temperature was measured in the infrared and visible regions with the application of photoelectric radiation receivers, the results obtained encompass altogether the spectral range of λ=220 to 1300 nm. The brightness temperature of the front measured by different means was identical for different sections of the spectrum and coincided with the calculated temperature of the gas beyond the front (see Figure 39). On movement of the shock wave

with constant velocity when the geometric thickness of the heated gas increased, the radiation intensity from the front remained unchanged. The noted event is evidence of the great optical thickness of shock-heated air in the experiments.

Figure 44. Spectral moving image camera recordings of the radiation of shock waves obtained on the SP-111 in the range of λ=220 to 420 nm
1 -- xenon, 2 -- krypton, 3 -- argon, 4 -- neon, 5 -- argon (λ=460 to 660 nm); the spectra are marked off by the reference lines from a mercury lamp

Thus, the above-presented results confirm the conclusion that in the air the shock waves emit in a defined range of amplitudes as an absolutely black body. It is hardly possible to mention another high-temperature source which radiates similarly in such a wide spectral range. Based on the results obtained, the authors proposed the use of an amplitude-stable shock wave in the air as a high-temperature standard of the radiation of an absolutely black body [12-14]. The explosion type emitter suitable for photometric purposes is described in Chapter VI.

A study was made of the radiation spectrum of shock waves in neon, argon, krypton and xenon formed on exit of the detonation from the TG 40/60. The spectrum was recorded in the range of λ=220 to 450 nm (for argon, in the range of λ=220 to 660 nm) with resolution in time. The impressions of the spectral moving image camera recordings are presented in Figure 44. The radiation spectrum of the

shock waves in inert gases turned out to be continuous; however, weak absorption lines were superposed on the continuous background of the shock wave radiation in argon, krypton and xenon.[1] Different radiation intensities in the lines and the adjacent continuum did not exceed 5%. The detected lines were collected in Table 4. For identification of the lines, the information from [150] was used. It was possible to establish that almost the lines belong to the atoms and ions of the gas through which the shock wave was propagated. Lines Nos 1, 2, and 3 observed in the experiments with argon constituted an exception. Of them, only line No 1 belonging to atomic hydrogen is identified for sure. Another characteristic feature of these three lines is appearance of them not immediately after the beginning of shock wave glow, but after ~1 microsecond (the remaining lines appeared simultaneously with the continuum). Similarly to this, the occurrence of these lines is connected with photoexcitation of the admixtures ahead of the front by the ultraviolet radiation of the shock wave. The appearance of not only lines, but also typical molecular bands ~10 microseconds after the beginning of glow was observed in the experiments with neon.

The intensity of the emission from the front increased sharply during the first moment after exit of the detonation, and then it dropped slowly. The reduction in the radiation intensity arose from gradual damping of the shock wave observed in the preliminary experiments (§4 of Chapter II). This is indicated by the fact that the brightness temperature of the front measured at different points in time coincided with the temperature of the gas after the front which was calculated by the velocities measured at the same points in time. The nonsteady shielding of the radiation described in the preceding section could also lead to

---

[1]The greater part of the lines on the moving image camera recordings are so weak that they did not print on Figure 44.

Table 4. Wave Lengths of Lines in the Emission of an Inert Gas Plasma

Line No	λ, Å	Identification	Line No	λ, Å	Identification
	Argon				
1	6562.85	H	8	4300.10	Ar
	6562.73	"		4272.17	"
2	6407	-		4277.55	Ar^+
3	6186	-		4266.29	Ar
4	5606.73	Ar	9	4259.36	"
	5572.55	"		4266.53	Ar^+
5	5559.62	"	10	4251.19	Ar
	5558.70	"	11	4200.68	"
6	4510.74	"		4198.32	"
	4522.32	"	12	4191.03	"
7	4323	-		4190.71	"
			13	4158.59	"
			14	3545.84	Ar^+
				3545.58	"

	Krypton			Xenon	
	4418.77	Kr	1	4193.15	Xe^+
1	4417.24	Kr^+	2	4180.10	"
	4416.88	Kr	3	3967.54	Xe
	4386.54	Kr^+	4	3948.16	"
2	4389.72	"	5	3083.54	Xe^{++}
	4385.27	"		3082.62	Xe^+
3	4369.69	"	6	3073.49	Xe^{++}
4	4351.36	Kr	7	3054.49	"
	4351.02	Kr^+			
5	4317.81	Kr^+			
6	4268.81	"			
	4268.57	"			
7	4259.44	"			

small additional reduction in the intensity. In this connection let us note that the reduction of the brightness temperature as the shock wave damps occurred faster than the reduction in the temperature of the gas behind the front calculated by the wave velocity. However, the accuracy of the measurements was insufficient to record these small differences with certainty (not exceeding ~2000°K). The absence of significant shielding is also indicated by the nature of the spectrum itself -- the presence of only weak absorption lines in it.

The buildup of the radiation intensity at the first point in time after the beginning of glow is explained by the fact that immediately afer exit of the detonation the layer of shock-heated gas is still very thin and emits volumetrically. Therefore the radiation intensity proportional to the thickness of the layer increases as the shock wave is propagated until the layer becomes optically dense. In experiments with xenon and krypton the buildup of the radiation intensity in the range of λ=220 to 450 nm occurred rapidly (judging by the spectral moving image camera recordings, in 0.6-0.1 microsecond). In the same time the radiation intensity built up in the range of λ=300 to 660 nm in experiments with argon. Inasmuch as time resolution on the spectral moving image camera recordings was 0.1 microsecond, the actual intensity buildup possibly occurred even faster. However, in the range of λ=220 to 300 nm the buildup time of the radiation intensity in the experiments with argon noticeably exceeded the time resolution, and for λ=220 nm it reached 2 microseconds. The radiation intensity from the front built up still more slowly in the experiments with neon; for example, for λ=450 nm, in 2 microseconds; for λ=260 nm, in 4 microseconds.

By the buildup of the radiation intensity after exit of the detonation it is possible to measure the radiation absorption coefficient in the shock-heated gas. The intensity of the radiation of the flat layer in the direction of the normal is

$$I = I_0(1 - e^{-\varkappa' d}), \tag{4.3}$$

where χ' is the absorption coefficient, d is the thickness of the layer, I_0 is the radiation intensity for $\chi' d \gg 1$ when the layer is optically dense. In turn, the thickness of the layer of shock-heated gas is

$$d = D \cdot t/\delta, \tag{4.4}$$

where t is the time after detonation exit, D is the shock wave velocity, δ is the gas compression in the wave. From (4.3) and (4.4) it is easy to obtain

$$\frac{\chi'}{\delta} = -\frac{1}{Dt}\ln\left(1-\frac{I}{I_0}\right). \qquad (4.5)$$

The variation of the intensity I/I_0 with time and also the wave velocity D are measured in the experiments. The gas compression δ can be calculated quite exactly from the shock ratios or measured directly in the experiment as Christian did [133]. The shock compression cannot be considered in general and the absorption coefficient χ'/δ found reduced to the gas density ahead of the front. Thus, the absorption coefficient of red light (λ=650 nm) was measured in shock-heated air by I. Sh. Model' [29]. The measurements were performed for two temperatures: χ'/δ=3.7 cm^{-1} for T=10900°K, χ'/δ=1.66 cm^{-1} for T=7480°C; the temperatures themselves were determined experimentally by the intensity I_0. Analogous measurements on emanation of the detonation from the TG 40/60 into the argon were performed by Roth [28]. In these papers the radiation of the individual sections of the spectrum was isolated by light filters and recorded by the moving image camera [29] or photomultiplier [28]. However, for detailed measurements of the absorption coefficients of heated gases it is more convenient to use the spectral moving image camera permitting a broad range of the spectrum to be encompassed in one procedure. Although in our experiments this problem was not specially stated and, in particular, the time resolution on the spectral moving image camera recordings was not always sufficient for performance of precise measurements, the results obtained are still of defined interest.[1] These results, just as the results of Roth are presented in Table 5.

[1] In his experiments I. Sh. Model' placed a metal plate between the explosive and the gas. As a result of this, on the one hand, mixing of the explosion products with the shock-heated gas was prevented, and on the other hand, the damping of the shock wave near the charge was less. The plate also separated the glow of the explosion products from the glow of the shock-heated gas (in experiments with inert gases the latter was ~10^2 times more intense). In the Roth experiments the plate was placed between the explosive and the gas only in a few control experiments and, as it turned out, had no significant influence on the measurement results. In our experiments the plate was not used.

Table 5.

λ, nm	600	500	450	400	300	230	Remarks
χ'/δ, cm^{-1}	8.8	7.4	6.2	5.2	-	-	Roth experiments [28]
χ'/δ, cm^{-1}	10	10	10	10	4	1	Our experiments with argon

In the experiments with neon the following values of the absorption coefficients were measured: $\chi'/\delta=1$ cm^{-1} for $\lambda=450$ nm and $\chi'/\delta=0.3$ cm^{-1} for $\lambda=260$ nm. For xenon and krypton in the entire investigated range of the spectrum $\chi'/\delta\geq 10$ cm^{-1}. In the experiment with krypton Roth [28] obtained a value of $\chi'/\delta=10.1$ cm^{-1} for $\lambda=450$ nm.

It is interesting to note that theory predicts an increase in transparency of the heated gas with a decrease in the radiation wave length λ, especially sharply manifested for $\lambda<\lambda_1$ when all of the excited levels are involved in the absorption. For argon and neon the limiting wave lengths λ_1 are 290 and 260 nm, respectively. The radiation intensity buildup time in the experiments increased rapidly with these values of λ.

Thus, the radiation intensity from the front initially built up as a result of an increase in the optical thickness of the heated gas; then it decreased as a result of damping of the shock wave. The distribution of the brightness temperature of the front with respect to the spectrum corresponding to the maximum radiation intensity is presented in Figure 40. The brightness temperature of the shock wave front in argon in the region of $\lambda=300$ to 600 nm was constant with respect to spectrum and it coincided with the gas temperature beyond the front calculated by the velocity on emergence of the detonation (D=9.4 km/sec). However, for $\lambda<300$ nm, a reduction in brightness temperature was observed. The reduction was caused by the fact that the time of formation of the optically dense layer of heated argon in this part of the spectrum was comparatively long and in this time damping of

the shock wave turned out to be noticeable. If we compare the brightness temperature not with the argon temperature at the first point in time after emergence of detonation, but with the temperature at the time of occurrence of the maximum radiation intensity, good agreement is obtained (see Figure 40). Two microseconds after emergence of detonation when the shock wave became optically dense in the entire investigated region, the brightness temperature was constant with respect to spectrum. For neon the buildup of the radiation intensity was still more prolonged than for argon, and the effect of the shock wave damping on the spectral dependence of the brightness temperature was also stronger. The buildup of intensity slowed sharply for $\lambda<260$ nm in neon and $\lambda<290$ nm in argon. Rapid decrease in brightness temperature occurred from these values of λ on approaching the ultraviolet end of the spectrum (see Figure 40).

For xenon and krypton the maximum in the spectral dependence of the brightness temperature is characteristic. The damping of the shock wave had no influence on the type of function, for the radiation intensity built up rapidly. The presence of the maximum is, in our opinion, connected with the peculiarities of the structure of the front in these two gases as a result of their high atomic weight and high temperature beyond the front. We shall discuss the interpretation of this and other experimental results in more detail in the following chapter.[1]

---

[1]It was noted earlier that the brightness temperature of the front in the visible part of the spectrum measured after the light filters is lower than the temperature of the shock-heated xenon even for comparatively low velocities D=4 to 10 km/sec. The spectral dependence in Figure 40 confirms these results. Let us also note that the decrease in brightness temperature toward the red end of the spectrum obviously continues also for $\lambda>450$ nm. Thus, according to the data of [41], the brightness temperature of the front for D=8.3 km/sec (corresponds to the emanation of detonation in xenon) is equal to 26000°K in red light.

The presence of absorption lines in the spectrum and the deviations in the spectral distribution of the radiation intensity indicate that the shock waves emit as a black body on emergence of detonation only in the roughest approximation. At the same time it is worthwhile to consider the results obtained without going into all of the details. The intensity of the radiation from the front was determined primarily by the gas temperature after the front which increased on going to gases with larger atomic weight.[1] The increase in temperature as a result of an increase in the atomic weight of the gas frequently was felt in the fact that the shock wave velocity on emanation of detonation into heavier gases decreased. Thus, if on going from neon to xenon the velocity did not change, then the temperature after the front would be 50000°K. The temperature of 40000°K obtained on emanation of detonation in xenon is quite high. The possibility of obtaining higher temperatures and larger radiation fluxes on emanation of detonation into heavy inert gases constantly attracts reseachers to this type of experimentation. Special hopes in this respect come from the use of more powerful explosives. Accordingly, let us note that in two experiments with argon instead of TG 40/60 hexogene was used pressed to a density of 1.74 g/cm^3. The intensity of the visible radiation in these experiments was 10% higher, and ultraviolet, 15-20% higher.

The measurements of the spectral brightness most completely characterize the radiative properties of shock waves. With respect to intensity of the visible

---

[1]Comparing the results of the measurements for different gases to each other, it is necessary to consider that the error in the relative measurements was three times less than the error in the absolute measurements noted in Figure 40. Let us also note that the dispersion of the experimental points from experiment to experiment reached the error in the absolute measurements (in Figure 40 the curve for each gas is averaged with respect to three experiments), but the relative arrangement of the experimental curves was retained.

radiation on emanation of the detonation from the TG 40/60 into argon, Roth [28] measured the brightness temperature of the shock wave. In his experiments the radiation was isolated by narrow interference light filters, and it was recorded by a photomultiplier. The brightness standard was a tube with a strip of tungsten. The following values of the brightness temperature were measured at the time of maximum intensity.

λ, nm	600	500	450	400
T, °K	31,500	30,000	29,000	29,000

The error in the measurements was estimated at $\pm$1000°K (except the section with λ_{eff}=600 nm where the error was larger). The spectral distribution of the radiation intensity corresponded to the color temperature of the front of 29000$\pm$ 1000°K. In the experiment with krypton the brightness temperature of the front in the section with λ_{eff}=450 nm was 38000°K.[1] The results obtained by Roth and the results of our experiments compare with each other within the limits of error.

Conger, et al. [7] measured the color temperature of the front by the ratio of the intensities of ultraviolet and visible radiation on emanation of the detonation into argon. In these experiments the shock wave excited on explosion of spherical pentolite or cyclonite charges (explosive filler to TG 40/60). The ultraviolet radiation λ=230 to 300 nm was separated by a liquid filter and recorded using a luminophor and photomultiplier. The color temperature of the front turned out to be 20000°K. The spectral function in Figure 40 corresponds in this case to the color temperature of the front of 19000°K.

---

[1] In this unique experiment the couvette was first filled with argon which was then displaced by krypton. As a result of the limited amount of krypton it was not certain that it forced all of the argon out.

Thus, using our data it is possible, at first glance, to relate the results of references [7, 28] which do not agree with each other.

Anderholm [30] measured the integral density of the radiant energy flux from an explosion in argon for the section of λ=200 to 600 nm. In his experiments a cylindrical shock wave was used, the velocity of which dropped from 9.3 to 5 km/sec during the time of recording the radiation. The flux density from the front measured using a photomultiplier varied from $5 \cdot 10^5$ to $1 \cdot 10^5$ watts/cm^2. The maximum flux density in the Anderholm experiments correspond, according to our estimates, to the integral brightness temperature of the front of 23000°K. Comparing this value with the results presented in Figure 40, it is necessary to consider that the primary contribution to the radiant energy flux was made by the ultraviolet radiation. In this region of the spectrum the brightness temperature in our experiments was lower, and it was on the average the same 23000°K.

Taylor and Kane [31] measured the brightness temperature of the front on emanation of detonation from TG 40/60 to argon. The shock wave velocity in the experiment varied within the limits of 9 to 8 km/sec. The radiation was divided by gas plates into two photomultipliers, bypassing the light filters with effective wave lengths of λ_{eff}=545 and 405 nm and halfwidth $\Delta\lambda$=20 nm. The brightness standard was a pulsed gas discharge tube. The measurements for different sections of the spectrum gave identical results. The brightness temperature of the front in the experiments varied within the limits of 26000 to 21000°K. The reduction in brightness temperature is connected with damping of the shock wave. The maximum value of 26000°K coincides with the results of our measurements within the limits of error.

One of the first measurements of the color temperature of the front of shock waves formed during explosions was performed by Stettbacher [27]. The

shock wave was excited on emergence of the detonation from the explosive (tetranitromethane+toluene) which is similar with respect to effect to the TG 40/60. The color temperature of the front in visible light was 27000°K for argon.

Thus, it is possible to prove good coincidence of the results of our measurements with the data of other authors. The distribution of the brightness temperature presented in Figure 40 has bound the available disparate results together pertaining to the different sections of the spectrum and obtained in different ways.

A comparison of the results of the papers known to us would be incomplete if we did not discuss the radiation spectra of shock waves presented by a number of authors. Conger, et al. [7] recorded the explosion radiation in argon in a spectrograph. The radiation spectrum turned out to be continuous with powerful argon lines superposed on the late stages of the explosion when the shock-heated gas expanded and luminesced volumetrically. Roth [28] and Anderholm [30] mention obtaining time-resolved spectra on emanation of the detonation into argon. The spectra were continuous. Roth notes the appearance of absorption lines 3 microseconds after emergence of detonation. The results of such experiments were described in more detail by Taylor and Kane [31]. The spectrum was recorded in the range of λ=400 to 700 nm. Weak absorption lines and radiation were observed against the background of the continuum. In this paper a spectral moving image camera recording is presented on which the absorption lines arising simultaneously with the continuum are visible.

4. Instability of the Flat Front When Shock Waves Move in Channels

In 1954 Shreffler and Christian [151] described experiments in which they observed bending of the plane front during propagation of a shock wave in a tube. The shock wave was generated after discharge of a plane detonation wave from an explosive to a boundary with a gas. The shock wave was propagated through the tube over a period of several microseconds, maintaining a plane front. But a difference between the velocity of all sections of the front adjacent to the tube walls and the velocity of the front in the central part of the tube then occurred suddenly. The front was propagated more rapidly near the walls and "ran ahead" with respect to the remaining part of the front (Figure 45). The front easily seen in Figure 46 acquired this shape. Upon further motion, the shock wave was gradually attenuated and the front again became plane. Experiments were conducted with different gases, but bending of the front near the tube walls was observed only with those gases in which high temperatures were reached behind the front (argon and chlorine). This circumstance served as the basis for the hypo hesis that bending of the front is related in some manner to heating of the tube walls and the gas adjacent to them by the shock wave radiation. Other characteristics of the phenomenon, for example, disappearance of bending as the shock wave was attenuated or an increase of the time between formation of the shock wave and the occurrence of bending with a decrease of tube cross section, also became understandable with this explanation. Shreffler and Christian varied their experiments. Specifically, a wire was extended along the tube and then bending of the front in the direction of motion of the shock wave was observed near it, as near the walls of the tube. Experiments in which different obstacles were placed in the path of the shock wave are of great interest. Thus, it was possible to establish that bending near the walls has a sharply defined front and significant destructive force.

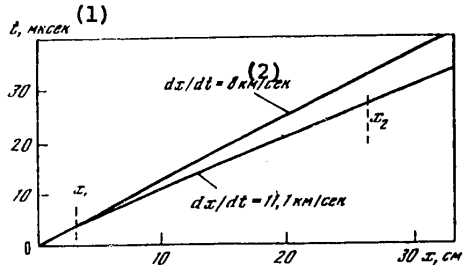

Figure 45. "x-t" Diagram of Shock Wave Motion in Tube Filled With Argon: at $x > x_1$, the velocity of the front near the tube walls increases intermittently and on the section $x_1 < x < x_2$ comprises 11.1 km/s (10 km/s at $x > x_2$). The plane front not affected by wall disturbances propagates at velocity of 8 km/s

Key:
1. Microseconds
2. km/s

The shock wave velocity did not exceed 9 km/s in Shreffler and Christian's experiments and the problem of which shape a front of stronger shock wave acquires remained unclear. The investigations of Yu. A. Zatsepin et al [42] provided the

answer to this question. Moreover, we detected a significant effect of the instability of a plane front on the radiating properties of strong shock waves.

Development of a section of front near the cuvette walls, sharply differing in brightness, was observed in the first experiment with argon and helium set up to investigate the radiating properties of strong shock waves in these gases. The brightness temperature of this formation hardly varied over the entire investigated range of shock wave amplitudes and was comparatively low: 15,000-25,000°K in experiments with argon and 25,000-35,000°K in experiments with helium. Within 5-10 microseconds the bright central section of the front disappeared completely, being absorbed by this formation (Figures 28 and 47). This decrease of radiation intensity could not be the result of the small optical thickness of a shock-heated gas. In the given case a smooth decrease of radiation intensity at an angle of 45° was not observed as it approached the wall of the cuvette, as occurred at comparat vely low shock wave velocities. The intensity decreased intermittently and was identical for radiation at an angle of 45° and for normal radiation. Due to recording of radiation emerging at an angle of 45° to the cuvette axis, it was possible to measure separately the velocities of the bright and diffuse sections of the front. It turned out that the brightness of the front near the walls is approximately 20 percent higher than that in the central part of the cuvette. It immediately became obvious that this difference of velocities should lead to bending of the front. Specially run experiments confirmed this hypothesis. We made use of the circumstance that the glow was cut off at the moment the shock wave touches the end window of the cuvette to investigate the shape of the front.* The moments of arrival of different sections of the front to the end window of the cuvette were recorded by cutoff of the glow in the experiments. Knowing the time difference of arrival of individual sections of the front and the velocity of the front, it is easy to restore its shape. To follow the variation of shape of the front during motion, the end window was placed at different distances from a diaphragm, after rupture of which a plane shock wave was generated in the cuvette.

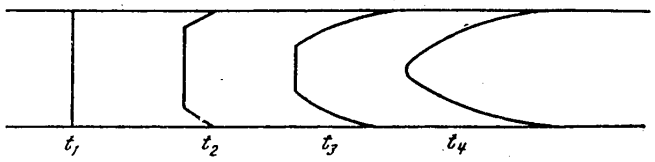

Figure 48. Bending of Front During Motion of Strong Shock Wave in a Channel

The results of these experiments are qualitatively illustrated by Figure 48. The front plane the first 1-2 microseconds after generation of the shock wave near the walls began to be bent in the direction of motion. This process was especially

* A slight surge and then a sharp surge within approximately 0.1 microsecond was observed when a strong shock wave was reflected from the window and there was a decrease of radiation intensity. Cut-off of the glow was apparently caused by breakdown of the transparent material of the window.

intensive if the temperature behind the front exceeded 30,000°K. The plane section of the front then disappeared completely within 5-10 microseconds. The front acquired a funnel shape which was maintained during subsequent motion. The brightness temperature of this front was approximately constant, 15,000-17,000°K, over the entire area in experiments with argon (it was somewhat higher, approximately 25,000°K) in the ultraviolet section) and was 25,000-30,000°K in experiments with neon and helium. The experimental conditions were sometimes such that the shock wave attenuated rapidly during propagation in a cuvette. If the shock wave velocity decreased to 7-8 km/s in argon or to approximately 20 km/s in helium, then the front again became plane and the front immediately became equalized over its entire surface. A front when at least a small plane section remained in the central part of the cuvette was equalized in a completely different manner. In this case the entire process proceeded in opposite order--the plane bright section increased while the diffuse bent section near the cuvette walls decreased until it disappeared completely. Yet another characteristic feature should also be noted--some increase of brightness temperature of the plane section of the front near the boundary with the bent section. Although the difference was slight, only approximately 3,000°K, it was always distinguished on a background of random fluctuations of brightness temperature along the surface of the front. The distribution of the brightness temperature of the front through the diameter of the cuvette reflecting this characteristic is given in Figure 49.

Unique deformation of the front was observed in those experiments in argon where the shock wave was created upon detonation of an explosive rod placed in a steel tube. A shock wave with brightly illuminated plane front was initially propagated in the channel formed by the tube walls and the rod. But slightly illuminated bends, which increased and soon encompassed in the entire front, occurred both near the tube walls and near the rod within approximately 5 microseconds.

Bending of the front of strong shock waves was also recorded in experiments with other gases. In experiments with xenon this process proceeded more slowly at identical temperatures behind the front than in argon or helium. This significant difference of brightness of the plane and bent section of the front was not observed. An increase of brightness temperature was frequently recorded near the walls of the cuvette prior to the occurrence of bending.

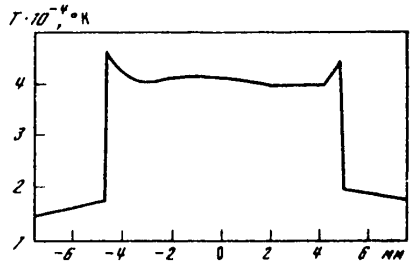

Figure 49. Distribution of Front Temperature Along Cuvette Diameter in One of Experiments With Argon (D = 14 km/s)

The results of experiments in which the cuvettes were filled with argon with an air impurity are of special interest. In this case a front with insignificant bending

near the walls (as at moment t_2 in Figure 48) was established during motion of the shock wave. The fact that the presence of an air impurity in argon prevented bending of the front quite specifically indicates the important role of radiation in th the occurrence of instability of a plane front. Estimates show that air absorbs approximately 70 percent of the radiant flux going to the area of transparency of pure argon near the front with shock-heated gas temperature of 30,000°K.

The instability of the plane front was generally not observed in air over the entire investigated range of shock wave amplitudes. Only very slight bending of the front occurred near the walls without variation of brightness. The hypothesis was made that the instability of the front in air could not be manifested within the 15-20 microseconds during which the shock waves in our experiments propagated along the cuvette. One can conclude from the experiments with inert gases that an increase of shock wave amplitude and of the cuvette cross section contributes to instability. The time between excitation of a plane shock wave and the occurrence of bending of the front was reduced in this case. A special experiment was set up in regard to all this. A shock wave in air with velocity of 14 km/s, produced upon detonation of a shaped charge, was propagated along a long steel tube 18 mm in diameter within 50 microseconds. The brightness temperature of the front was measured in the region of the spectrum at λ_{ef} = 432 nm. During the first 30 microseconds the brightness of the front was identical over its entire surface. The measured value of brightness temperature of 25,000°K coincided with the calculated temperature of the gas behind the front. However, slightly illuminated sections with brightness temperature of 15,000°K then occurred near the tube walls. Slightly illuminated sections, upon increasing, encompassed the entire front within another 15 microseconds. The front had a funnel shape (as at moment t_4 in Figure 48) at the moment the shock wave was reflected from a window installed on the end of the tube. Thus, the instability of a plane front can also be manifested in air under specific conditions.

In experiments with reduced argon pressure, the instability of the front was manifested more strongly than in experiments with argon at atmospheric pressure. The front in these experiments, being bent near the walls in the direction of motion, frequently acquired an irregular shape. Photochronograms of two of these experiments are presented in Figure 50. One can judge the shape of the front at the moment the shock wave is reflected from the window of the cuvette by the cutoff of the glow.

The effect of the wall material on the development of instability was observed in the experiments. A plane front was usually deformed more slowly in steel tubes than in glass tubes. This process proceeded even more slowly in glass tubes lined inside by polished aluminum foil.

The results of experiments in which instability of the plane front was observed during propagation of shock waves in channels was stressed repeatedly among a number of specialists. The most contradictory opinions were advanced with respect to the nature of this phenomenon. In most cases attempts were made to explain the occurrence of bending by friction of the gas against the wall. However, it remained unclear how friction could lead not to a decrease but rather to an increase of the velocity of the front near the wall. Hypotheses were also advanced that

the front bends due to reflection of the shock wave from the wall. As is known, during inclined impingement of a shock wave on a rigid obstacle, so-called Mach reflection occurs in which the front bends near the surface in the direction of propagation of the wave. The possibility of this flow was first linked to the presence in the experiments of a unique conical channel formed by the broken-down walls of the cuvette that flew in all directions. But this explanation had to be rejected after the instability of the plane front was recorded in experiments with thick-walled steel tubes which did not break down. Authors have recently tended to assume that the flow converging with transient Mach reflection could occur due to the presence of a layer of heated gas near the wall.

Comparison of the results indicates that the instability of a plane front is caused by heating of the walls and the gas adjacent to it by the shock wave radiation. The phenomenon was observed only at sufficiently high temperatures behind the front and consequently at high radiant fluxes from the front. The instabilities developed more rapidly in helium, argon and xenon than in air. Actually, inert gases with their high ionization potential are more transparent to ultrabiolet radiation than air, which absorbed a considerable fraction of the radiation of a shock-heated gas before the front. Thus, helium absorbs only approximately 2 percent of the Planck energy flux at a temperature of 30,000°K behind the front, argon absorbs 13 percent, xenon absorbs 29 percent and air absorbs 71 percent. Even more convincing of the relationship of the phenomenon to shock wave radiation is the fact that a slight addition of air to argon prevented the development of the instability. The thermodynamic characteristics of the gas in a shock wave, specifically the temperature behind the front, essentially did not change in this case, but the optical characteristics of the gas before the front varied considerably. Air absorbed a considerable part of the radiant flux from the front and consequently heating of the walls and the gas adjacent to them by radiation decreased.

We note yet another characteristic of the phenomenon--bending of a plane front increased earlier and proceeded more rapidly with an increase of cuvette diameter. Actually, the radiant flux density on the walls decreased more slowly as the distance of the wave front increased with large cuvette diameter than in small-diameter cuvettes. Therefore, the gas near the walls in large-diameter cuvettes was heated more strongly by the moment the shock wave arrived. The effect of the wall material, observed in experiments, was apparently determined by heat dissipation, more intensive in the case of metal walls.

It is very difficult to estimate at which temperature the cuvette walls were heated by radiation. Experiments will be described in Chapter 6 in which intensive evaporation of different materials, including metals, was observed due to the effect of shock wave radiation. The effect of radiation was weaker in the experiments described here due to the small cuvette dimensions. The temperature of the inner surface of cuvettes rather did not reach the boiling point but even so was rather high.* The temperature of a narrow layer of gas coming into contact with the wall may be even higher since energy transfer by the electrons formed during the photoeffect from the surface occurred along with ordinary thermal conductivity.

*It was noted in [151] that nails placed into the tube were heated to incandescence due to the effect of shock wave radiation.

According to some data [148], these "hot" photoelectrons may carry off up to approximately 10 percent of the incident radiant energy.

Assuming a decrease of gas density ρ_0 near the wall due to heating and constant pressure p_1 in the plug of a shock-heated gas due to the subsonic nature of flow behind the shock wave front, it is easy to explain the increase of front velocity near the wall. The following relation is valid for a strong shock wave

$$p_1 = \frac{2}{\gamma + 1} \rho_0 D^2. \tag{4.6}$$

In order that pressure p_1 be identical at all points behind the front, a decrease of gas density ρ_0 near the wall should be compensated for by an increase of velocity D.

Based on these concepts, the authors are tempted to artificially induce bending of the front near the axis rather than near the walls of the cuvette. To do this, the output end of the cuvette was smoothly joined to an expansion nozzle. The configuration of the channel was such that the cuvette walls were partially shaded against radiation of the shock wave initially propagating through the nozzle. Absorbing ultraviolet radiation by impurities, the argon in the cuvette was heated and it was heated more strongly near the axis. A sharp discharge of the front near the axis was observed in these experiments.

Shreffler and Christian [151] gave a somewhat different interpretation of the experimental results that they obtained. They link the occurrence of bending to heating, radiation and rapid expansion of the gas adjacent to the wall. Acting similar to a piston, the expanded gas, they feel, forms a secondary shock front adjacent to the shock wave front near the tube wall. Reference is made in this case to the fact that a sharply defined luminous front occurred above a target placed in the tube even before the arrival of the shock wave. But investigations [9, 11] showed that the occurrence of this glow was caused by evaporation and subsequent ionization of the target material.

The target in these types of experiments was located normally to the incident flow and therefore was subjected to a more powerful effect than the walls. But nevertheless the velocity of the luminous vapor boundary was always somewhat lower than the propagation velocity of disturbances from the tube wall to its axis. Bending

---

* Interesting data that confirm these ideas of the mechanism of disturbances near the wall were kindly presented by V. V. Adushkin to the authors. Experiments were conducted in which the shock wave of an explosion propagated along steel plates. The shape of the wave front was recorded by a system of pressure piezosensors. Radiation of the wave could not be taken into account since its amplitude was comparatively small. The plate was first brought to red heat by a burner and bending of the front near the surface in the direction of motion of the shock wave was then observed. G. I. Taganov first explained the "thermal layer" effect (see [172]).

of the front in a tube lined on the inside with aluminum foil could be observed in the same experiment, whereas a luminous region did not occur above a target of the same foil placed in the tube. All this indicates the difference of phenomena coming into play during interaction of a strong shock wave with the wall of a channel, on the one hand, and upon irradiation of solids by a powerful luminous flux, on the other hand.

Some features make the phenomenon of instability of a plane front similar to that of transient shielding of the radiation of the front described in Section 2, Chapter 4. They were both observed in experiments with inert gases and almost always simultaneously. The typical times of development of the processes coincide by an order of magnitude. The dimensions of the cuvette affected the course of the processes in both cases and this effect was identical--the course of the processes slowed down with an increase of cuvette diameter. Both one and the other phenomenon led to a significant decrease of the brightness of the shock wave front. The difference here is perhaps only quantitative--bending of the front was accompanied by a more significant decrease of brightness. There is also similarity of the phenomena in the fact that transient shielding was manifested most frequently in the form of dark spots which, spreading, encompassed the entire front. A unique feature existed which made it possible to confidently separate these two phenomena if the shape of the front was not monitored during the experiment. Bending was always distinguished by a sharp drop of brightness on the boundary with the plane section of the front while clear boundaries had no spots.

Based on the internal similarity of the two phenomena, it is interesting to suggest that they are essentially the same phenomenon. An important confirmation of this would be achieved if the occurrence of dark spots could be related to deformation of the front. The section of the front on photochronograms not affected by wall bending seemed to be only approximately plane. However, we were unable to establish any correspondence between the spots and the uneven surfaces of the front.

It is difficult to judge the extent to which one or another details are significant when the nature of the phenomena has not yet been finally determined. The question remains open whether the disturbances caused by heating the gas near the wall are capable of leading to total disappearance of the plane front, as was observed in experiments.* Although further investigations are required to determine the mechanism of interaction of a strong shock wave with the channel wall, already available experimental material permits one to make two important conclusions. First, the flow mode with a plane shock front is not stable and is replaced by a flow mode with convex, funnel-shaped front during propagation of strong shock waves in channels. A number of problems (attenuation of shock waves in channels, their effect on obstacles placed in the channels and so on) has not yet been resolved in practic tice, for which the result is of considerable interest. Second, conversion to a

*At one time S. P. D'yakov [152] noted that a flow with a plane shock front is in itself not always sufficiently stable. The criteria of stability which he derived to small disturbances can be violated under certain conditions (specifically, upon dissociation and ionization of the gas behind the front).

flow mode with convex front is accompanied by a significant decrease of the radiating capability of the shock wave. This circumstance should be taken into account when the question arises of the luminous effect of a strong shock wave, especially when designing explosive sources of radiation.

EVALUATION OF THE INFLUENCE OF THE FRONT STRUCTURE ON SHOCK WAVE RADIATION

Moscow IZLUCHATEL'NYYE SVOYSTVA UDARNYKH VOLN V GAZAKH in Russian 1977

[Chapter 5 from the book "Radiating Properties of Shock Waves in Gases," by M.A. Tsikulkin and Ye. G. Popov, Izdatel'stvo "Nauka," 173 pages]

[Text] During the propagation of a shock wave, a sharp, discontinuous variation of the parameters of the medium -- pressure, density and temperature -- takes place. The shock wave, the amplitude of which at distances of several radiation path lengths varies insignificantly; it almost repeats the classical example of an absolutely black radiator: the optically dense region of uniformly heated material is bounded by a surface with a sharp temperature discontinuity. All of the differences from the radiation of a black body are determined in the given case by the nature of variation of the parameters of the medium in the wave front, that is, the structure of the front.

Shock compression and heating of the gas take place in a very narrow layer, the so-called viscous shock compression. The width of the layer is comparable to the free path length of the gas molecules. Inasmuch as the radiation path length is several orders higher under the same conditions, the layer is transparent and has no influence on the shock wave emission.

In high-amplitude waves, dissociation, ionization and other processes leading to the establishment of thermodynamic equilibrium in a heated gas take place after the short-term shock compression. These processes also determine the structure of the transition layer. In the conclusions with respect to the influence of the layer on the shock wave emission caution must be exercised, for the

width of the layer approaches the path length of the radiation in the heated gas.

In addition, with an increase in weight amplitude the radiant flux from the shock-heated gas increases rapidly, and beginning with some amplitudes it makes up a noticeable proportion of the hydrodynamic energy flux in the wave. The radiant heat exchange changes the structure of the front significantly. The gas cools after viscous shock compression, radiating. Partially absorbing this radiation, the cold gas is heated before the shock compression. The width of the transition layer now is determined by the radiation path length -- the largest scale of length. The structure of such a layer has the most direct influence on the radiative properties of the shock wave.

However, before analyzing the effect of the front structure, it must be emphasized that even in the simple approximation of a temperature discontinuity the shock wave is not identical to an absolutely black radiator. Light is reflected from the front of the wave, just as from the interface of two media that are different in optical respects -- a shock compressed heated gas and the cold gas before the front. The estimates proposed below indicate that this fact sometimes must be taken into account.

Let us use the simple expression for the reflection coefficient with a normal decrease in light

$$r = \left(\frac{n_1 - n_0}{n_1 + n_0}\right)^2, \tag{5.1}$$

where n_1 and n_0 are the indexes of refraction of the gas on both sides of the wave front (for example, in air of normal density n_0=1.0003 for visible light). The relation of the index n to the gas density ρ is described by the expression

$$n = 1 + K\rho,$$

where K is the Gladstone-Daly constant, or the specific refraction. Even with tenfold shock compression of the air $n_1=1.003$ and the reflection coefficient turns out to be negligibly small $r=2\cdot10^{-6}$.

In reality, the reflection coefficient is still smaller, for a real shock wave is not an ideal discontinuity. Such an approximation is valid only in the case where the thickness of the front is much less than the light wave length. In gases of normal density the thickness of the viscous shock compression is on the order of 10^{-5} cm, that is, comparable to the wave length of visible radiation. In this case the reflection coefficient depends strongly on the structure of the transition layer. The latter fact was used by Horning, et al. [153, 154] when he investigated the structure of the front of weak (Mach number 2-4) shock waves. They compared the values of the reflection coefficients calculated for different angles of incidence and under different assumptions with respect to the structure of the front with the values measured experimentally. The primary difficulty consisted in measuring the reflection coefficient which, as was expected, turned out to be very small -- within the limits of 10^{-5} to 10^{-7} for different gases.

Thus, it is possible to neglect the reflection of the light in shock waves of small amplitude. Usually weak shock waves do not emit as an absolutely black body for another reason -- as a result of transparency of the volume of the shock-heated gas. Powerful shock waves in which ionization of the gas takes place after compression (causing their intense glow) are of the greatest interest to us. The presence of free electrons greatly decreases the index of refraction of the gas. The propagation of electromagnetic waves in a plasma is determined by the value of the dielectric constant which in the absence of a magnetic field has the form

$$\varepsilon = 1 - \frac{4\pi e^2 N}{m_e \omega^2} \frac{1}{1 - i\frac{\nu}{\omega}}, \tag{5.2}$$

where ω is the angular frequency of the electromagnetic wave, N is the number of charged particles per cm^3 of plasma, γ is the frequency of the electron collisions in the plasma. It is possible to find the collision frequency from the formula

$$\gamma = \frac{2 \cdot 10^{-6} N_i Z}{T_e^{3/2}(\nu e)}.$$

For plasma the magnetic permeability $\mu=1$ so that the index of refraction $n=\sqrt{\varepsilon}$. Inasmuch as the imaginary part of the dielectric constant corresponds to the absorption of the radiation, when calculating the index of refraction only the real part is taken into account.

Let us consider an example which is characteristic of our experiments. A shock wave with a velocity D=14 km/sec is propagated through air of normal density. The gas behind the front is tenfold compressed, heated to a temperature of 25000°K, completely dissociated and singly ionized (Z=1, $N=10^{21}$ cm^{-3}). From (5.2) and (5.1) for the reflection coefficient of red light with $\lambda=6.5 \cdot 10^{-5}$ cm we obtain r=0.2%; for infrared radiation with $\lambda=1.3 \cdot 10^{-4}$ cm r=0.5%. If the air in the wave is heated to 50000°K (D=23 km/sec), second ionization occurs (Z=2). Under these conditions we obtain r=1% for red light and r=6% for infrared radiation.

Thus, with an increase in the shock wave amplitude the reduction coefficient increases. Inasmuch as formula (5.1) does not take into account the thickness of the front, it is possible to expect only significant reflection of the infrared radiation, the wave length of which is greater than the front width. Noticeable reflection from the front of the electromagnetic waves from the adjacent superhigh frequency region is known to researchers studying plasma in shock tubes. In our experiments the plasma approached metals with respect to the free electron

concentration. Therefore the effects connected with distortion of the radiation during reflection must be manifested more strongly.[1]

§1. Effect of the Relaxation Layer

In powerful shock waves, the relaxation layer in which ionization, dissociation, electron excitation and other processes develop leading to the establishment of thermodynamic equilibrium in the shock-heated gas, is adjacent to the viscous shock compression. Usually the width of the layer is determined by the ionization relaxation of the gas as the slowest process. The possibility of shielding the radiation of the equilibrium-heated gas behind the front by this layer was noted by the authors of [13, 32]. Let us consider this problem in more detail here.

For estimation of the layer width let us use the paper by M. B. Zheleznyak and A. Kh. Mnatsakanyan [73] in which the data were gathered on the structure of the relaxation layer of shock waves in the air. With a wave velocity D=14 km/sec recalculated for the initial air pressure p_0=760 mm Hg, the width of the layer is $\ell=7\cdot10^{-5}$ cm.

Now let us note the radiation path length under these conditions. The coefficient of photoionization absorption will be found by the Biberman-Norman formula [91]

(5.3)

where N_0 is the number of atoms per cm^3 of ionized gas; $\xi=\xi_0(\nu, T)$ is the factor taking into account the nonhydrogen-likeness of the absorption cross section by the excited atoms (Figure 51); γ is the ratio of the number of halflevels of the atom corresponding to the given quantum numbers n and ℓ to the analogous value

[1] It is known that the incandescent metals do not emit as an absolutely black body as a result of the reflection of light from the interface.

for the hydrogen atom; Σ_0 is the statistical sum of the states of the atom. The braking absorption coefficient will be found by the Kramers formula

$$\varkappa_{\nu 2} = 3{,}69 \cdot 10^8 \frac{Z^2 N_i N_e}{T^{1/2} \nu^3} \text{ см}^{-1}. \tag{5.4}$$

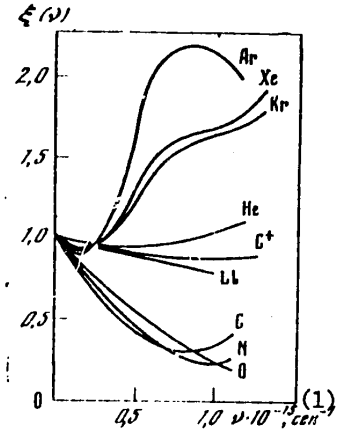

Figure 51. Calculation of the coefficient of photoionization absorption by heated gases. Values of the factor ξ by the data of [92, 100]

Key:
1. sec^{-1}

In order to consider the effective decrease in the absorption as a result of forced emission (see §1, Chapter III), the total absorption coefficient is multiplied by $1-e^{h\nu/kT}$. Then for the radiation path length we have

$$1/l_\nu = (\varkappa_{\nu 1} + \varkappa_{\nu 2})(1 - e^{h\nu/kT}). \tag{5.5}$$

For example, let us calculate the path length of a quantum of red light $\lambda = 6.5 \cdot 10^{-5}$ cm ($\nu = 0.46 \cdot 10^{15}$ sec^{-1}). Here, according to [91] in formula (5.3) the factor $\xi = 0.5$. The splitting of the levels on nitrogen and oxygen is $\gamma = 15$ judging by [155]. The concentrations of the atoms, ions and electrons will be taken from tables in [147]. After substitution of the numerical data in (5.3)-(5.5), we obtain $l_\nu = 6 \cdot 10^{-4}$ cm.

As is obvious from the presented estimates, the path length of a quantum of red light is an order larger than the thickness of the relaxation layer. For radiation with a shorter wave length the path length is still longer so that the

layer shields the visible and near ultraviolet radiation weakly. On the contrary, in the infrared region of the spectrum the shielding is significant. Thus, for $\lambda=1.3\cdot10^{-4}$ cm the estimates give the path length of $\ell_\nu=10^{-4}$ cm comparable to the layer thickness. Even if we consider that in the relaxation layer the concentrations N_i, N_e and the electron temperature T are lower than behind the front and we take the values that are half the equilibrium values as the average for the layer, we obtain $\ell_\nu=2\cdot10^{-4}$ cm. In the last example the optical thickness of the layer is

$$\tau=\int_0^l \varkappa_\nu dx=\underset{(1)}{\varkappa_{\nu\,\text{средн}}}\int_0^l dx=\frac{l}{l_\nu}=0{,}3. \tag{5.6}$$

Key: 1. average

The intensity of the radiation normal to the front must decrease noticeably after passing through the layer

$$I=I_0e^{-\tau}=0{,}7I_0. \tag{5.7}$$

The oblique beams will be attenuated still more strongly.

Now let us see how the shielding capacity of the layer varies on variation of the shock wave amplitude. With a decrease in amplitude, the temperature of the shock heated gas decreases, and the radiation path length increases very rapidly. As for the width of the layer, in the velocity range of D=5 to 14 km/sec it varies nonmonotonically. The largest value of $\ell=5\cdot10^{-4}$ cm is reached for D=10 km/sec. However, the radiation path length turns out to be much greater (estimates by the gas parameters behind the front give $\ell_\nu=10^{-2}$ cm for $\lambda=6.5\cdot10^{-5}$ cm and $\ell_\nu=2\cdot10^{-3}$ cm for $\lambda=1.3\cdot10^{-4}$ cm). Consequently, with a decrease in the shock wave amplitude the relaxation layer becomes more transparent.

For the velocities D>14 km/sec the information about the ionization structure of the front is extremely meager. V. A. Bronshten and A. N. Chigorin [18] performed the calculations for three values of the velocity D=16, 47 and

75 km/sec. For the initial concentration of the atoms after dissociation $N_0=10^{20}$ cm^{-3} and a velocity D=16 km/sec the relaxation time will be $t=3\cdot10^{-9}$ sec. If the shock wave is propagated through air of normal density, then after compression and dissociation in the wave front the initial atom concentration $N_0=3\cdot10^{20}$ cm^{-3} and, correspondingly, $t=10^{-9}$ sec. Let us estimate the width of the relaxation layer as follows:

$$l = tD/\delta,$$

where δ is the average compression of the gas for the layer. After dissociation of the air $\delta=6$, and the equilibrium value of $\delta=11$. As the average let us take $\delta=8$. Then the width of the layer $l=2\cdot10^{-4}$ cm. Now let us estimate the radiation path length. As the averages for the layer let us take the values of the charged particle concentrations and temperature half the equilibrium values. Then the calculations by (5.3)-(5.5) give $l_\nu=6\cdot10^{-4}$ cm for $\lambda=6.5\cdot10^{-5}$ cm and $l_\nu=10^{-4}$ cm for $\lambda=1.3\cdot10^{-4}$ cm.

Thus, with an increase in the wave amplitude the radiation path length approaches the width of the relaxation layer. In order to be convinced of this noteworthy trend, let us also consider the results of estimates for a shock wave with a velocity D=47 km/sec. In this case the ionization relaxation time (for $N_0=10^{20}$ cm^{-3}) will be $t=6.4\cdot10^{-10}$ sec. In the recalculation for normal air density ahead of the front $t=3\cdot10^{-10}$ sec, and the layer width $l=2\cdot10^{-4}$ cm (it is of interest to note that although the relaxation time has decreased, the layer width does not change). According to the data of [18], setting the averages for the layer $N_e=10^{21}$ cm^{-3}, $N_i=5\cdot10^{20}$ cm^{-3}, $Z^2=4$ and $T_e=6\cdot10^4$ °K, we obtain $l_\nu=10^{-4}$ cm for $\lambda=6.5\cdot10^{-5}$ cm and $l_\nu=6\cdot10^{-5}$ cm for $\lambda=1.3\cdot10^{-4}$ cm. The radiation path length now is less than the layer thickness.

Let us collect the results of the estimates together; the degree of transparency of the relaxation layer will be characterized by its optical thickness $\tau \approx \ell/\ell_\nu$.

D, km/sec	10	14	16	47
$\tau(\lambda=6.5\cdot10^{-5}$ cm)	0.02	0.06	0.3	2
$\tau(\lambda=1.3\cdot10^{-4}$ cm)	0.1	0.3	2	3

From the presented data it is obvious that as the wave amplitude increases the relaxation layer becomes less transparent for radiation of the equilibrium heated gas behind the front. The shielding first begins in the infrared region of the spectrum, and at sufficiently high amplitudes it extends to the visible region.

In experiments at high velocities the brightness temperature of the front was noticeably below the air temperature behind the front (see Figure 30). In red light this difference occurred at velocities of D=10 to 35 km/sec. In yellow, blue and violet sections of the spectrum the lagging of the brightness temperature occurred at somewhat higher velocities D=25 to 35 km/sec. The lagging of the brightness temperature and also the difference in brightness of the front at different angles recorded experimentally indicate the shielding of the radiation in powerful shock waves. Up to now this phenomenon was explained by the shielding effect of the heated layer which is formed on absorption by cold gas ahead of the short-wave radiation front of the shock wave. However, by the estimates of Yu. P. Rayzer and Ya. B. Zel'dovich [34-37]. This shielding becomes noticeable only at the air temperature behind the front $T_1=9\cdot10^4$°K (D=36 km/sec). At this temperature the intensity of the red light emerging normally to the front must be attenuated by 12%. In the experiment the intensity is attenuated by 27% already at $T_1=6\cdot10^4$°K when the radiant flux heating the gas ahead of the front is ~5 times

less than for $T_1=9\cdot10^4$°K. It is hardly possible to explain the results of the measurements behind yellow, blue and violet light filters only by the effect of the heated layer. Obviously, for $T_1<9\cdot10^4$°K the primary role in the shielding of the radiation was played by the relaxation layer.

The influence of the relaxation layer on the shock wave emission in argon can be estimated using the data collected in the paper by L. M. Biberman and I. T. Yakubov [66]. For $T_1=25000$°K the relaxation time in argon is 6 times greater than in air. Hence, the greater width of the layer $\ell=3\cdot10^{-4}$ cm. However, the lower degree of ionization of the argon and smaller initial number of atoms (air dissociates) lead to the fact that the path length of the visible light turns out to be ~100 times longer than the thickness of the layer.

We do not have information about the width of the relaxation layer of more powerful shock waves in inert gases available. The problem of the structure of the layer is complicated in the region of primary ionization by the mechanism of the appearance of nucleating electrons. The estimate of the width of the relaxation layer depends significantly on which of the propositions we begin with when solving this problem. However, the part of the layer where the initial ionization of the gas develops in practice is transparent for light in view of the low concentration of ions and excited atoms in it. In addition, N. M. Kuznetsov [67] demonstrated that the problem of nucleating electrons in sufficiently powerful shock waves is removed in general as a result of photoionization of the gas by radiation of the equilibrium-heated region in gases of normal density with ionization potential I~13 ev for $T_1>24000$°K. In such shock waves in a heated gas an electron avalanche develops immediately, and the relaxation time is determined by the energy exchange time between the ions and electrons, which is proportional to the atomic weight of the gas. These arguments can be confirmed, comparing the relaxation times in argon and air by the available experimental data and the

calculations. The atomic weight of argon is 3 times greater than the average atomic weight of air. The initial concentration of the argon atoms is approximately 2 times less, for the air dissociates. Therefore in argon the relaxation time must be 6 times greater, which agrees with the data of [66, 73].

It is possible to expect that in xenon, the atomic weight of which is 9 times greater than the average atomic weight of air, the relaxation layer is much wider, and its shielding effect is stronger. Beginning with the above-presented arguments, we estimate the width of the relaxation layer in heavy inert gas at $T_1=3\cdot10^4$°K. The results of the estimates in the comparison of them with the average path length of red light for the layer appears as follows:

	Air	Argon	Krypton	Xenon
ℓ, cm	$2\cdot10^{-4}$	$1.1\cdot10^{-3}$	$1.7\cdot10^{-3}$	$2.2\cdot10^{-3}$
ℓ_ν, cm	$6\cdot10^{-4}$	$1.4\cdot10^{-2}$	$9\cdot10^{-3}$	$5\cdot10^{-3}$

It is obvious that in such gases as xenon and krypton the relaxation layer must shield the radiation of the shock wave noticeably. In the experiments the brightness temperature of the shock waves in xenon is appreciably less than the gas temperature after the front. The difference is especially high for the red section of the spectrum (see Figure 32). The decrease in the brightness temperature toward the red end of the spectrum was observed also on emergence of the detonation in krypton and xenon (see Figure 40). A reduction in brightness of the front was recorded at a comparatively low gas temperature behind the front when the shielding of the radiation by the heated layer was absent. Unconditionally, at high temperatures $T_1\sim10^5$°K and higher; a powerful heated layer is formed ahead of the shock compression which has a decisive influence on the radiative properties of the shock wave. However, as for the reduction in brightness of the front detected experimentally at temperatures of $T_1=2\cdot10^4$ to $6\cdot10^4$°K, it must be attributed to the shielding by the relaxation layer.

The experiment provided another proof of shielding of the radiation by the relaxation layer. On emergence of the detonation in heavy inert gases, the absorption lines of multicharge ions were recorded. The number of lines belonging to different ions is in accordance with the ionization composition of the shock-heated gas (see Table 4 and the tables in the Appendix). Let us note that the gas temperature in the heated layer was below 10^4°K in these experiments. The presence in the spectrum of the lines with excitation potential of ~20 ev cannot be explained by shielding by the heated layer.

§2. Radiation Heat Exchange at the Shock Wave Front

With an increase in the shock wave amplitude, the radiant flux from the front $S=\sigma T_1^4$ increases rapidly. The short-wave radiation is absorbed by the cold gas ahead of the front, and this heats this gas to a temperature of T_-.[1] The shock wave is now propagated through the advance-heated gas, and the temperature after the discontinuity T_+ is higher than in the absence of heating. The shock-heated gas cools, radiating, and its temperature drops from T_+ to T_∞. Thus, on propagation of a powerful shock wave the gas first is heated by the emission, and experiencing shock heating, is cooled, releasing part of the energy which also goes to the creation of the radiation flux S (Figure 52).

In gases of normal density the effect of the radiation on the structure of the transition layer will become noticeable for temperatures of about $T_1=10^5$°K where the radiant flux S becomes comparable to the energy flux of the material in the wave. The layer width is determined by the path length of the quanta with energy of several tens of electron volts near the maximum of the Planck

[1]In the next section it is demonstrated that the thermodynamic equilibrium cannot occur in the gas ahead of the front, and it is necessary to talk about its temperature provisionally. However, we have retained this notation in accordance with references [33-37].

distribution. In contrast to the less energetic quanta of visible and infrared radiation these quanta are not so intensely absorbed by the heated gas. Their path length turns out to be at least an order higher than the width of the layer in which the ionization of the shock-heated gas develops. Therefore when investigating the structure of the transition layer in the large plan, the details connected with ionization relaxation of the gas disappear.

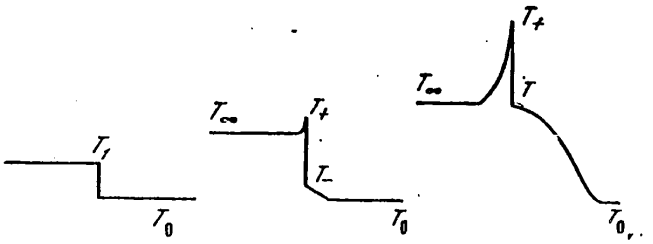

Figure 52. Temperature profiles of shock waves of different amplitude

Table 6. Ratio of the Radiant Flux $S=\sigma T_1^4$ to the Energy Flux of the Material $\rho_0 D^3/2$, %

$T_1 \cdot 10^{-4}$°K	3	4	5	6	7	8	9	10
Helium	3.9	4.1	5.3	7.7	11.2	14.4	17.7	20.2
Neon	4.7	6.9	9.4	12.3	14.7	18.0	22.0	25.9
Argon	4.3	5.6	8.4	11.8	14.0	16.7	19.9	28.5
Krypton	5.9	8.6	12.6	18.1	25.3	31.9	37.8	43.0
Xenon	6.7	8.7	12.1	16.5	21.2	27.5	35.6	44.0
Air	1.8	3.1	4.9	6.9	9.4	10.6	13.0	15.5

In Table 6 data are presented from which it is obvious that with an increase in amplitude the radiant flux increases faster than the energy flux of the material in the wave. At the same time the energy losses to radiation in the shock waves are limited and usually small. The fact is that ahead of the front the gas is not transparent for quanta, the energy of which exceeds the ionization potential of the atoms and molecules. In addition to photoionization, other absorption mechanisms occur in molecular gases. Let us present the boundary

gases of the shock waves λ beginning with which continuous absorption is observed in the gases (the values are taken from the book by A. N. Zaydel' and Ye. Ya. Shreyder [148]).

Gas	Helium	Neon	Argon	Krypton	Xenon	Air
λ, nm	50.4	57.5	78.7	88.6	102.2	190

At high temperature the flux S_∞ for the region of transparency of the gas is a small fraction of the total flux S. With an increase in temperature T_1, this fraction decreases still more. At the limit of very high temperatures the flux S_∞ belongs to the Rayleigh-Jeans part of the spectrum so that the losses are proportional not to the fourth, but the first power of the temperature.

The effect of the radiation on the gas parameters in a shock wave will be taken into account if the radiation energy flux is included in the relation at the discontinuity along with the energy flux of the material. The relation between the final and the initial parameters of the gas will be determined from the expression (e is the internal energy)

$$\begin{aligned} &\rho_\infty u_\infty = \rho_0 D, \\ &p_\infty + \rho_\infty u_\infty^2 = \rho_0 D^2, \\ &\rho_0 D\,(e_\infty + p_\infty/\rho_\infty + u_\infty^2/2) = \rho_0 D^3/2 - S_\infty. \end{aligned} \tag{5.8}$$

It is important to note (and this is obvious from equations (5.8)) that the final state of the gas depends not on the total flux S, but on the part S_∞ of it which belongs to the region of transparency of the gas ahead of the front and goes to "infinity" without inhibition.

Table 7 gives the ratio of the radiant flux S_∞ to the energy flux of the material in the wave characterizing the radiation losses and their influence on the final state of the gas.

From this table it is obvious that the radiation losses in the shock waves are limited. At low temperatures almost all of the radiation goes to the region of transparency of the gas ahead of the front, and the flux $S_\infty \approx \sigma T_1^4$ increases with an increase in the temperature more rapidly than the energy flux of the material. However, as the maximum of the radiated energy in the spectrum shifts to the region of nontransparency of the gas ahead of the front, the situation changes -- the flux S_∞ lags behind the energy flux material $\rho_0 D^3/2$. For each of the gases there is a completely defined value of the amplitude (it corresponds to the maximum of the ratio in Table 7), for which the radiation losses and their influence on the final state of the gas reach the highest value. The negligible radiation losses in the air -- no more than 0.5% of the hydrodynamic energy flux -- attract attention. Therefore for calculations of the air parameters behind the front the flux S_∞ is usually neglected in expressions (5.8).

Table 7. Ratio of the Radiant Flux S_∞ to the Energy Flux of the Material $\rho_0 D^3/2$, %

$T_1 \cdot 10^{-4}$°K	2	3	4	5	6	7	8	9	10	12
Helium	2.8	3.2	3.9	4.5	5.6	6.9	7.4	7.6	7.4	7.2
Neon	4.4	4.7	5.2	7.1	7.5	7.6	7.6	7.8	7.5	6.5
Argon	3.5	3.7	4.6	4.6	4.9	4.8	4.7	4.5	4.3	3.7
Krypton	3.7	4.8	5.2	5.6	6.0	6.2	5.7	5.3	4.9	-
Xenon	3.4	4.8	4.4	4.3	4.3	3.8	3.8	3.7	3.5	-
Air	0.4	0.5	0.5	0.4	0.4	0.4	0.4	0.3	0.2	-

In contrast to the air, the region of transparency of the inert gases extends far in the direction of the vacuum ultraviolet. Hence, we have significant radiation losses approaching 10%. When calculating the shock adiabats of inert gases these losses must be taken into account. The corrections to the gas parameters behind the front are easily found by representing them in the form $\rho_\infty = \rho_1 + \Delta\rho_\infty$, $u_\infty = u_1 + \Delta u_\infty$, and so on. Separating the terms of different order of

smallness in the system of equations (5.8) and using the equation of state $e=(1/(\gamma-1))(p/\rho)$, it is easy to obtain the following expressions:

$$\begin{aligned}
&\frac{\Delta\rho_\infty}{\rho_1} = \frac{\delta}{\delta-1}\frac{2S_\infty}{\rho_0 D^3},\\
&\frac{\Delta p_\infty}{p_1} = \frac{\delta}{(\delta-1)^2}\frac{2S_\infty}{\rho_0 D^3},\\
&\frac{\Delta e_\infty}{e_1} = -\frac{\delta(\delta-2)}{(\delta-1)^2}\frac{2S_\infty}{\rho_0 D^3},\\
&\frac{\Delta T'_\infty}{T'_1} = 0{,}67\cdot\frac{\Delta e_\infty}{e_1} + 0{,}08\cdot\frac{\Delta\rho_\infty}{\rho_1}.
\end{aligned} \tag{5.9}$$

Here $\delta=\rho_1/\rho_0=(\gamma+1)/(\gamma-1)$ is the shock compression of the gas. We found the correction to the temperature using the interpolation formula $e=aT^{1.5}\rho-0.12$ which describes the results of the exact calculations well (see the Appendix).

The expressions (5.9) are also applicable for calculating the corrections to the gas parameters at the shock compression. For this purpose it is necessary only that the flux S_∞ be replaced by the flux $-(S-S_\infty)$. Actually, in contrast to (5.8) the relations at the discontinuity have the form

$$\begin{aligned}
&\rho_+ u_+ = \rho_0 D,\\
&p_+ + \rho_+ u_+^2 = \rho_0 D^2,\\
&\rho_0 D\,(e_+ + p_+/\rho_+ + u_+^2/2) - S = \rho_0 D^3/2 - S_\infty.
\end{aligned} \tag{5.10}$$

A specific representation of the influence of the radiation on the parameters of the shock-heated gas can be presented by the following example. A shock wave with a velocity D=36.5 km/sec is propagated through neon. Without considering the radiation the gas parameters in the wave are as follows: T_1=100 000°K, p_1=10600 atm, ρ_1/ρ_0=9.15. Considering the radiation we have T_∞=96000°K, ρ_∞=10700 atm, ρ_∞/ρ_0=9.9; T_+=110 000°K, p_+=10300 atm, ρ_+/ρ_0=7.3.

If we limit ourselves to the investigation of shock waves in gases of normal density, the presented example illustrates, perhaps, the case of a strongest influence of the radiation on the final state of the gas after the front.

The radiation can be felt much more strongly on the state of the gas at the front. This is caused by the fact that the radiant flux $S-S_\infty$ increases with an increase in the wave amplitude faster than the energy flux of the material. For small amplitudes the flux $S-S_\infty$ pertains to the Wien part of the spectrum and increases very rapidly with temperature T_1. At high amplitudes when in practice all of the emission is absorbed in the heated layer, the flux is proportional to the fourth power of the temperature T_1. From Tables 6 and 7 it is obvious that the ratio $2(S-S_\infty)/\rho_0 D^3$ increases monotonically with an increase in the amplitude.

The relations at the discontinuity (5.8), (5.10) supplemented by the equation of state $e=(1/(\gamma-1))(p/\rho)$ can be solved directly without assuming smallness of the corrections. The increase in precision of the parameters of the shock-heated gas obtained in this way does not exceed 1% for $2\sigma T_1^4/\rho_0 D^3<20\%$. For $2\sigma T_1^4/\rho_0 D^3>20\%$ these increases in precision will be approximate, for it is necessary to consider the difference of the radiant flux S from σT_1^4. In essence, when the temperature profile of the shock wave begins to differ noticeably from the ideal discontinuity, the relations at the discontinuity must be resolved jointly with the radiation transport equations (3.29), (3.7). In addition, it is necessary to be given the relation between the internal energy of the gas, its density and temperature. Joint solution of all these equations is a highly difficult mathematical problem. The situation is simpler with the gas parameters behind the front. For any amplitudes the flux S_∞ is a small fraction of the hydrodynamic energy flux in the wave. Therefore expressions (5.9) are applicable for calculation of the corrections. There will also be no large error in considering the flux S_∞ as part of the Planck flux at a temperature T_1 for the region of transparency of the cold gas ahead of the front. Moreover, for quite large amplitudes when the radiation is almost completely absorbed in the heated layer,

it is possible to neglect the flux S_∞ altogether, setting $T_\infty=T_1$, $e_\infty=e_1$, and so on. Here the gas parameters in the wave front are more simply found, for the radiation transport equations permit averaging over the spectrum.

In powerful shock waves the radiation has, although significant, limited effect on the state of the gas in the front. The heating temperature T_- is proportional to the radiation flux $S-S_\infty$, and therefore it increases rapidly with an increase in the wave amplitude. The amount that the temperature T_+ exceeds the final temperature T_∞ increases correspondingly. At some temperature behind the front $T_\infty=T_{cr}$ the heating temperature T_- reaches T_∞. This temperature T_{cr} (equal to approximately 300,000°K for air) can be called critical, for it separates the two significantly different cases of the structure of the shock wave front. For the temperatures behind the front $T_\infty>T_{cr}$ the quantum energy flux will suffice to heat the layer on the order of the path length in which the quanta are absorbed to a temperature of $T_->T_\infty$. However, such high heating cannot be realized, for the heated layer would begin to emit intensely and would quickly cool to a temperature of T_∞. The occurrence of the state with $T_->T_\infty$ would indicate that in the closed system the heat is spontaneously pumped from the less heated layers of the gas to the more heated ones -- a contradiction with the second principle of thermodynamics.[1] Indeed, the energy picked up by the radiation from the gas heated at the shock compression is reemitted and heats the thicker layers before the discontinuity.

Thus, in waves of large, supercritical amplitude the shock compression is propagated through the gas first heated to a temperature of $T_-=T_\infty$. Taking this into account, for the gas temperature after the discontinuity T_1 it is possible to

---

[1]Strict proof of the impossibility of the state with $T_->T_\infty$ is presented by Ya. B. Zel'dovich [33].

obtain the following expression [37]: $T_+=(3-\gamma)T_\infty$. For $\gamma=1.25$ we have $T_+=1.75\ T_\infty$. If we use the interpolation formula $e=aT^{1.5}\rho^{-0.12}$ considering inconstancy of the heat capacity of the ionized gas, we obtain $T_+=1.6\ T_\infty$.

The existence of a temperature peak at the front of a powerful shock wave can be characteristically felt in its radiative properties. The width of the peak is determined by the path length of the quanta with energy $h\nu\sim$(3 to 5) kT which plays a primary role in the radiant cooling of the shock-heated gas. The low-energy quanta ($h\nu<<kT$), in particular, the quanta of the visible light, are absorbed by the ionized gas more strongly. The region of the temperature peak for these quanta is nontransparent. The brightness temperature of the front must coincide with the temperature T_+, that is, be higher than the gas temperature after the front.

In the experiments no noticeable excess of the brightness temperature of the front over the gas temperature behind the front was observed. Moreover, at high shock wave velocities the inverse picture was observed. The divergence should be considered the result of radiation shielding. Measuring the brightness of the front at different angles, it was possible to estimate the optical thickness of the shielding layer and reproduce the true temperature of the gas radiating to the outside. This temperature always turned out to be above the temperature of the gas after the front (see Figures 30-33).

On emergence of the detonation in xenon and krypton, the maximum in the brightness temperature distribution over the spectrum was recorded (see Figure 40). As we have already noted, the drop in brightness temperature toward the red end of the spectrum obviously was caused by shielding of the radiation by the relaxation layer in which ionization of the shock-heated gas developed. The transparency of the region of the temperature peak for ultraviolet radiation could be the cause of a decrease in the brightness temperature toward the other end of the spectrum.

In the conclusion of this section let us discuss the papers by Griem, L. M. Biberman, K. N. Ul'yanov and N. M. Kuznetsov [156-158] indicating that the radiation losses sometimes lead to disturbance of the thermodynamic equilibrium in an optically thick medium, which, in turn, is felt in its radiative properties. Although we are investigating optically dense shock waves, this has direct bearing on the layer of gas several radiation path lengths wide radiating to the outside. According to reference [157], the equilibrium population of levels with the main quantum number n is insured if

$$N_e \geqslant 7 \cdot 10^{18} \frac{(Z+1)^7}{n^{17/2}} (kT_e/I_Z)^{1/2},$$

where I_Z is the ionization potential of an ion with the charge Z-1. The estimates show that for normal gas density ahead of the front in the temperature range of $T_1=10^4$ to 10^5°K, the condition of equilibrium population of the excited levels is satisfied. According to reference [158], the temperature difference of the electrons T_e and the ion temperature T_i in a stationary optically thin plasma is

$$\frac{T_i - T_e}{T_e} \approx 3{,}5 \cdot 10^{-9} \frac{AT_e}{\Lambda} \left(1{,}2 \frac{I_Z}{kT_e} + \frac{1}{2}\right),$$

where A is the atomic weight of the ion, Λ is the Coulomb logarithm. The estimates give $(T_i-T_e)/T_e<10^{-2}$ for $T_e<10^5$°K. Thus, under the conditions of our experiments the radiation losses did not lead to significant violation of the thermodynamic equilibrium in the shock-heated gas.

§3. Radiation Shielding by Heated Layer

The cold gas ahead of the shock wave absorbs quanta, the energy of which exceeds the ionization potential of the atoms and molecules of the gas. Quanta are also absorbed which cause resonance excitation of the atoms and molecules. As a result, the radiation spectrum of the shock wave acquires the form detected in

Figure 53 -- the short wave part of the spectrum is "cut off", and the individual narrow lines are "cut out." In molecular gases the lines usually overlap, forming broad absorption bands.

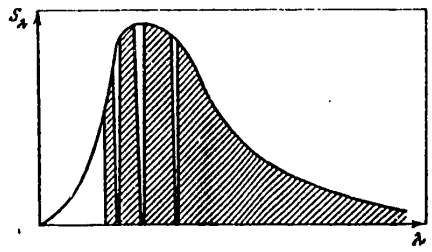

Figure 53. Shielding of the radiation of the shock-heated gas by cold gas ahead of the front

However, the "distortion" of the emission of a shock-heated gas is not limited to only this. At high amplitudes the gas ahead of the discontinuity is heated by short-wave radiation so strongly that it begins to absorb in the regions of the spectrum where, being cold, it is less transparent. First of all, the small quanta of infrared and visible radiation are delayed, the absorption coefficient of which by the heated gas is especially high. The brightness temperature of the front in these sections of the spectrum will become lower than the true temperature of the shock-heated gas: the heated layer shields the highly heated gas after the shock wave.

In the visible part of the spectrum the shielding becomes noticeable when the radiation path length is comparable to the width of the heated layer. As a result of shock dependence of the absorption of visible light on the temperature and, in turn, the quite sharp dependence of the heating temperature on the wave amplitude, the beginning of shielding sets in when the amplitude increases quite explicitly. The brightness temperature of the front initially coincides with the temperature of the shock-heated gas, but as the wave amplitude increases, it lags behind it, it passes through a clearly expressed maximum and quickly decreases to some limiting value caused by the natural glow of the heated layer.

Let us discuss the quantitative estimates of the shielding performed by Yu. P. Rayzer [35] in more detail for a shock wave in air of normal density. The temperature profile of the heated layer was calculated from the expression

$$S = De\rho_0, \tag{5.11}$$

where S is the radiant flux heating the gas before the shock wave, e is the internal energy of the gas in the heated layer. This relation is observed with good accuracy in waves of subcritical amplitude and also in the forward zone of the heated layer in waves of supercritical amplitude. The decrease in the flux S with respect to the spectrally averaged optical coordinate τ was taken in the diffusion approximation:

$$S = S_0 e^{-\sqrt{3}\tau},$$

where $S_0=\sigma T_1^4$. Being given the Boltzmann relation for the absorption coefficient of visible light as a function of temperature, $\varkappa_\nu = \text{const}\cdot\exp\left(-\frac{I-h\nu}{kT}\right)$, and considering the average absorption coefficient χ constant and also using the interpolation relation $e\sim T^{1.4}$, it is easy to obtain the following expression for the optical thickness of the heated layer:

$$\tau_\nu(T) = \int_0^\infty \varkappa_\nu\, dx = \int_{T_-}^{0} \varkappa_\nu \frac{dx}{dT}\, dT = \int_{T_-}^{0} \frac{\text{const}}{\varkappa}\cdot\frac{1{,}4}{\sqrt{3}} e^{-\frac{I-h\nu}{kT}} \frac{dT}{T} \approx$$
$$\approx \frac{1{,}4}{\sqrt{3}} \frac{kT_-}{I-h\nu}\cdot\frac{\varkappa_\nu(T_-)}{\varkappa}.$$

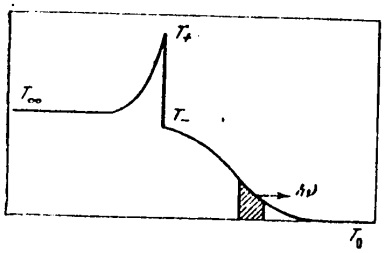

Figure 54. Position of the layer radiating to the outside in very powerful shock waves

In a shock wave with T_1=65000°K in which the temperature ahead of the discontinuity T_-=9000°K, the shielding is absent. However, when T_1=90000°K, when

T_-=20000°K, the optical thickness of the heated layer for red light (λ=650 nm) is $\tau_\nu \sim 0.12$. Here the brightness temperature of the front $T_b \sim 80000$°K. With a further increase in the wave amplitude the optical thickness of the layer increases, and the brightness decreases; for example, with a rise in temperature by a total of 10000°K, for T_1=100,000°K, T_-=25000°K, $\tau_\nu \sim 0.37$ and $T_b \sim 67000$°K, that is, the brightness temperature is already less than 80000°K.

Thus, the brightness maximum corresponds to the temperature after the front T_1=90000°K, and the maximum brightness temperature in the air is $T_{b\ max}$=80000°K. For a temperature behind the front T_1=140,000°K, $T_- \sim 50000$°K, $\tau_\nu \sim 1.5$ and the shielding is almost complete. Under these conditions not only the high temperature light from the gas after the discontinuity is absorbed in the heated layer, but also the light of the strongly heated layers ahead of the discontinuity. The moderately heated layer remote from the discontinuity emits to the outside (crosshatched in Figure 54), in front of which the gas is so hot that the radiation is noticeably shielded. The gas temperature in this layer is found from the condition that the length of path of the red light in it compares with the path length of short-wave radiation heating the gas (in more heated layers where the path length is shorter, the light is emitted, but it is immediately absorbed; the less heated layers do not absorb and do not emit because of their transparency). This temperature, which is the maximum brightness temperature of very powerful shock waves in the air, is approximately 17000°K.[1]

---

[1] Since the absorption coefficient within the visible region of the spectrum varies slightly, the estimated values of the brightness temperatures approximately pertain not only to red light, but also in general to the entire visible region of the spectrum.

In experiments with air the shielding began at significantly lower amplitudes of shock waves than follows from the presented estimates. As has already been noted, when explaining the experimental results it is necessary to consider the additional shielding effect of the relaxation layer in which the ionization of the shock-heated gas develops.

Quantitative estimates of the shielding by the heated layer analogous to the above-presented estimates for air were made in accordance with the primary measurements of the brightness temperature of powerful shock waves in inert gases. It turned out that the maximum brightness temperature in such gases as argon, krypton and xenon must reach approximately the same values as in the air. However, in the first experiments the brightness temperature of quite powerful shock waves did not exceed 40000°K. In spite of all of the efforts more precisely to define the calculations, no agreement with the experimental data was obtained. The impression was made that the gas temperature in the heated layer for some reason was higher than follows from the estimates. One of the possible causes of the divergences -- absence of thermodynamic equilibrium in the heated layer -- was noted by the authors in reference [42] and is substantiated in [43].

The width of the heated layer is determined by the path length of the quanta ℓ absorbed by the cold gas ahead of the discontinuity, and the time the gas is in the layer, by the value of $t=\ell/D$. In argon, krypton and xenon of normal density $\ell\sim10^{-3}$ cm and for D=10 km/sec we obtain the time $t\sim10^{-9}$ sec which, as we shall see below, is comparable to the time of the relaxation processes in the heated gas.

The internal energy E of the gas ahead of the discontinuity will be found from the expression

$$S = DE, \tag{5.12}$$

where, in contrast to (5.11), E is the energy of 1 cm^3 of gas, and

$$S = 2\pi c^{-2}h^{-3}\int_I^\infty [\exp(\varepsilon/kT_1)-1]^{-1}\varepsilon^3\,d\varepsilon$$

is the short-wave radiation flux causing ionization of the gas ahead of the discontinuity $\varepsilon=h\nu$. The number of photoelectrons N_e per cm^3 is determined analogously:

$$s = DN_e, \tag{5.13}$$

where

$$s = 2\pi c^{-2}h^{3}\int_I^\infty [\exp(\varepsilon/kT_1)-1]^{-1}\varepsilon^2\,d\varepsilon$$

is the quantum flux causing photoionization. From (5.12), (5.13) we obtain the average energy of the photoelectrons ε_e:

$$\varepsilon_e = S/s - I. \tag{5.14}$$

The values of N_e and ε_e calculated by (5.13), (5.14) for a shock wave in argon of normal density are presented in Table 8. We shall use these values to estimate the time of the different relaxation processes in the heated layer which will occur as a result of photoionization of the gas.

Table 8

$T_1\cdot10^{-3}$, °K	30	35	45	60	70	80
$N_e\cdot10^{-17}$, cm^{-3}	1,7	5,9	18	65	110	170
ε_e, ев	3,5	4,2	5,8	8,4	10	12
t^*/t	4,3	1,2	0,4	0,09	0,05	0,03
t_i/t	0,9	0,3	0,06	0,02	0,01	0,01
t_{ei}/t	55	25	16	10	9	8
$T''_e\cdot10^{-3}$, °K	11	12,5	15,4	18,7	22,0	29,0
$T_e\cdot10^{-3}$, °K	1,7	5,0	13,5	17,6	20,7	24,0

The electron excitation relaxation time t* will be estimated by the formula

$$t^* = 1/(\beta^* N_e), \tag{5.15}$$

where $\beta^* = \sigma^* \frac{g_1}{g^*}\left(\frac{E^*}{kT_e}+2\right)v_e$ is the deactivation rate constant, v_e is the average electron velocity. For argon levels with excitation potential E*=11.5 ev

and a statistical weight g*=8, the effective excitation cross section $\sigma^*=C^*kT_e$, where $C^*=0.7\cdot10^{-17}$ cm^2/ev [37].

The ionization relaxation time will be estimated by the formula

$$t_i = \frac{1}{\alpha_i N_a}, \tag{5.16}$$

where $\alpha_i = \delta_i\left(\frac{I}{kT_e}+2\right)\exp\left(-\frac{I}{kT_e}\right)\bar{v}_e$ is the ionization rate constant, $\sigma_i=C_ikT_e$ is the effective ionization cross section (in argon $C_i=2\cdot10^{-17}$ cm^2/ev [37]), N_a is the atom concentration.

The results of the estimates are also presented in Table 8. For a temperature behind the front $T_1>3.5\cdot10^4$°K the relaxation times of the electron excitation and ionization are much less than the time the gas is in the heated layer: $t^*/t\ll1$ and $t_i/t\ll1$. Consequently, the "hot" photoelectrons will "cool" in inelastic collisions with atoms. For $T_1<3.5\cdot10^4$°K (D<12 km/sec) the excitation and ionization of the gas in the heated layer cannot be completed: $t^*/t>1$ and $t_i/t>1$.

Now let us consider whether the photoelectrons are able to put the "cold" particles -- atoms and ions -- into thermal motion. The electron-ion relaxation time will be estimated by the Landau formula

$$t_{ei} = \frac{3{,}15\cdot10^8 A T^{3/2}\,(ev)}{N_i Z^2 \Lambda}, \tag{5.17}$$

where A is the atomic weight of the ions, Λ is the Coulomb logarithm (under our conditions for Z=1 Λ=5 [37]). The values of t_{ei} turn out to be at least an order higher than the time the gas is in the layer (see Table 8). Let us note that the electron relaxation takes place much more rapidly: $t_{ee}/t_{ei}\sim m_e/m_i\sim10^{-5}$. In the heated layer the electron temperature is set up. The electron-atomic relaxation time can be estimated by the formula

(5.18)

where $\overline{\sigma}_{ea}$ is the eleastic scattering cross section of the electron on the atoms averaged with respect to Maxwell distribution (the values of σ_{ea} were taken from [159]). The estimates give $t_{ea}/t=10$ to 30.

Thus, the energy from the "hot" photoelectrons is not transferred to the heavy particles -- atoms and ions -- and they remain "cold" in the heated layer. The entire excess energy of the photoelectrons is spent on further ionization and excitation of the gas atoms. Inasmuch as the absorption of light is determined at the same time by the degree of ionization and excitation of the gas, it is necessary to expect stronger shielding of the radiation than in the case of thermodynamic equilibrium.

A comparison of the relaxation times of the different processes indicates that in the heated layer only partial thermodynamic equilibrium can be set up when only the degrees of ionization and excitation of the gas correspond to the electron temperature. The values of the temperature T'_- ahead of the discontinuity calculated considering expression (5.12) for the case of partial thermodynamic equilibrium are presented in Table 8. In the calculations only the contribution of the ionization, excitation and kinetic energy of the electron to the internal energy of the gas was taken into account. For comparison values of the temperature T_- ahead of the discontinuity are presented which correspond to complete thermodynamic equilibrium of the gas in the heated layer. The absorption coefficient of the light by the heated gas depends quite sharply on the temperature. Therefore, comparing the values of the temperatures T'_- and T_- to each other, it is necessary to consider that the difference in the absorption coefficients and, consequently, in the optical thicknesses of the heated layer will be more significant.

The partial thermodynamic equilibrium is established not throughout the entire thickness of the heated layer. On going away from the discontinuity the

temperature T' decreases, and the relaxation processes in the gas are retarded. Approximately at T'=13000°K the excitation relaxation time compares with the time the gas is in the layer.[1] Far from the discontinuity the photoelectrons, losing their energy in inelastic collisions with atoms and in elastic collisions with secondary electrons, quickly "cool" to a temperature of $T_e \approx 13000$°K. Thus, the relaxation processes remain incomplete. The state of the gas here is significantly nonequilibrium. Only at a temperature after the front $T_1 > 3.5 \cdot 10^4$°K does the radiant flux heat the gas near the discontinuity to a temperature of T'>13000°K. Then the relaxation processes in some part of the heated layer adjacent to the discontinuity are completed by establishing partial thermodynamic equilibrium. This peculiarity reflects the temperature profile of the heated layer presented in Figure 55.

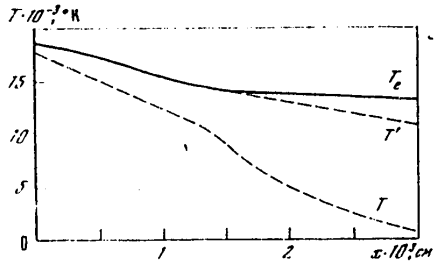

Figure 55. Temperature profile of the heated layer

The comparatively broad region of strongly nonequilibrium gas far from the discontinuity obviously makes a small contribution to the radiation shielding. Although here the electron temperature is relatively high, their concentration

[1]The ionization relaxation time estimated by (5.16) for T'=13000°K turns out to be even greater than the time the gas spends in the heated layer. However, at low temperatures the equilibrium concentration of the electrons is established predominantly by the ionization of the excited atoms.

decreases quickly (exponentially) on going away from the discontinuity. This region of the gas absorbs the radiation more weakly than would be absorbed if partial thermodynamic equilibrium had been set up in it. Then the degree of ionization and excitation of the gas would be higher. However, even for such ionization and excitation the path length of the visible radiation turns out to be much longer than the possible width of the heated layer. Thus, for T'=13000°K the estimates by (5.3)-(5.5) give $l_\nu \sim 10$ cm. Therefore for simplication of the calculations it was proposed that the partial thermodynamic equilibrium is established in the entire thickness of the heated layer.

The temperature profile of the heated layer was calculated by the formula (5.12) where the radiant energy flux at different distances from the discontinuity was found from the expression

$$S = 2\pi c^{-2}h^{-3}\sum_{m=1}^{n} f(\tau_m)\int_{\varepsilon_n}^{\varepsilon_{m+1}} [\exp(\varepsilon/kT_1)-1]^{-1}\varepsilon^3\,d\varepsilon, \qquad (5.19)$$

where $f(\tau_m) = 2\int_0^\infty e^{-\tau_m\xi}\xi^{-3}\,d\xi$ is the function taking into account the absorption of the flux with respect to the optical coordinate $\tau_m = \int_0^x \varkappa_m\,dx$ (Table 9). The sections of the spectrum $\varepsilon_m<h\nu<\varepsilon_{m+1}$ were selected in such a way that the absorption coefficient χ_m within the limits of the section varied weakly. The boundary of the first segment was the transparency limit of the cold gas, that is, ε_1=I. The number of sections was n=5 to 10 depending on the nature of variation of the absorption coefficient χ.

Table 9. Values of the Function $f(\tau) = 2\int_1^\infty e^{-\tau\xi}\xi^{-3}\,d\xi$

τ	0	0,1	0,2	0,3	0,4	0,5	0,6	0,7	0,8	0,9	1,0
f	1,000	0,833	0,709	0,600	0,514	0,443	0,383	0,332	0,288	0,251	0,219
τ	1,2	1,4	1,6	1,8	2,0	2,5	3,0	4,0	5,0		
f	0,168	0,127	0,100	0,077	0,061	0,033	0,018	0,006	0,001		

The absorption coefficient was calculated by the formula

$$\varkappa = \sum_{i=0}^{k} N_i \sigma_i, \tag{5.20}$$

where σ_i and N_i are the absorption cross section and concentration of the ions of i-th multiplicity in the ground state.[1] Broad experimental data [148] are available on the absorption cross sections of atoms σ_0. This data was used for the calculations. The absorption cross sections of the ions were assumed to be hydrogen-like:

$$\sigma_i = 7{,}9 \cdot 10^{-18} (i+1)^4 \left(\frac{I_H}{\varepsilon}\right)^3 \text{ см}^2.$$

Double ionization of the gas in the heated layer was considered to be sufficient in practice, that is, the sum (5.20) included no more than three terms for the calculations.

The equations (5.12), (5.19) and (5.20) were solved jointly by the method of successive approximations. In the first approximation it was assumed that the gas ahead of the discontinuity absorbs as a cold gas (the sum (5.20) consisted of only the first term). Using the tables of internal energy and ionization composition of the gas (see the Appendix), the temperature profile of the heated layer was found, and the absorption coefficient was more precisely defined (5.20). Usually after three or four approximations the temperature profile did not change.

The optical thickness of the heated layer for radiation normal to the front is

$$\tau_\nu = \int_0^\infty \varkappa_\nu \, dx. \tag{5.21}$$

The light absorption coefficient χ_ν was calculated by the formula (5.3)-(5.5), where the braking absorption by the electrons in the field of the multicharge ions

[1] The primary role in the heating of the gas ahead of the discontinuity was played by the quanta $h\nu \sim (3\text{-}5)kT$ which were weakly absorbed by the excited ions.

and also the light absorption by the excited ions, was taken into account in the heated layer. The factor ξ in (5.3) for Ar, Kr and Xe atoms was taken from reference [92]. We had no information about the value of ξ for the He and Ne atoms or ions. However, from references [92, 100] it follows that in the visible region for different atoms (and especially ions) $\xi \approx 1$. Judging by [155], the splitting of the highly excited levels responsible for absorption of visible light, $\gamma \approx 15$ for atoms and $\gamma = 45$ for ions.

The brightness temperature T_b was determined from the following expression under shielding conditions

$$(e^{h\nu/kT_B} - 1)^{-1} = (e^{h\nu/kT_+} - 1)^{-1} e^{-\tau_\nu}. \tag{5.22}$$

Here we consider the fact that the temperature peak after the discontinuity is opaque for visible light. When $\tau_\nu > 0.1$ the natural glow of the heated layer was considered:

$$(e^{h\nu/kT_B} - 1)^{-1} = (e^{h\nu/kT_+} - 1)^{-1} e^{-\tau_\nu} + \int_0^\infty (e^{h\nu/kT} - 1)^{-1} e^{-\tau'_\nu} \varkappa_\nu \, dx, \tag{5.23}$$

where, in contrast to τ_ν, $\tau'_\nu = \tau'_\nu(x) = \int_x^\infty \varkappa_\nu \, dx$.

The calculations were performed for fixed values of the gas temperatures behind the front beginning with $T_1 = 6 \cdot 10^4$°K and then every 10^4°K until total shielding and establishment of the maximum brightness temperature occurred.

The obtained relations for the brightness temperature of shock waves in blue ($\lambda = 430$ nm) and yellow ($\lambda = 560$ nm) light are presented in Figure 56 as a function of the front velocity. Under the conditions of partial thermodynamic equilibrium in the heated layer the shielding comes sooner (the solid curves in Figure 56) than in the case of total thermodynamic equilibrium (the dotted lines). However, the difference is small. The difference in the curves corresponding to the yellow and blue light for which the absorption coefficient χ_ν differed by 2-3 times was also small. The differences are concealed by the sharp dependence of the heating temperature on the wave amplitude.

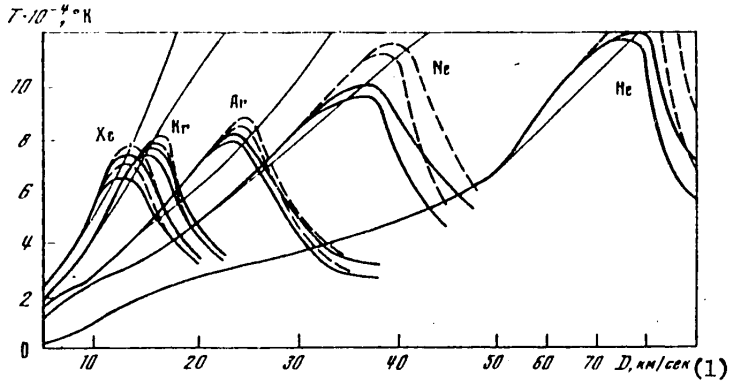

Figure 56. Brightness temperature of shock waves in inert gases. The boldface solid curves are the partial thermodynamic equilibrium of the gas in the heated layer; the dotted curves are complete thermodynamic equilibrium. The curves for blue light (λ=430 nm) are above the curves for yellow light (λ=560 nm). The fine solid lines are the temperature T_1 of the gas behind the shock wave front.

Key:
1. km/sec

Nonsteady shielding of the radiation was observed in the experiments with inert gases. Possibly the effect was caused by gradual development of a broad region of nonequilibrium heated gas ahead of the discontinuity. However, at the first point in time after excitation of the shock wave ahead of the discontinuity only a narrow heated layer could occur. The values of the brightness temperature measured at the first point in time (and these were maximal for the given temperature velocity) fit the curves in Figure 56 well.

The absorption of the radiation in the lines not taken into account by our calculations leads to additional shielding. In the radiation spectrum of the powerful shock wave there must be a large number of absorption bands, where the lines appear at lower velocities D when the shielding in the continuum is still unnoticeable. At such velocities the thermodynamic equilibrium of the gas ahead of the discontinuity leads to a qualitative difference of the spectrum from the case of thermodynamic equilibrium. Thus, for D=10 km/sec, the ionization and

excitation of argon ahead of the discontinuity correspond to a temperature of $T'_- \sim 10^4$°K. Under these conditions it is possible to expect weak shielding in the individual atomic lines, whereas for the equilibrium temperature $T_- \sim 10^3$°K the argon is still entirely transparent.

§4. Shielding of Radiation Front in Gas Mixtures

The possibilities of the shock wave as a source of light are easily expanded by adding specially selected gas. The latter, playing the role of the primary filter would permit adjustment of the spectral composition of the shock wave emission. On the other hand, the negligible and not always controllable admixtures sometimes change the radiative properties of the shock wave significantly. For example, in argon with an admixture of 0.01% air the radiation flux in the spectral region λ=79 to 190 nm, to which at $T_1 = 3 \cdot 10^4$°K 80% of the energy emitted from the front belongs, is attenuated by 5 times at a distance of 1 meter from the front.

The presence of the impurities can lead to shielding of the radiation also in parts of the spectrum where the gas mixture is transparent. For example, it is possible to show that an insignificant admixture having no influence on the shock adiabat of the gas can cause shielding of the front at low velocities D for which shielding is absent in the pure gas. Moreover, by decreasing the admixture concentration it is possible to amplify and not attenuate the effect. The temperature profile of the heated layer in a gas with admixture is depicted in Figure 57. The impurity heated layer caused by absorption of radiation by the impurity extends in front of the narrow layer occurring as a result of absorption of the short-wave radiation by the basic gas.

One of the causes of earlier shielding is preliminary heating of the gas to a temperature of T_{--} in the admixture layer. Figure 58 shows the results of

calculating the brightness temperature of argon with an admixture of air considering this additional heating (curve 4). Curve 5 for pure argon is presented for comparison. During the calculations it was assumed that the admixture layer is quite broad and the relaxation processes in it are entirely complete. As is obvious from Figure 58, the effect of the admixture in the given case is small. The fact is that at high temperatures $T_1 \sim 10^5$°K the greater part of the radiant flux is absorbed by the argon in the basic heated layer.[1]

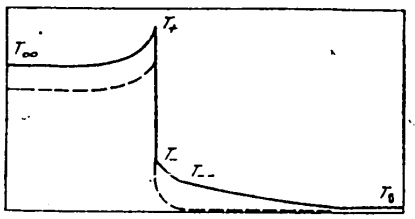

Figure 57. Temperature profile of the shock wave in a gas with impurity (dotted line in pure gas)

A more significant contribution to the shielding of the radiation can be made by the impurity heated layer. In pure argon the shielding becomes noticeable at a temperature of $T_- \approx 3 \cdot 10^4$°K when the path length of the visible light compares with the path length of the radiation causing the heating. For many gases this temperature is appreciably lower. Let, for example, the shock wave be propagated in argon with an admixture of the vapor of alkali metals. The light path length in

[1]Comparing curves 4 and 5 in Figure 58 it is easy to note a curious detail -- the brightness temperature at D<20 km/sec in argon with an admixture is higher than in pure argon. The increase in emissivity in the region of transparence of air λ>190 nm is directly related to worsening of it in the region λ=79 to 190 nm. The absorption of ultraviolet radiation by air leads to a rise in temperature behind the discontinuity (see Figure 57). This effect is small in the investigated example. However, in other cases, in particular for low gas densities, when the radiant fluxes are comparable to the hydrodynamic energy flux, the possibility of increasing the emissivity of the shock wave with the help of impurities in certain sections of the spectrum at the expense of others is of interest.

the vapor compares with the radiation path length during the heating in the admixture layer at a temperature of $6 \cdot 10^3$°K or for D=10 km/sec. In this example the argon does not participate directly in the shielding -- the width of the admixture heated layer and the light path length in it are determined by the optical properties of the admixture. However, argon is a direct cause of premature shielding. At low concentration of the admixture and temperatures below 10^4°K, the gas mixture behaves as an ideal monoatomic gas. With identical internal energy and heated layer the temperature in the mixture will be appreciably higher than in the admixture gas alone (in the vapor of alkali metal). However, the maximum brightness temperature for gas admixture can be lower than for each of the components of the mixture separately.

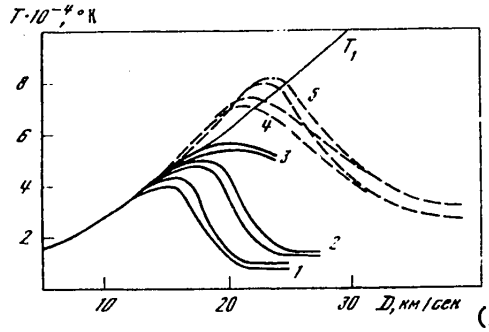

(1)

Figure 58. Brightness temperature of shock waves in argon with air admixture.
Curves 1, 2 and 3 correspond to 0.01, 0.1 and 1% air in the argon; 4 -- without considering shielding by the admixture heated layer; 5 -- for pure argon. In each pair of curves 1-3 the upper is yellow light (λ=560 nm), the lower is blue light (λ=430 nm), and for the dotted curves 4 and 5, vice versa.

Key:
1. km/sec

Let us return to the shock waves in argon with air admixture. The gas temperature in the admixture heated layer is comparatively low. Thus, for $T_1=7 \cdot 10^4$°K the gas is heated in it to a temperature of ~$1.5 \cdot 10^4$°K and it absorbs the light weakly. However, it is always possible to select a quite low concentration of the admixture for which the admixture heated layer will be so broad that

it will begin to shield the visible light. The lower the air concentration, the broader the layer, and the less shielding occurs. This feature is reflected by the results of calculating the brightness temperature in argon with air admixture presented in Figure 58 (curves 1-3).

The influence of the air admixture on the brightness of the shock waves in argon was detected experimentally. The data obtained here agree well with the above-presented arguments. The significance of the broad admixture heated layer is indicated by the weak glow of the gas ahead of the front recorded experimentally. The glowing region extended a distance of about 1 cm. The width of the layer is easily estimated also by the buildup of the brightness with approach of the front to the end window of the couvette. When adding 5% air to the argon, the buildup lasted $t \sim 0.4$ microsecond. The front velocity was D=13.5 km/sec. The width of the layer $\ell \sim tD \sim 0.5$ cm. The estimate of the width of the layer by the air concentration gives the same value with respect to order of magnitude. Actually, in air of normal density the radiation path length λ=79 to 190 nm is $\ell \sim 10^{-2}$ cm, and for air concentration of 5%, $\ell \sim 0.2$ cm.

Both in the experiments and in the calculations the maximum brightness temperature of the shock waves in argon with air admixture is much lower than in the argon and air individually. The quantitative divergences of the experimental curve in Figure 35 with the calculated curves in Figure 58 can be ignored. The fact is that when calculating curves 1-3 in Figure 58 the coefficient of absorption of short-wave radiation by air was assumed to be invariant. The heating and the dissociation of air ahead of the front lead to the disappearance of the molecular mechanisms of absorption. The heated layer will be broader. The braking absorption of light by the electrons on the atoms, which plays a significant role at low temperatures in the admixture heated layer, was also not taken into account. All

of this must intensify the shielding so that for stricter calculations it is necessary to expect better quantitative agreement with the experiment.

In the experiments with inert gases nonsteady shielding of the radiation was detected. The characteristic features of the phenomenon indicate the development of a broad shielding layer ahead of the discontinuity. This could be an admixture heated layer. The experiments in which the argon was specially diluted by a small amount of air gave only a more sharply expressed effect. In the majority of experiments the procedure for filling the couvettes obviously kept the admixtures from getting into the gas except those already in it -- 0.01% in argon and xenon; 0.005% in helium.[1] By the concentration of the admixtures and their absorption coefficients the width of the admixture heated layer $\ell \sim 1$ m, and the delay in its formation $t \sim \ell/D \sim 100$ microseconds. Under the conditions of our experiments this layer not only did not, but could not occur as a result of the small dimensions of the couvette. Obviously, the above-investigated peculiarities of the shielding in the gas with admixture can be manifested fully only in large-scale experiments in which the couvette dimensions are greater than the width of the admixture heated layer.

Volumetrically absorbing a small part of the shock wave emission by the admixtures, the gas in the couvette was heated, according to the estimates, to $\sim 10^3$°K. If all of the radiation were absorbed, the gas temperature in the admixture heated layer would reach ~15000°K in experiments with xenon, ~18000°K in experiments with argon and ~30000°K in experiments with helium. At these temperatures the gas layer ~1 cm wide absorbs intensely. Possibly the initial heating as a result of

[1] Let us present the composition of the impurities in the argon, going by the certificate on the bottle: 0.01% nitrogen, no more than 0.003% oxygen, 0.03 g/m^3 moisture for a gas pressure of 760 mm Hg.

the admixtures leads to an increase in the absorption and gradual heating of the gas in the couvette with the formation of a broad shielding layer ahead of the front.

Analysis of the possible causes of nonsteady shielding will be incomplete if we do not discuss the paper [45]. In 1959 L. M. Biberman and B. A. Veklenko demonstrated that as a result of absorption of resonance quanta in the wings of the lines and subsequent acts of reradiation similar to diffusion, a broad layer of excited atoms is formed ahead of the shock wave front. The level population in the layer is close to Boltzmann at a temperature equal to the gas temperature behind the front, and the layer itself grows without limit with time (the excitation wave goes to infinity). Considering the extinguishing of the excitation in gas-kinetic collisions, the layer width is finite. In atomic gases the probability of extinguishing is very low, and it is determined more frequently by the presence of molecular admixtures. Thus, with air concentration in the argon of 0.01% and an initial pressure of the gas p_0=10 mm Hg, the width of the layer $\ell \sim 1$ m, and the time of its formation $t \sim 10^{-4}$ sec. Recalculation for the case of p_0=760 mm Hg will give $\ell \sim 1$ cm and $t \sim 1$ microsecond. It would appear that in the formation of such a layer it is also necessary to find the explanation for the experimental results. Recently Vulliet [160] calculated that an optically dense layer of excited aron atoms is formed after the shock wave is propagated 2 cm at a velocity of D=8 km/sec.

The authors of references [45, 160] did not take the extinguishing (photoionization) of the excited atoms by the shock wave radiation into account in the calculations. This approach is to some degree justified for optically thin shock waves which emit weakly in the continuum, but is suitable for optically dense shock waves. Thus, at a temperature behind the front of $T_1 \sim 3 \cdot 10^4$°K for each resonance

quantum capable of exciting an atom ahead of the front, an optically dense shock wave emits ~10^2 quanta capable of extinguishing excitation. Therefore only that concentration of excited atoms will be set up ahead of the shock wave front for which the layer will absorb no more than ~10^{-2} of the visible and near ultraviolet radiation. The heating of the gas as a result of this radiation absorption is of the same order as for ~0.01% admixtures.[1]

Some authors, analyzing the results of experiments in shock tubes, discuss the possibility of diffusion of the "hot" electrons from the region of the shock-heated gas to the region ahead of the front. The process is similar to thermoelectron emission from the surface of incandescent metals. In reference [44], the argon temperature ahead of the front (supposedly as a result of energy transport by such electrons) reached 8000°K. The phenomenon has been studied insufficiently to estimate its role in our experiments.

In references [161-163] a study was made of the glow of xenon in a shock tube. In spite of comparatively low temperatures T_1=6000 to 9000°K, a continuous glow spectrum was observed which appeared with a delay. An extraordinary explanation for this phenomenon is proposed -- the continuous glow spectrum is related to the formation of Xe_2^* quasimolecules and transition of them from the excited stable state to the ground unstable state. Possibly these processes, occurring ahead of the shock wave front in our experiments, were responsible for nonstationary

---

[1]The kinetic model describing the photochemical reactions ahead of the shock wave front was proposed recently by Dohhins [46]. The investigation included radiation transport far from the wave front in the wings of the resonance absorption lines, partial capture of this radiation, subsequent photoionization of the excited atoms, photoionization of the atoms in the ground state and certain recombination and deexcitation processes. It is proposed that this model is applicable to powerful shock waves in argon. The case of a shock tube is especially considered.

shielding of the radiation. The other authors of [94] consider that the xenon glow observed in [161-163] is ordinary braking radiation of the electrons on the ions. In our opinion, at such low temperatures braking radiation of the electrons on the atoms predominated.

It is of interest to note that the phenomenon of brightness absorption has been observed by many authors in spark discharges [164]. Increasing the rate of input of energy to the spark discharge channel, beginning with some value of this rate, will not lead to an increase in the brightness temperature. On the contrary, a decrease in brightness of the channel with time was observed. In addition to quantitative similarity of the phenomena there is an interesting quantitative correspondence between the maximum brightness temperatures of the spark and the shock wave.

	Xenon	Argon	Air
Spark (according to [164])	27000°K	40000°K	45000°K
Shock wave (our experiments)	66000°K	80000°K	75000°K

Higher temperatures -- about 90,000°K in air -- were observed during discharges in capillaries. The absorption effect is perhaps connected with shielding of the high temperatures in the spark channel to some degree similar to shielding in a shock wave.

EXPLOSION RADIATION SOURCES

Moscow IZLUCHATEL'NYYE SVOYSTVA UDARNYKH VOLN V GAZAKH in Russian 1977

[Chapter 6 from the book "Radiating Properties of Shock Waves in Gases", by M. A. Tsikulkin and Ye. G. Popov, Izdatelstvo "Nauka", 173 pages]

[Text] Measured temperatures (70,000-140,000°K) place the shock wave in the same series with brighter radiators. Based on condensed explosives in heavy inert gases, one can create very compact light sources having many advantages. These sources are superior to the widely used pulsed gas-discharge lamps in the output of visible and especially of ultraviolet radiation. Explosive flash lamps have long been used successfully in photography of high-speed processes. And explosive sources have recently been used as a tool for investigating the effect of high-density radiant fluxes on solids. Unlike lasers, having a broad radiation spectrum propagated into the vacuum ultraviolet region, these sources permit more complete simulation of the phenomena that accompanied the motion of cosmic bodies in the atmosphere and strong explosions. The sources can also be used successfully for other diverse purposes, for example, to investigate photochemical reactions or as a standard of an absolutely black body at high temperatures.

1. Explosion Radiator for Photometry Purposes

Light sources with an incandescent body as a radiator are widespread in photometric technology. An example is a measuring lamp with a tungsten strip or a uniformly heated cavity with an opening that simulates an absolutely black body. The temperature of these radiators does not exceed 3,000°K whereas one encounters brightness temperatures of 10^4-10^5°K and above when investigating some phenomena. The great difference of brightnesses of an object under investigation and the comparison standard frequently makes it very difficult to calibrate radiation detectors. A high-temperature standard is convenient for this. The need for this standard aris arises in measurement in the ultraviolet region of the spectrum where incandescent bodies are not suitable in practice due to their low brightness. Attempts to adapt the electric discharge in gases for these purposes were rather successful. The recently developed EV-39 (EV-45) pulse source radiates like a black body with temperature of 41,000°K in the section λ = 200-600 nm [143, 144].

Experiments show that shock waves in air at temperatures of 10,000-50,000°K behind the front radiate like an absolutely black body over a very broad spectral range that encompasses the ultraviolet and infrared regions. The problem of using a

shock wave as a black body radiation standard at high temperatures was considered by the authors of [12-14].

To know the brightness temperature of a shock wave, using it as a pulsed radiation standard, it is sufficient to follow the velocity of the wave front. Measuring the velocity with accuracy of $\pm$ 1 percent by means of the SFR-2 photorecorder and resorting to calculated adiabatic shock curves, one can determine the temperature with an accuracy of $\pm$ 3 percent. However, it is preferable in practice to have a source with a previously known brightness temperature constant over some time segment. To meet these requirements, we used an explosive shaped charge to produce shock waves stable in amplitude (see Figure 9). The charge was cast from TG 40/60 and had the following dimensions: d = 8 mm, $\varnothing$ = 30, l = 120, L = 150 mm, depression under the detonator cap δ = 10 mm and weight of the charge of 168 grams. Careful measurements of the velocity of a stable shock wave in air formed upon detonation of this charge yield a value of 13.6 $\pm$ 0.1 km/s. If one uses the calculated adiabatic shock curve of air from [147], then the gas temperature behind the front of 24,000 $\pm$ 700°K corresponds to the measured velocity. The dimensions of the charge were selected so that inaccuracies of observing them have a weak effect on the shock wave velocity. As already noted (section 2, Chapter 2), maximum velocity whose value is almost independent of diameters $\varnothing$ and d (see Figure 12) at $\varnothing/d \geq 4$ is established in the charge channel at $l > 8d$. If an increase of charge weight plays no role, then selection of the highest possible ratio of $\varnothing/d$ is justified. The shock wave temperature also increases in this case. Thus, for charges with $\varnothing$ = 60 mm ($\varnothing/d$ = 7.5), a velocity of 16.7 km/s and temperature of 32,000°K were measured. However, the weight of these charges is fourfold greater.

The type of radiation pulse upon detonation of a shaped charge can be judged by Figures 10 and 41. With the selected dimensions, the glow time of a stable shock wave in the charge channel is 5 microseconds. If a tube of cardboard or other dense material not more than 160 mm long is attached to the charge, the shock wave propagates through it without appreciable attenuation and the glow time is extended to 17 microseconds (Figure 59).

Sometimes, for example, during photographic recording of the time-integral radiation by spectrograph or in measurements of radiation with a calorimeter, it is convenient to have a calibrated square-wave pulse. The time of stable shock wave formation is reduced from 5 to 2 microseconds if one uses an elongated charge (L = = 180 mm), the bottom of which is not flat, as in Figure 9, but is in the form of a conical recess. One can reduce the leading edge of the pulse even more--to 0.1 microsecond. To do this, the initial part of the channel where a stable shock wave is established must be separated by a thin opaque screen (for example, carbon paper). The screen is destroyed by the shock wave without introducing appreciable disturbances. The trailing edge of the pulse is cut off within approximately 1 microsecond when the shock wave encounters a quartz or glass window attached to the end of the accessory tube (Figure 60).

The results of measuring the brightness temperature of a stable shock wave in air with velocity of 13.6 km/s are presented in Figure 39. The temperature fluctuations in time and to the channel cross section did not exceed $\pm$ 1,000°K. A temperature variance was included in this same range from experiment to experiment.

The brightness temperature was approximately 1,000°K lower for charges manufactured from TG 50/50. Avoiding inhomogeneities in casting the charge and initiating the charge strictly along the axis, it was possible in some experiments to reduce the temperature fluctuations to ± 400°K.

It is obvious from Figure 39 that a shock wave in a channel radiated like an absolutely black body with temperature of 24,000°K over a wide spectral range of λ = = 220-1,300 nm. The radiation spectrum was continuous. The lines were not recorded even on spectrograms with resolution of 0.1 Å. In this regard the proposed source is similar to incandescent lamps although it differs from them by tenfold higher brightness temperature.

Having replaced the air by another gas, one can increase the radiation temperature and can penetrate the vaccum ultraviolet region. In several experiments the charge channel was filled with neon; in this case the temperature increased to 32,000°K. The temperature was raised to 40,000°K when the channel was filled with argon. However, transient shielding and instability of the plane front complicated production of stable radiation pulses in argon and heavier inert gases.

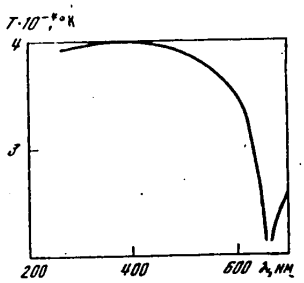

Figure 61. Dependence of Brightness Temperature of EV-39 Source on Radiation Wavelength Measured by Means of Explosive Brightness Standard

Thus, shock waves in air formed upon detonation of a shaped charge were a sufficiently stable radiator. The source described here was used by the authors as a brightness standard in laboratories and under field conditions. Its capabilities are illustrated in this regard by Figure 61, in which the dependence of brightness temperature of the EV-39 source on wavelength λ is shown [13]. The low weight and "pocket" size, the independence from an electrical system and other power sources and the absence of noise typical for pulsed sources with an electric charge make this radiator a convenient means of investigating explosive processes.

2. Installation of an Ultraviolet Shock

The effect of powerful ultraviolet radiation pulses on solids is accompanied by a number of interesting physical and gas-dynamic phenomena. These phenomena can be studied experimentally by means of special explosive installations in which a strong shock wave is radiated in an inert gas [9-11]. These installations are similar to existing pulsed lasers by the radiant flux density and are far superior to them in the value of the radiated energy.

We achieved the maximum radiant flux density from the front of a shock wave in experiments with helium. At shock wave velocity of D = 78 km/s the density of the ultraviolet radiation (shielding of which can be disregarded) was estimated at $S_\infty = 3 \cdot 10^8$ W/cm^2.

However, development of devices designed to investigate the effect of radiation on matter consist not only in producing maximum fluxes from the wave front but in providing those geometric ratios which would permit fuller use of the radiated energy to affect the target being investigated. In this regard devices used to achieve high shock wave velocity were ineffective. It follows from formula (3.16) for a disk radiator that the flux density on the target depends on the square of the sine of the angle at which the radiator is visible. Therefore, the flux density on the target $\Phi = 3 \cdot 10^8$ W/s^2 could be produced only for a very short time, on the order of 10^{-7} second, when the wave would be in the immediate vicinity of the irradiated surface. The integral energy density in time $E = \int_0^t \Phi \, dt$ distinguished on the target would also be low, approximately 10 J/cm^2.

The weight of the charge, which was limited to 1 kg in our experiments, is also no less important when designing the installation. To compare explosive radiation sources to each other, it is convenient to introduce the efficiency of the source

$$\eta = \frac{ES}{Gq}, \tag{6.1}$$

where E is the radiant energy density released on the target during operation of the installation, S is the output cross-sectional area where the target is placed, G is the weight of the explosive charge and q is the heat value of the explosive. Devices to achieve record velocities and temperature had an efficiency of only $\eta \sim 0.001$ percent.

An explosive radiation source, under the effect of which intensive evaporation and flight of different solids was detected, is described in [9]. The sources was a shaped charge filled with argon (Figure 62). The inner walls of the channel were lined with polished aluminum foil that reflected part of the radiation to the target. The mean velocity of the shock wave in the channel was D = 9 km/s and the brightness temperature in blue light was T_{ya} = 26,000°K.* The plane front lost stability and began to bend near the walls approximately 10 microseconds after generation of the shock wave. Its temperature dropped in this case to T_{ya} = = 17,000°K.

The radiant flux density Φ and the surface energy density E near the target axis were calculated from the results of measuring the brightness temperature of the front in blue light and its position in time. The inhomogeneity of the brightness of the front through the channel cross section was taken into account in the calculation. It was assumed that the shock wave radiated like an absolutely black body up to the transparency threshold of argon. Circular regions of the mirror

*The value of brightness temperature refined compared to [9] is presented here.

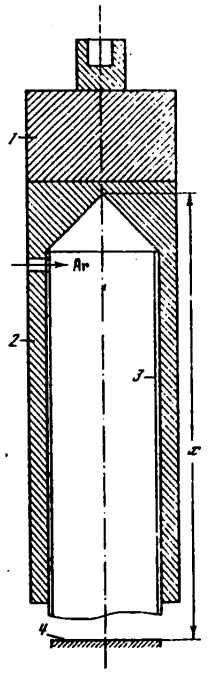

Figure 62. Explosive Radiation Source: 1--lens providing plane detonation front; 2--charge of cast TG 40/60 weighing 400 grams (outer diameter of 60 mm, inner diameter of 45 mm and length of charge of 165 mm); 3--polished aluminum foil; 4--target

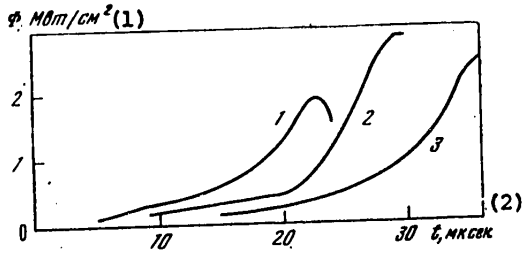

Figure 63. Flux Density Φ with Different Positions of Target: 1--x = 21 cm, E = 15 J/cm^2; 2--x = 27 cm, E = J/cm^2; 3--x = 33 cm, E = 15 J/cm^2

Key:
1. MW/cm^2
2. Microseconds

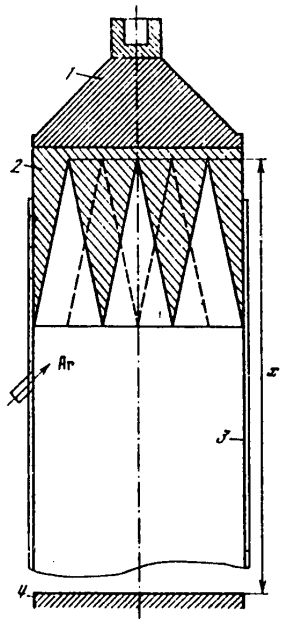

Figure 64. Explosive Radiation Source: 1--lens providing plane detonation front; 2--charge of cast TG 40/60 weighing 400 grams, diameters of 84 mm and length of 70 mm; 3--polished aluminum foil; 4--target

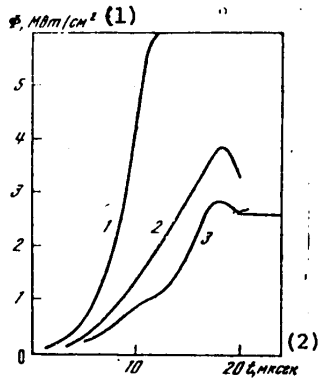

Figure 65. Flux Density Φ with Target in Different Positions: 1--x = 15 cm, E = 20 J/cm^2; 2--x = 25 cm, E = 31 J/cm^2; 3--x = 27 cm, E = 32 J/cm^2

Key:
1. MW/cm^2
2. Microseconds

image of the shock wave front bounded by beams at angles of θ_0 (without reflection), $\theta_1 - \theta_0$ (single reflection), $\theta_2 - \theta 1$ (double reflection) and so on, are formed on the reflecting walls of the channel. In this case formula (3.16) for a disk radiator acquires the form

$$\Phi = a\sigma T^4 [\sin^2 \theta_0 + k(\sin^2 \theta_1 - \sin^2 \theta_0) + k^2 (\sin^2 \theta_2 - \sin^2 \theta_1) + \ldots + k^n (\sin^2 \theta_n - \sin^2 \theta_{n-1}) + \ldots], \quad (6.2)$$

where K is the reflection coefficient of foil and a is a multiplier that takes into account the opaqueness of argon for photons $h\nu > 15.7$ eV. According to [148], the reflection coefficient of aluminum is weakly dependent on the angle of incidence and hardly varies in the spectral region of interest to us. The mean reflection coefficient for the spectrum was assumed equal to k = 0.5.

The results of calculating the radiant flux density Φ and energy density E on the target are presented in Figure 63. There is an optimum distance for installation of the target x = 27 cm for which the flux density Φ and energy density E are maximum. The shock wave reached the highest amplitude at this distance. The contribution of reflection from the foil to energy E comprised approximately 30 percent. The efficiency of the source was estimated at η = 0.01 percent.

The source described above was used to investigate the effect of powerful radiation with continuous spectrum on a solid. A number of interesting results was obtained. However, some deficiencies of the source were also determined during the experiments. More than half the explosive products of the charge flew off to the sides and did not participate in formation of the shock wave in the channel. The wave due to detonation of the channel walls was intensified only toward the end of action of the source when the temperature near the walls decreased due to bending of the front. The aluminum foil with which the channel walls were lined reduced the shock wave amplitude somewhat.

Experiments were conducted from the results of which a more improved design of the source was developed (Figure 64). The latter is a charge cast from TG 40/60 in the form of a cylinder with seven conical recesses, placed in a tube of polished aluminum foil. The tube diameter is two times greater than the channel diameter of the source of the old design. The mean velocity of the shock wave when the source is filled with argon is D = 11 km/s and brightness temperature in blue light is 30,000°K. The results of calculating the radiant flux density Φ and the energy density E at the center of the target are presented in Figure 65. The maximum flux density Φ = 6 MW/cm^2 is reached near the charge at x = 15 cm. The amplitude of the shock wave is highest at this location. The integral energy density in time E is maximum when the target is installed at a farther distance, x = 27 cm. Although the flux density on the target Φ decreases in this case, the time of operation of the source and the energy E increase. The efficiency of the source at this distance is η = 0.07 percent.

It is significant that the source of new design permits irradiation of a target 84 mm in diameter (the maximum target diameter was 40 mm in the previous design). Because of this, evaporation and scattering of the target material proceeded under conditions similar to one-dimensional, which facilitated analysis and interpretation of the results. The flux density distribution Φ through the target

radius is presented in Figure 66. The nonuniformity of illumination initially increased (it was maximum at a distance of y = 4 cm from the wave to the garget) and then decreased as the shock wave approached the target. Reflection from the tube walls was not taken into account in calculations of distribution but it is qualitatively clear that it reduces the nonuniformity of irradiation.

Experiments were conducted on evaporation of sulphur targets to compare the source of the old and new design. The rate of rise of the luminous threshold of the vapors comprised 0.8 km/s for the old design and 1.1 km/s for the new design. More intensive glow of the vapors was also observed in the latter case.

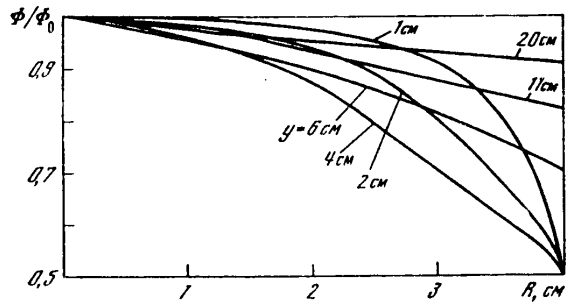

Figure 66. Flux Density Distribution Φ Through Target Radius, Related to Density Φ_0 at Center (y is the distance from the shock wave to the target)

By using inert gases heavier than argon, one can reach higher temperatures at lower velocities D. Although the region of gas transparency decreases in this case, an increase of temperature leads in the final analysis to an increase of flux density Φ on the target. The energy density E released on the target increases even more strongly since the operating time of the source is extended.

Experiments were conducted in which the source was filled with xenon. To avoid losses of the scarce gas, the source was filled by preliminary evacuation rather than by purging. Changes were introduced in the design of the source for this purpose compared to Figure 64. A charge with foil and the target were inserted in a glass tube hermetically sealed on both ends by plates. The charge was initiated by a lens through the plate. The velocity and temperature of the front in blue light at the beginning of operation of the source comprised D = 12 km/s and T_{ya} = 55,000°K, but dropped to values of D = 5.3 km/s and T_{ya} = 30,000°K within 27 microseconds. Despite the fact that xenon is transparent only to photons of $h\nu < 12.1$ eV (argon is transparent for $h\nu < 15.70$ V), the flux density Φ and energy density E increased appreciably (Figure 67). When the target was installed at distance of x = 14 cm, the flux density was maximum, Φ = 15 MW/cm^2. The integral energy density in time was maximum at x = 21 cm and was equal to E = 130 J/cm^2; the efficiency of the source for this distance was estimated at η = 0.3 percent.

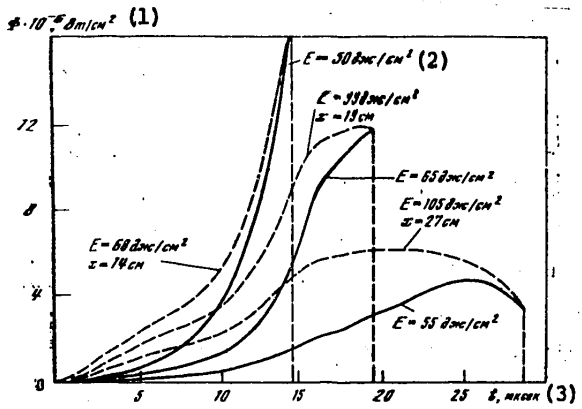

Figure 67. Flux Density Φ and Energy Density E at Center of Target With Source Filled With Xenon: the solid curves correspond to foil reflection coefficient of 0.5; dashed line--without regard to reflection

Key:
1. W/cm^2
2. J/cm^2
3. Microseconds

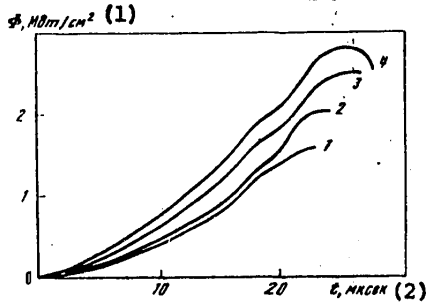

Figure 68. Flux Density Φ at Center of Target Installed at Distance of x = 27 cm with Different Initial Pressures of Argon: 1--p_0 = 50 mm Hg (E = 14 J/cm^2); 2--p_0 = 100 mm Hg (E = 18 J/cm^2); 3--p_0 = 300 mm Hg (E = 27 J/cm^2); 4--p_0 = 760 mm Hg (E = 34 J/cm^2)

Key:
1. MW/cm^2
2. Microseconds

The source was filled with xenon to produce harder radiation with photon energy up to $h\nu$ = 21.5 eV. The mean wave velocity on the section of x = 27 cm was D = 13 km/s and temperature was T_{ya} = 30,000°K. The radiant flux density reached Φ = 4 MW/cm^2 and energy density E = 30 J/cm^2.

Table 10

p_0, mm Hg	760			300			100			50		
y, см	20	8	1	20	8	1	20	8	1	20	8	1
D, км/s	9.8	10.4	10.2	10.0	10.6	10.8	10.6	11.2	11.4	11.0	11.3	11.8
$T \cdot 10^{-3}$, °K	26	29	28	24.5	27	28	23.5	26	27	23	25	26.5

The use of different inert gases in the source permits one to study the effect of the spectral composition of radiation and the density of the surrounding medium on the target. The parameters of the source when it was filled with argon of reduced density were also measured in this regard. The values of temperature and velocity of a shock wave for three distances y to the target (x = 27 cm) at different initial argon pressure are presented in Table 10.

Although the temperature does not vary very strongly with variation of the initial pressure, the difference in the fluxes is significant (Figure 68). The difference is even greater for energy E since the wave velocity increases with a decrease of pressure and the operating time of the source is reduced. The energy E decreases by a factor of 2.4 upon transition from initial pressure p_0 = 760 mm Hg to p_0 = 50 mm Hg. But if one takes into account the energy released during the same time, for example, during the first 22 microseconds, this difference decrases to a factor of 1.6.

§3. Efficiency of Explosion Sources

Under laboratory conditions when the weight of the used explosive charge is limited, it is possible to achieve an increase in radiant energy only by increasing the efficiency of the source. Its highest value $\eta=0.3\%$ was obtained in a blast source with xenon. This is approximately 100 times more than in ordinary devices designed to obtain powerful shock waves. The preliminary results of several experiments indicate that as a result of further improvement of the structural designs of the source it is possible to achieve an efficiency of $\eta=1\%$. For this purpose it is necessary to use a sufficiently strong tube which will not be destroyed on passage of the shock wave and which at the same time will insure slower damping of the wave. Between the charge and the walls of the tube it is necessary to leave a wedge-shaped gap, as a result of which the flight of the blast products to the sides will also be used for the creation of a shock wave in the tube. It is necessary to use a higher quality mirror coating which is obtained by depositing aluminum in a vacuum. Significant reflection in the ultraviolet region can be achieved if we avoid contact of the coating with air, for example, immediately after deposition, fill the tube with an inert gas [148].

For further significant increase in radiant energy yield, theoretically new solutions are needed. The source efficiency introduced in the form of (6.1) is in essence the product of three cofactors:

$$\eta = \eta_1\eta_2\eta_3, \tag{6.3}$$

where η_1 is the energy transfer coefficient from the explosive charge to the shock wave, η_2 equals the efficiency of the shock wave as a radiator, η_3 is the radiant energy transfer coefficient from the shock wave to the target. Let us discuss each of these coefficients in more detail.

The energy transferred to the wave is made up of the internal energy of the heated gas and its kinetic energy. In a powerful shock wave they are equal to each other, and for a unit mass of gas it is possible to write

$$e = u^2/2. \tag{6.4}$$

Expressing the gas velocity in terms of the front velocity $u=(2/(\gamma+1))D$, we obtain the following expression for the energy transfer coefficient to the wave:

$$\eta_1 = \frac{4}{(\gamma+1)^2}\frac{\rho_0 D^2 V}{Gq}, \tag{6.5}$$

where V is the initial volume occupied by the gas (the volume of the working chamber of the source), D is the average shock wave velocity, G is the weight of the charge, q is the calorific value of the explosive.

Shaped charges give higher shock wave velocity in the required direction. The coefficient η_1 is higher for them. For example, the charge which we used which had seven shaped depressions created a shock wave with an average velocity of D=11 km/sec in argon. The charge cast without the shaping and having 1.3 times more weight created a shock wave with an average velocity of D=8 km/sec in the working chamber of the source. Thus, as a result of shaping the coefficient η_1 was increased by 2.5 times.

A significant effect can be achieved on going over to high-density gases. Although the average shock wave velocity is somewhat lower in this case, the combination $\rho_0 D^2$ increases. Thus, on going from argon to xenon, the average

velocity in the section x=27 cm decreased altogether from 11 to 10 km/sec, and the density ρ_0 increased by 3.3 times. As a result the energy transfer coefficient increased by 3.3 times, reaching a value of η_1=18%. The dependence of the coefficient on the density is such (Figure 69) that on filling the source with xenon with pressure of p_0=3 to 4 atm it is possible to approach a value of η_1=50%. There is a limit somewhere here, for the blast products expand in all directions, and part of the charge energy is consumed on creation of the shock wave in the surrounding air. If the charge is separated from the air by a massive rigid shell, then this limit can be shifted away.

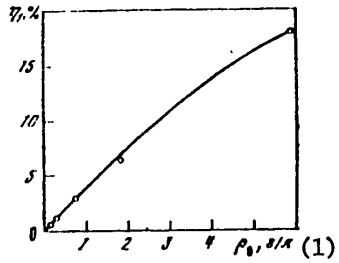

Figure 69. The coefficient η_1 as a function of gas density ρ_0 constructed according to experimental data

Key:
1. g/liter

The greatest reserves for increasing the efficiency of blast sources consist in increasing the effectiveness of the shock wave as a radiator. The work done by a piston creating a powerful shock wave in a gas if it is reduced to a unit time and a unit surface of the front is

$$A = p_1 u = \rho_0 u^2 D = \frac{4}{(\gamma+1)^2}\rho_0 D^3. \tag{6.6}$$

The energy emitted from the unit surface of the front per unit time is

$$S = a\sigma T^4, \tag{6.7}$$

where a is the factor considering the opaqueness of the gas ahead of the front for the quanta $h\nu > I$. Then for the shock wave-emitter efficiency we have

$$\eta_2 = \frac{(\gamma+1)^2}{4}\frac{\sigma T^4}{\rho_0 D^2}. \qquad (6.8$$

From Table 11 it is obvious that with an increase in the temperature the coefficient η_2 first increases and then decreases (this smooth dependency is distorted somewhat by the peculiarities of ionization in each specific gas). For each gas there is a defined temperature range in which the radiation yield is maximal.

Table 11. Coefficient η_2 for Different Temperatures, %

$T \cdot 10^{-4}$°K	3	4	5	6	7	8	9	10	12	14	16
He	2,7	2,5	2,8	3,6	4,5	5,0	4,9	4,7	4,1	4,6	5,2
Ne	2,9	3,2	4,5	4,8	4,8	4,8	4,9	4,8	4,0	3,8	3,4
Ar	2,4	2,9	2,8	3,1	2,7	2,6	2,3	2,7	2,4	1,9	1,6
Kr	2,9	3,2	3,5	3,8	3,9	3,7	3,5	3,1	—	—	—
Xe	3,1	2,8	2,8	2,7	2,5	2,5	2,5	2,3	—	—	—

Helium and neon are distinguished by high value of the energy deexcitation coefficient $\eta_2 \approx 5\%$. The application of these gases is expedient at temperatures above 60000°K when, along with high efficiency, large radiation flux densities with respect to absolute magnitude are achieved. Accordingly, experiments were set up [165] in which couvettes 25 mm in diameter and the devices described in §3 of Chapter II were used. For several microseconds the shock waves glowed with a temperature of ~100,000°K. The radiant flux density was estimated at 10^8 watts/cm^2. The deficiency of the devices was the low energy transfer coefficient to the wave $\eta_1 \sim 1\%$. For gases with high atomic weigh the deexcitation coefficient η_2 is smaller, but it is higher than the energy transfer coefficient to the wave η_1 so that on the whole the efficiency of the source gains. Obviously the shaped charges used in combination with xenon or krypton insure the highest radiant energy yield.

It is possible to determine the effect of the initial gas pressure on the efficiency of a shock wave emitter according to the data in Table 12.

Table 12. Coefficient η_2 for Different Argon Pressures, %

$T \cdot 10^{-4}$°K	2	3	4
p_0=760 mm Hg	2.3	2.4	2.9
p_0=300 mm Hg	4.2	5.3	5.6
p_0=100 mm Hg	9.2	12	14
p_0=50 mm Hg	15	22	23

The radiation yield increases quite rapidly as the gas pressure drops. The growth is such that it almost compensates for the decrease in the energy transfer coefficient to the wave (the product $\eta_1\eta_2$ at p_0=760 mm Hg is a total of 1.2 times greater than for p_0=50 mm Hg). On the other hand, if the pressure increases above atmospheric, the variation of the coefficient η_1 slows (see Figure 69) whereas the value of the coefficient η_2 persistently decreases. Therefore the optimal initial pressure insuring the highest source efficiency must be realized. According to the data presented in Figure 68 for argon this pressure is approximately equal to atmospheric pressure.

Intentionally selecting various gases, we have complained many times that in nature there is no gas with such a high atomic weight as xenon and with such high ionization potential as helium. As a result of the high atomic weight this gas would be heated to high temperatures with effectiveness energy transfer to the wave. As a result of the high ionization potential, the cold gas ahead of the front would remain transparent in the far ultraviolet region so that a significant proportion of the radiation from the heated gas would be emitted to the outside. Considerations about this question have led us to the conviction that a medium with the required properties can be obtained artificially.

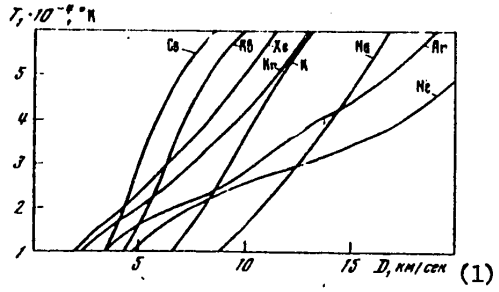

Figure 70. Shock adiabats of alkali metal vapor and inert gases

Key:

1. km/sec

All of the alkali metals have low primary, but quite high secondary ionization potentials. The estimates which follow below indicate that the radiation of a powerful shock wave propagated in alkali metal vapor is capable of singly ionizing the vapor far ahead of the front. However, the singly ionized vapor absorbs quanta weakly with energy less than the second ionization potential. Therefore as a result of the fast ionization of the body of the vapor powerful radiation begins to reach the target uninhibited.

Let us try to substantiate this picture quantitatively. In Figure 70 we see the temperature of shock-heated vapor as a function of the wave front velocity (the initial vapor temperature was assumed equal to the boiling point at atmospheric pressure; see the Appendix). A comparison with the analogous relations for inert gases which are also presented in Figure 70 is of interest. The energy expenditure on the primary ionization of alkali metals is much less. Therefore in practice for equal atomic weight (A_{Ne}=20.18 and A_{Na}=22.99, A_K=39.10 and A_{Ar}=39.94, A_{Kr}=83.80 and A_{Rb}=85.48, A_{Xe}=131.3 and A_{Cs}=132.9) higher temperatures are reached in the alkali metal vapor. The noted characteristic feature itself leads to noticeable increase in the energy deexcitation coefficient of the shock wave.

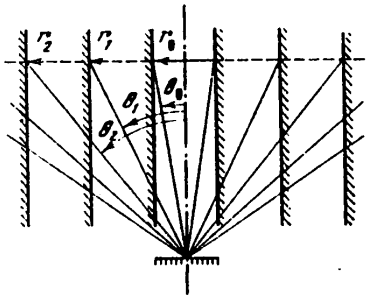

Figure 71. Calculation of the flux density in the center of the target

Let us demonstrate that the radiation is capable of quite fast ionization of the body of the vapor separating the front and the target. Alkali metal vapor at a temperature of ~1 ev in practice is entirely ionized. The expenditures on eating the cesium vapor to this temperature, for example, are 6.9 ev/atom. In 1 cm^3 of vapor under atmospheric pressure at the boiling point (963°K), there are $7.6 \cdot 10^{18}$ atoms so that the expenditures on heating 1 cm^3 of cesium vapor amount to 8.4 joules. For heating a column of vapor 1 cm^2 in cross section and 30 cm long it takes 250 joules. At the temperature behind the front $T_1=10^5$°K this energy is emitted from 1 cm^2 of front surface in ~0.5 microseconds. Thus, fractions of microseconds are needed for the ionization of the body of the vapor separating the front and the target. As a result, inasmuch as the ionized vapor absorbs very weakly[1], the powerful radiation reaches the target.

Beginning with the fact that the quanta less than the second potential of cesium ($h\nu<33$ ev) are not absorbed ahead of the front, the values of the "deexcitation" coefficient η_2 are calculated by formula (6.8).

$T_1 \cdot 10^{-4}$°K	3	4	5	6	7	8	9	10	12
η_2, T	26	48	35	27	36	44	50	55	60

[1]The estimates according to (5.4) give a path length in the vapor $\ell_\nu \sim 0.7$ cm for small visible quanta $h\nu \sim 2$ ev. However, for the quanta $h\nu \sim 10$ to 30 ev for which almost all of the emitted energy is needed, the paths turn out to be longer, $\ell_\nu \sim 1$ to 20 meters.

The presented figures indicate that by using alkali metal vapor it is possible to increase the efficiency of blast sources by tenfold.

Let us discuss the last of the cofactors which determines the efficiency of the blast source -- the energy transfer coefficient from the shock wave to the target. In the sources which we used this coefficient was $\eta_3 \approx 0.2$, but it could be increased, improving the quality of the reflector. For reflecting walls of the cube the emitter will be not only the wave front, but also annular regions -- reflections of the front in the tube walls (Figure 71). The radiant flux density at the center of the target can be represented in the form of a series (6.2) or by grouping the terms of the series in pairs, in the form

$$\Phi = S(1-k)\sum_{n=0}^{\infty} k^n \sin^2 \theta_n = S(1-k)\sum_{n=0}^{\infty} k^n \frac{r_n^2}{r_n^2 + y^2}. \tag{6.9}$$

Here S is the flux density from the front, k is the reflection coefficient. From Figure 71 it is obvious that $r_n=(2n+1)r$, and instead of (6.9) we have

$$\Phi = S(1-k)\sum_{n=0}^{\infty} k^n \frac{(2n+1)^2 r^2}{(2n+1)^2 r^2 + y^2}. \tag{6.10}$$

The energy density E at the center of the target released during operation of the source t will be

$$E = \int_0^t \Phi\, dt = \int_x^0 \Phi \frac{dt}{dy}\, dy = \int_0^x \frac{\Phi}{D}\, dy, \tag{6.11}$$

where x is the distance from the charge to the target, D=-dy/dt is the front velocity. Integrating this series (6.10) by terms and setting D=const, we obtain

$$E = \frac{Sr(1-k)}{D}\sum k^n (2n+1) \operatorname{arctg} \frac{x}{(2n+1)r}. \tag{6.12}$$

If we assume that this target is installed quite far from the charge and we set $\operatorname{arctg} \frac{x}{(2n+1)r} = \frac{\pi}{2}$ in (6.12), then for the energy density we obtain the following expression:

$$E = \frac{\pi}{2}\frac{Sr}{D}\frac{1+k}{1-k}. \qquad (6.13)$$

The data for the other distances are presented in Table 13.

Table 13. Values of the Energy Density E in Units of $(\pi/2)(Sr/D)$ for Different Reflection Coefficients and Distances

x/r	1	2	3	4	5	7	∞
$k=0$	0,50	0,71	0,80	0,84	0,88	0,90	1
$k=0,5$	0,56	0,94	1,22	1,43	1,60	1,74	3
$k=0,7$	0,59	1,06	1,44	1,77	2,05	2,29	5,67
$k=0,9$	0,62	1,19	1,72	2,23	2,70	3,15	19

In the case where D=const the greatest gain from increasing the reflection coefficient is obtained when installing the target at the maximum distance $x \to \infty$. Under real conditions when the shock wave damps, there is an entirely defined distance from the charge to the target in which the energy density is maximal. The role of the reflector decreases here. Thus, in the previously described sources the contribution of reflection was about 30%. However, with an increase in the reflection coefficient the optimal distance of installing the target also increases. On the whole, as the estimates show, for k=0.7, as a result of the reflector it is possible to achieve doubling of the energy released on the target. For a reflection coefficient k=0.9 which is actually attainable only for the visible and near ultraviolet regions, the contribution of the reflector can exceed the contribution of the shock wave by several times. The most radical path of increasing the energy transfer coefficient to $\eta_3=1$ is to "stop" the shock wave in direct proximity to the target. On braking the wave it would also be possible to increase the temperature of the shock-heated gas, which would provide an additional effect. However, it is quite difficult to implement this idea. It is possible,

for example, to place a transparent wall in front of the target. However, first, the most transparent materials (fluorite, lithium fluoride) intensely absorb the radiation with a wave length λ shorter than 110 nm [148] and, secondly, after the impact of the wave against the wall the latter cracks and completely eliminates transparency.

It is possible to use the interaction of the shock wave with a magnetic field. For effective braking of the shock wave fields are required with an intensity on the order of [166]

$$H = \left[\frac{16\pi(3\gamma-1)}{\gamma^2-1}\rho_0 D^2\right]^{1/2}. \tag{6.14}$$

For $\rho_0=10^{-3}$ g/cm^3, $\gamma=1.2$ and D=10 km/sec, we obtain $H=6\cdot10^5$ oersteds. The pulse magnetic fields of such intensity are entirely attainable under laboratory conditions (for example, using magnetic shaped-charge generators in which obviously it is possible to use the blast energy of the charge of the source itself).

The original method of braking the shock wave was proposed by the author I. V. Nemchinov. It is necessary to separate the gas with high atomic weight (xenon) from the target by a layer of gas with low atomic weight, but high ionization potential (helium). Then after passage of the shock wave the interlayer of helium is forced out and the xenon heated to high temperature brakes on the target. As a result of low atomic weight the helium is heated insignificantly and remains transparent. It is still better to use cesium vapor as the gas with high atomic weight. The fact is that a narrow layer of xenon at the interface with helium quickly cools by radiation and begins to shield the internal region heated to high temperature. The shielding of the cesium plasma is negligible until it cools to a temperature of $\sim10^4$°K.

The possibility of creating a light source in which the energy of a gas cooling as a result of radiation yield has been studied experimentally by I. I. Divnov. In the experiments a device of the shock wave tube was used which made it possible to obtain a moving xenon-helium interface in a tube 15 mm in diameter and then heat the xenon by an explosive blast. The diagram of the experiments is presented in Figure 72. Two tubes filled with xenon (2) and helium (4) are separated by the diaphragm (3). The latter is ruptured when the helium pressure rises to a given value. After rupture of the diaphragm a shock wave is formed in the xenon behind which the contact "xenon-helium" interface moves. When the wave reaches the ionization sensor (6), the charge is exploded (1). The powerful shock wave created by the blast heats the xenon. In order for a rarefaction wave not to occur after the shock wave reaches the interface with the helium in the xenon, the helium density must be no less than the xenon density. This condition could be satisfied by selecting the initial gas pressures p_0=0.05 atmospheres in xenon and p_0=20 atmospheres in helium (calculating the rupture decay formed during rupture of the diaphragm it follows that on both sides of the contact interface the gas pressure and densities are identical and equal to $p_1 \simeq 3$ atmospheres and $\rho_1 \simeq 10^{-3}$ g/cm^3).

Figure 72. Device for attaining a stationary volume of gas heated to high temperature.
1 -- explosive charge, 2 -- blast tube with xenon, 3 -- diaphragm, 4 -- metal tube with helium, 5 -- glass window, 6 -- ionization sensor

In the experiments the brightness temperature of the glow was measured through the window (5) using the FR-10M camera. The velocity of the shock wave front was measured simultaneously (the recording diagram appears in Figure 27, a). The brightness temperature as a function of time is presented in Figure 73 for one of the experiments. Up to the time t_1 the blast shock wave was propagated in the xenon of the initial density; an increase in brightness temperature was caused by the acceleration of the shock wave in the charge channel. At $t_1<t<t_2$ the blast shock wave moves through the xenon previously heated and compressed to density of $\rho_1 \approx 4\rho_0$ in the shock wave formed after the rupture of the diaphragm. The time t_2 corresponds to the shock wave reaching the interface with the helium. The decrease in brightness for $t>t_2$ is naturally connected with radiant cooling of the xenon.

The shock wave velocity in the experiment at the time $t_1<t<t_2$ was 12.2 km/sec. This value of the velocity corresponds to the temperature in the wave of $7 \cdot 10^4$°K greatly exceeded the measured values of the brightness temperature. Obviously shielding of the visible radiation occurred in the wave front. However, on reaching the interface with the helium the shielding must disappear, and a brightness temperature peak must be observed at the first instant (shown in Figure 73 by the dotted line). However, in the experiment, sometimes as a result of insufficient time resolution (10^{-7} sec), and sometimes as a result of turbulent mixing of the helium and xenon the peak was not observed.

Let us note that the use of helium as the "light guide" makes it possible to obtain large radiation fluxes with "wide" spectrum -- to the limit of transparency of helium ($h\nu<24.6$ ev) -- for comparatively low shock wave velocities. In order to obtain such fluxes, heating the helium itself, a shock wave velocity that is much larger is required. A large deficiency of such devices is the fact that the helium interlayer separating the target from the highly heated gas does not

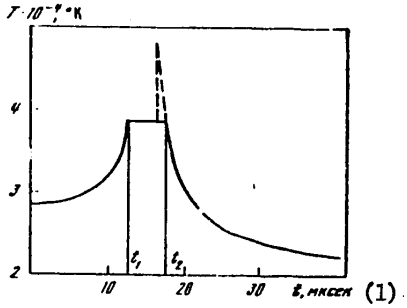

Figure 73. Brightness temperature (λ_{eff}=432 nm) as a function of time; the time the detonation reaches the bottom of the shaped channel is taken as the origin

Key:
1. t, microseconds

protect it from high pressures developing during braking of the shock wave. However, in some cases, for example, when the cosmic body is moving in the lower layers of the atmosphere, the simultaneous effect of powerful radiation and high pressure is typical. For simulation of such phenomena it is even simpler to get along without the helium interlayer, realizing braking of the shock wave by the target itself.

Up to now we have considered the blast devices as an instrument for the investigation of the effect of powerful radiation fluxes on matter. However, it can also be used for other purposes. In some experiments the gas in the shock wave was heated to temperatures above 10^5°K. On reflection of this wave from a rigid barrier the temperature would exceed $3 \cdot 10^5$°K, and the density would become 50 times greater than the gas density at atmospheric pressure. Such a dense hot plasma is a source of quite intense x-radiation. On expansion of 1 cm^3 of such plasma to atmospheric pressure, a glowing ball is formed about 0.5 meters in diameter with a temperature of about 30000°K. In essence, the existing devices using the chemical energy of an explosive permit simulation of many processes occurring during a nuclear blast -- irreversible heating of the gas in a powerful shock wave, adiabatic expansion of a shock-heated gas to atmospheric pressure with the

formation of a fire ball, slow cooling of the fire ball by radiation. An artificial miniball can turn out to be an effective source of light similar to the natural fire ball, from the surface of which a significant proportion of the nuclear blast energy is released (tens of percentages [37]).[1]

Let us also note that the application of a shock wave as a radiator for visible and near ultraviolet regions has its peculiarities. As we have already noted, the reflector can play an important role. The efficiency of the energy deexcitation in the different sections of the spectrum must be characterized, in contrast to (6.8) by the spectral deexcitation coefficient

$$\eta_\lambda = \frac{(\gamma+1)^2}{4}\frac{S_\lambda}{p_0 l)^3}, \qquad (6.15)$$

where S_λ is the spectral density of the radiation from a front surface. For each gas there is a defined amplitude of the shock wave for which the efficiency of the deexcitation on the given wave length λ is maximal -- this is obvious from Tables 14 and 15.

Table 14. Coefficient $\eta_\lambda(cm^{-1})$ in the visible part of the spectrum (λ=500 nm)

$T_1 \cdot 10^{-4}$, °K	10	15	20	25	30
He	38	63	60	56	33
Ne	88	118	102	60	39
Ar	120	123	73	41	36
Kr	168	136	79	56	47
Xe	188	139	77	62	55
Air	11	14	20	16	14

Table 15. Coefficient $\eta_\lambda(cm^{-1})$ in the near ultraviolet region of the spectrum (λ=300 nm)

$T_1 \cdot 10^{-4}$ °K	10	15	20	25	30
He	68	201	248	267	172
Ne	159	380	422	314	204
Ar	217	392	303	195	188
Kr	303	434	327	267	246
Xe	340	443	320	295	288
Air	20	45	83	76	74

[1] The idea of creating such a light source has been implemented to some degree in reference [167].

§4. Certain Results of Investigating the Effect of Radiation With a Continuous Spectrum on a Hard Substance

Applying the blast radiation source, I. V. Nemchinov, I. F. Zharikov and one of the authors of [9] observed the formation of a glowing region above the surface of the target which expanded at a velocity of about 500 m/sec. A rise in pressure at the radiated surface to several atmospheres was recorded. The formation of the glowing region was explained by intense evaporation and ionization of the material of the target, and the rise in pressure, by the reaction of the dispersing vapor. The correctness of this interpretation was later confirmed when A. A. Provalov [11] was able to obtain spectra of the glowing region containing the lines of the target material.

The picture of the effect of not very short radiation pulses on a solid material can be imagined as follows.

On irradiation of the solid state the surface layer of the material is heated up and evaporated. If the vapor weakly absorbs the incident radiation, then it penetrates deeper and deeper layers of the material, and evaporates them -- a transparency wave moves into the material [109]. However, even weakly absorbing the radiation, for example, as a result of thermal ionization, the vapor begins to heat up.

I. V. Nemchinov and G. G. Vilenskaya [116] performed calculations demonstrating that with high radiation intensity the heating of the vapor and the growth of absorption connected with it lead to the formation of a highly heated opaque layer at the surface.

Thus, independently of the initial transparency of the vapor it is necessary to expect the occurrence of a layer that shields the incident radiation. However, the shielding of the surface of the body still does not mean that

evaporation must cease. The heated vapor itself radiates. The intensity and the spectral composition of this radiation are determined not so much by the power of the primary radiation as by the optical properties of the evaporated material. Thus, it is possible to use a focused laser beam to heat up the vapor from the outside to very high temperature, but as a result of opaqueness of the vapor only the radiation of the comparatively cold inner layers reaches the surface of the body. The phenomenon is analogous to shielding in powerful shock waves when the radiation of the shock-heated gas and also the highly heated layer ahead of the front turns out to be blocked, and only the light from the remote, moderately hot layers penetrates to the cold transparent gas.

The above-described concepts of self-shielding of the surface of bodies, in spite of similarity to the already known shielding effect of powerful shock waves in gases, are in need of experimental confirmation. The theoretical calculations of the effect of the radiation of a continuous spectrum on a barrier were performed in references [9, 111, 168, 169].

In our experiments targets made of various materials were irradiated by a blast light source. The moving image camera recording of the dispersion of the target vapor is shown in Figure 74.

The fact of glow of the vapor above the target indicated that the temperature of this vapor was about 10000°K. The temperature could not be appreciably higher than this, for lines of neutral atoms and molecules were present in the glow spectrum. On the other hand, a noticeable continuum in the glow spectrum indicated significant ionization of the vapor and, consequently, quite high temperature. If we consider that the measured pressures in the vapor were from several units to several tens of atmospheres, from equation $p=nkT$ it is easy to estimate the particle density which turns out to be on the order of 10^{18} cm^{-3}.

Figure 74. Moving image camera recording of the dispersion of the vapor from a target pressed from HgCl powder
1 -- target, 2 -- vapor interface (interface velocity 400-600 m/sec, height of rise 7 mm)

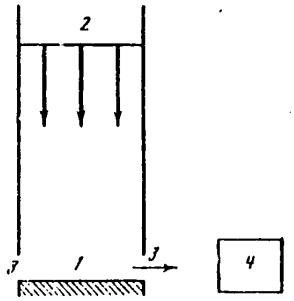

Figure 75. Diagram for obtaining the radiation spectra of heated vapor.
1 -- target, 2 -- shock wave front of the blast source, 3 -- window, 4 -- spectral moving image camera

In the experiments targets made of mercury applied to lead, pressed HgCl powder and also I_2 powder with 10% TlI admixture were irradiated. The blast source with seven shaped depressions held with argon was used (§2). The distance of the target from the charge was selected so that the energy density E released from the target will be maximal. The recording layout is shown in Figure 75, and the spectrum obtained, in Figure 76.

Figure 77 shows the radiation spectrum of mercury and lead vapor. First the spectrum consists of individual lines of the atoms of the target materials. The lines gradually broaden; some of them self-reverse with time, significant parts of the spectrum are overlapped by the intensifying continuum, against the background of which only the individual absorption lines remain. Let us present

the temperatures measured in mercury and lead vapor 3.5 mm from the target surface in 1 microsecond before the arrival of the shock wave in the vicinity of the vapor.

λ, nm	546	495	472	371	359	338	315	304
T, °K	9700	9600	9200	11000	11000	10600	10700	10200

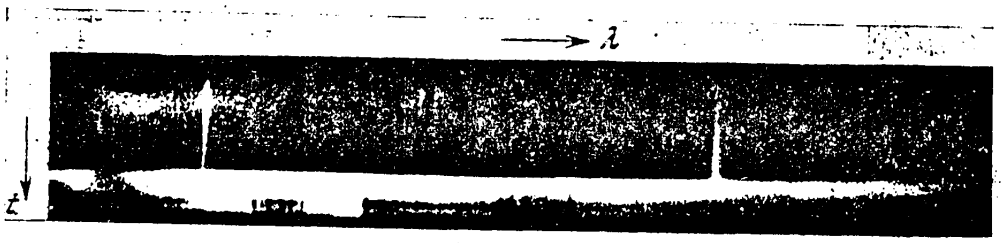

Figure 76. Spectral moving image camera recording of the glow of target vapor from pressed HgCl powder; distance from the target surface 2.5 mm. Light band -- shock wave vapor

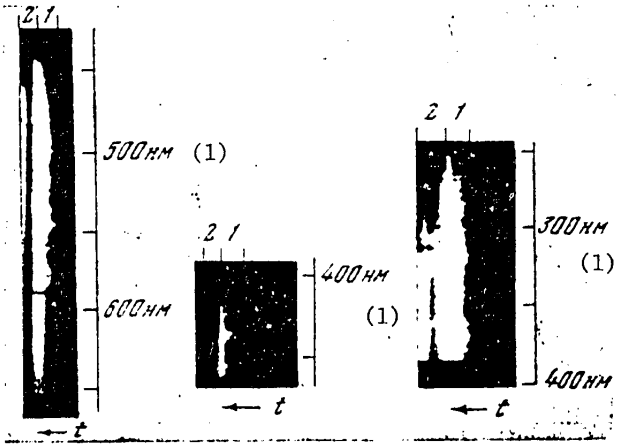

Figure 77. Spectral moving image camera recording of the glow of mercury and lead vapor in the visible and ultraviolet regions. 1 -- vapor emission spectrum, 2 -- shock wave spectrum of the source

Key:

a. nm

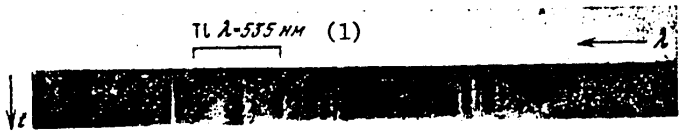

Figure 78. Radiation spectrum of vapor (I_2+10% T&I)

Key:
1. nm

The measurements were performed at the peaks of the most intense and broadest lines or with respect to an intense continuum. The temperatures turned out to be close. The radiation spectrum of the vapor of a mixture of iodine and tellurium iodide is shown in Figure 78.

Let us present the mean values of the temperatures measured at different distances h from the surface of the target 1 microsecond before the arrival of the shock wave.

h, mm	4.5	3.5	2.5
HgCl	-	8900	10900
Hg+Pb	9400	10300	7800
I_2+10% T&I	-	-	7900

Thus, the temperature measurements and estimates of the particle concentration demonstrated that the vapor was in the form of a dense plasma with a temperature of about 10000°K. The narrow outer layer of the expanding vapor was the brightest (see Figure 74) and emits in a continuous spectrum (see Figure 76) -- obviously the temperature there is higher.[1] With such parameters the vapor is in a position to absorb the radiation incident on it intensely.

However, as direct proof of shielding we have the results of recording the radiation reaching the surface of the target. This radiation was recorded through a small opening of the target (Figure 79). The target consisted of seven

[1] The measurements gave a temperature of the outer layer of vapor of about 15000°K, but it could be still higher, for this layer was not completely resolved on the spectral moving image camera recording as a result of the narrow width.

samples of different materials. In the center of each sample a hole 0.5 mm in diameter was drilled. The radiation recording was made using the SFR-2M moving image camera in which an iris limiting the field of view was installed in place of the slit. The brightness standard, just as in the other experiments, was the EV-39 source. The central part of the discharge in it was separated by a diaphragm of the same diameter as the openings in the samples.

Figure 80 shows the effective radiation temperature passing through the openings in the target. At the first point in time comparison with the blast source temperature was observed. This corresponds to the fact that all of the radiation leaving the shock wave front in the direction of the target reached the surface. At subsequent points in time, a sharp decrease in the effective temperature was detected for a number of samples. This is explained by the shielding effect of the vapor closing the opening.[1]

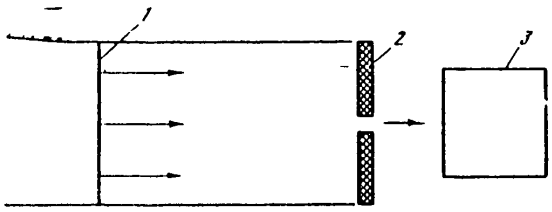

Figure 79. Diagram of the recording of radiation reaching the target surface.
1 -- blast source shock wave; 2 -- target with opening, 3 -- moving image camera or spectral moving image camera

[1] In several experiments the diameter of the opening in the targets was 1 mm, but in practice the same results were obtained as for a hole diameter of 0.5 mm. Consequently, the hole was quite small and had no influence on the development of the shielding layer above the surface of the target.

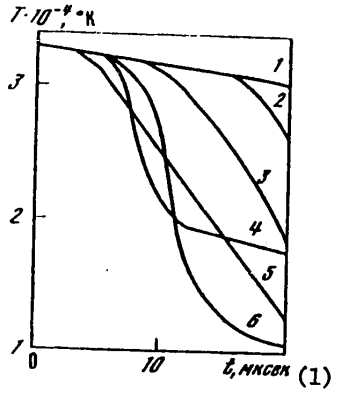

(1)

Figure 80. Radiation shielding by vapor.
1 -- brightness temperature of the source wave front;
2-6 -- brightness temperature of the holes in the samples of sulfur (2), lead (3), asbestos textolite (4), potassium chloride (5), carbon (6). The curves for the iron and aluminum compare with curve 1.

Key:
1. microseconds

In the experiments described above, the radiation was recorded through a light filter with λ_{eff}=432 nm. The shielding appeared still more clearly when the SP-111 device was used to record the radiation of a broad region expanded in a spectrum. Targets made of KCl were used in these experiments, and the source (in order to increase the irradiation power) was filled with xenon. A decrease in brightness was detected first in the individual lines and then with respect to the entire observed spectrum (Figure 81). The brightness temperature of the opening dropped from 50000°K (the shock wave temperature at the beginning of the effect of the source) to 6000°K during the time of operation of the source. Let us consider the difference in the temperature of 6000°K and 30000°K which the shock wave of the source had at the end of its operation. This difference corresponds to the fact that as a result of shielding ~100 times less light flux reached the surface of the target.

As a result of the recoil of the dispersing vapor, the pressure acts on the surface of the target. The first pressure measurements under the effect of

radiation from blast sources were made under conditions where the target vapor dispersed into argon at atmospheric pressure [9]. Later Yu. N. Kiselev investigated the mechanical effect of the radiation for different densities of the medium surrounding the target (argon and xenon for p_0=760 mm Hg; argon for p_0=300, 100 and 50 mm Hg). The results obtained are of interest also because the experiments were performed with more powerful radiation sources than in [9].

The pressure was measured by a piezoelectric sensor. The piezo pickup was calibrated (Figure 82) by an air shock wave of known amplitude formed on detonation of a spherical charge of PETN [19].

When investigating the pressure on the target as a function of the incident radiant flux, a source filled with xenon was used. Inasmuch as the reflection coefficient of the polished aluminum foil in the ultraviolet region is not known exactly, it was not used in the given experiments. This made it possible to calculate the flux density Φ on the target more precisely (the dotted line in Figure 67). A lead target was placed at a distance x=14 or x=27 cm from the charge which corresponded to different maximum flux densities $\Phi=15\cdot10^6$ and $\Phi=4.8\cdot10^6$ watts/cm^2, but of the same density of the released energy E=50 joules/cm^2. The pressure oscillograms obtained in these experiments are presented in Figure 83. The shape of the signal on the oscillograms repeats the variation of the flux Φ with time (compare Figures 67 and 83) -- the pressure on the target follows the decreasing flux. The instantaneous pressure as a function of the flux density measured in the different experiments is plotted on one curve (Figure 84).

Aluminum targets were installed in the experiments only at a distance x=14 cm. Greater delay of the beginning of evaporation τ=7.7 microseconds was

observed here (for lead when x=14 cm, τ=3.5 microseconds).[1] The maximum pressure recorded on the surface of the aluminum target was p=32 atmospheres.

In the experiments simultaneously with measuring the pressure by the SFR-2M, the dispersion of the vapor was recorded. The maximum velocities of ascent of the glowing lead vapor interface where u=370 and u=730 m/sec -- corresponding to the maximum fluxes $\Phi=4.8\cdot10^6$ and $\Phi=15\cdot10^6$ watts/cm^2. For aluminum vapor with a flux $\Phi=15\cdot10^6$ watts/cm^2, a velocity of u=650 m/sec was measured. The dispersing vapor excited a shock wave in the xenon. In the experiments with sulfur for which the fastest velocity of spreading was recorded (u=1000 m/sec), a slightly glowing shock wave front was observed ahead of the vapor interface. Let us compare the pressures $p_{shock\ wave}$ calculated by the velocity of the vapor interface (the piston velocity) with the pressures p_{piezo} measured by the piezopickup.

	Pb(x=27 cm	Pb(x=14 cm)	Al (x=14 cm)
p_{piezo}, kg/cm^2	16	45	32
$p_{shock\ wave}$, kg/cm^2	13	42	33

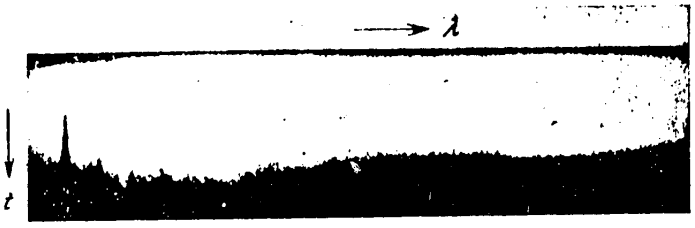

Figure 81. Spectral moving image camera recording of the brightness of the opening in a KCl target (λ=400-600 nm); the reference line of mercury λ=435.8 nm is visible)

[1]Let us note that in [9] a comparatively low-power source was used, and evaporation of the aluminum was not observed in general.

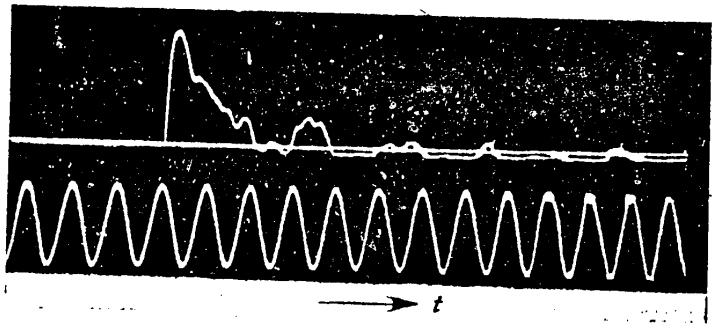

Figure 82. Oscillogram of the calibration signals; at the bottom is a 100 kilohertz sine curve

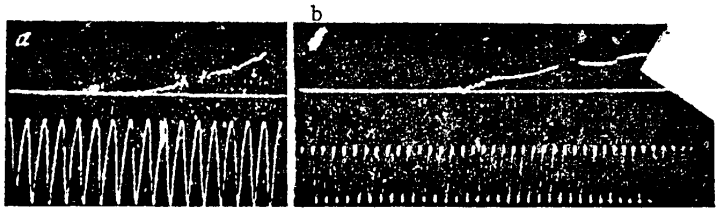

Figure 83. Pressure oscillograms on lead targets under the effect of the radiation of a source filled with xenon: a -- distance at which the target is installed x=14 cm, b -- x=27 cm. The time runs from left to right. The break in the recording corresponds to the arrival of the shock wave. At the bottom is a 1 megahertz sine curve.

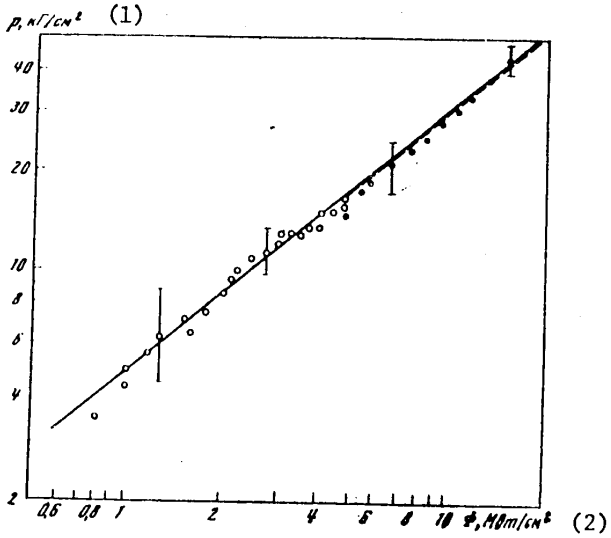

Figure 84. Pressure p on lead targets as a function of the radiation flux density Φ.
Circles -- for x=27 cm; dots -- for x=14 cm
Key: 1. p, kg/cm^2; 2. Φ, megawatts/cm^2

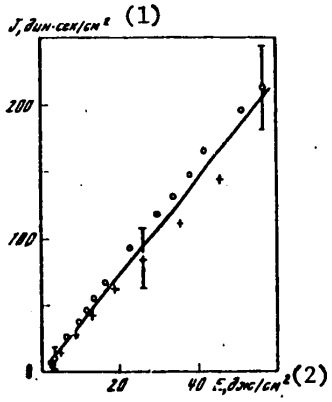

Figure 85. Pressure pulse J on the lead target for different densities of the released energy E (the notation is the same as in Figure 84)

Key:
1. J, dyne-sec/cm^2
2. E, joules/cm^2

Good agreement of the pressures on the target surface and in the shock-compressed xenon is present. Obviously, significant pressure gradients in the vapor layer are absent. This situation is possible when the speed of sound in the vapor exceeds the dispersion velocity. The speed of sound in the ionized lead and aluminum vapor (temperature ~10 000°K) is estimated at ~1000 and ~3000 m/sec, respectively.

The effect of the density of the surrounding gas was studied by varying the initial pressure of the argon filling the source. In Table 16 maximum pressures p_{piezo} and dispersion velocities of vapor u measured on lead targets and also the pressures in the shock-compressed argon $p_{shock\ wave}$ calculated by the velocity u are presented. The pressure pulse on the lead target is illustrated in Figure 85.

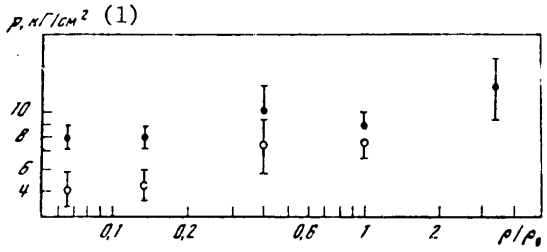

Figure 86. Pressure p on a lead target at different densities ρ of the surrounding gas reduced to argon density ρ_0 for p_0=760 mm Hg. Circles -- pressure in the experiments with argon at the time t=22 microseconds; dots -- pressure recalculated for one flux density Φ=3 megawatts/cm^2

Key:
1. p, kg/cm^2

Table 16

p_0 mm, Hg	Φ, megawatts/cm^2	p_{piezo}, kg/cm^2	u, m/sec	$p_{shock\ wave}$, kg/cm^2
760	2.7	13.3	580	8.4
300	2.6	11.0	860	7.1
100	2.1	8.4	1260	5.7
50	1.7	5.6	1760	4.9

In Figure 86 the pressure p_{piezo} is recalculated for one flux density $\Phi=3\cdot10^6$ watts/cm^2 (the recalculation was done by the experimental dependence of the pressure on the flux density presented in Figure 84). In spite of the variation of the surrounding gas density from 5.85 g/liter (xenon at p_0=760 mm Hg) to 0.118 g/liter (argon at p_0=50 mm Hg), the pressure on the target turned out to be constant.

BIBLIOGRAPHY
[Russian entries only]

4. [Russian title is the translation of the English book published by IL, Moscow, 1950]

9. Zharikov, I. F.; Nemchinov, I. V.; Tsikulin, M. A. PMTF [Applied Mechanics and Technical Physics], No 1, 1967, p 31.

10. Dremin, A. N.; Savrov, S. D. DAN SSSR [Reports of the USSR Academy of Sciences], No 179, 1968, p 624.

11. Popov, Ye. G.; Provalov, A. A.; Tsikulin, M. A. DAN SSSR, No 194, 1970, p 805.

12. Popov, Ye. G.; Tsikulin, M. A. VYSOKOTEMPERATURNYY IMPUL'SNYY IZLUCHATEL'. AVT. SVID. No 272611 [High-Temperature Pulsed Emitter. USSR Author's Certificate No 272611], 1968.

13. Popov, Ye. G.; Tsikulin, M. A. ZHETF [Journal of Experimental and Theoretical Physics], No 57, 1969, p 389.

14. Popov, Ye. G.; Tsikulin, M. A. PMTF, No 5, 1970, p 164.

15. Stanyukovich, K. P. NEUSTANOVIVSHIYESYA DVIZHENIYA SPLOSHNOY SREDY [Nonsteady Movements of a Continuous Medium], Moscow, Gostekhizdat, 1955.

16. Baum, F. A.; Kaplan, S. A.; Stanyukovich, K. P. VVEDENIYE V KOSMICHESKUYU-GAZODINAMIKU [Introduction to Space Gas Dynamics], Moscow, Fizmatgiz, 1958.

17. Bronshten, V. A. PROBLEMY DVIZHENIYA V ATMOSFERE KRUPNYKH METEORITNYKH TEL. [Problems of the Movement of Large Meteoritic Bodies in the Atmosphere], Moscow, Izd-vo AN SSSR, 1963.

18. Bronshten, V. A.; Chigorin, A. N. TEPLOFIZIKA VYSOKIKHTEMPERATUR. [High-Temperature Thermophysics], Vol 2, No 6, 1964, p 860.

19. Tsikulin, M. A. UDARNYYE VOLNY PRI DVIZHENII V ATMOSFERE KRUPNYKH METEORITNYKH TEL. [Shock Waves During Movement of Large Meteoritic Bodies in the Atmosphere], Moscow, Nauka, 1969.

21. Zel'dovich, Ya. B.; Leypunskiy, O. I. ZHETF, No 13, 1943, p 181.

22. Gershanik, Ya. K.; Zel'dovich, Ya. B.; Rozlovskiy, A. N. ZHFKH [Journal of Physical Chemistry], No 24, 1950, p 85.

29. Model', I. Sh. ZHETF, No 32, 1957, p 714.

32. Popov, Ye. G.; Tsikulin, M. A. ZHETF, No 57, 1969, p 522.

36. Zel'dovich, Ya. B.; Rayzer, Yu. P. UFN [Progress in the Physical Sciences], No 63, 1957, p 613..

37. Zel'dovich, Ya. B.; Rayzer, Yu. P. FIZIKA UDARNYKH VOLN I VYSOKOTEMPERATURNYKH GIDRODINAMICHESKIKH YAVLENIY [Physics of Shock Waves and High-Temperature Gas Dynamic Phenomena], Moscow, Nauka, 1966.

38. Voytenko, A. Ye. DAN SSSR, No 158, 1964, p 1278.

39. Voytenko, A. Ye. ZHTF [Journal of Technical Physics], No 36, 1966, p 178.

40. Voytenko, A. Ye. PMTF, No 4, 1966, p 112.

41. Voytenko, A. Ye.; Model', I. Sh.; Samodelov, I. S. DAN SSSR, No 169, 1966, p 547.

42. Zatsepin, Yu.A.; Popov, Ye. G.; Tsikulin, M. A. ZHETF, No 54, 1968, p 112.

43. Popov, Ye. G. PIS'MA V ZHETF [Letters to the Journal of Experimental and Theoretical Physics], No 9, 1969, p 176.

45. Biberman, L. M.; Veklenko, B. A. ZHETF, No 37, 1959, p 164.

47. Astanovich, I. S. METEORNYYE YAVLENIYA V ATMOSFERE ZEMLI [Meteor Phenomena in the Earth's Atmosphere], Moscow, 1958.

48. Posy, J. L.; Braswell, R. N. RADIOASTRONOMIYA [Radioastronomy], Moscow, IL, 1958.

49. Levin, B. Yu. FIZICHESKAYA TEORIYA METEOROV I METEORNOYE VESHCHESTVO V SOLNECHNOY SISTEME [Physical Theory of Meteors and Meteoric Matter in the Solar System], Moscow, Izd-vo AN SSSR, 1956.

52. Al'bitskiy, V. A., et al. KURS ASTROFIZIKI I ZVEZDNOY ASTRONOMII [Course in Astrophysics and Stellar Astronomy], Vol 1, Moscow, Gostekhizdat, 1951.

53. Astanovich, I. S. ASTRON. VESTN. [Astronomy Vestnik], Vol 5, No 2, 1971, p 89.

63. [The Russian title is the translation published by IL Press, Moscow, 1963].

65. [A translation of this article appeared in VOPR. RAKETN. TEKHN. [Problems of Rocket Engineering], No 4, 1964, p 63].

66. Biberman, L. M.; Yakubov, I. T. ZHTF, Vol 33, No 11, 1963, p 1344.

67. Kuznetsov, N. M. ZHTF, No 34, 1964, p 624.

68. Biberman, L. M.; Yakubov, I. T. TEPLOFIZIKA VYSOKIKH TEMPERATUR, Vol 3, No 2, 1965.

69. Biberman, L. M.; Yakubov, I. T. TEPLOFIZIKA VYSOKIKH TEMPERATUR, Vol 3, No 3, 1965.

70. Biberman, L. M., et al. IZV. AN SSSR. MEKH. ZHIDK. I GAZA [News of the USSR Academy of Sciences, Fluid and Gas Mechanics], No 6, 1967, p 46.

71. Losev, S. A.; Polyanskiy, V. A. IZV. AN SSSR. MEKH. ZHIDK. I GAZA, No 1, 1968, p 176.

72. Kozlov, G. I.; Rayzer, Yu. P.; Roytenburg, D. I. PMTF, No 1, 1968, p 140.

73. Zheleznyak, M. B.; Mnatsakanyan, A. Kh. TEPLOFIZIKA VYSOKIKH TEMPERATUR, Vol 6, No 3, 1968, p 390.

74. Zheleznyak, M. B. PMTF, No 6, 1970, p 126.

75. Magremova, N. N.; Pashchenko, N. T.; Rayzer, Yu. P. PMTF, No 5, 1970, p 11.

76. Unsold, A. VIZIKA ZVEZDNYKH ATMOSFER. [Physics of Stellar Atmospheres], Moscow, IL, 1949.

77. Bates, D. K. SOVREMENNYYE PROBLEMY ASTROFIZIKI I FIZIKI SOLNTSA [Modern Problems of Astrophysics and Solar Physics], Moscow, IL, 1950.

79. Ambartsumyan, V. A.; Mustel', E. R.; Severnyy, A. B.; Sobolev, V. V. TEORETICHESKAYA ASTROFIZIKA [Theoretical Astrophysics], Moscow, Gostekhizdat, 1952.

83. [A translation of this article appears in VOPR. RAKETN. TEKHN., No 11, 1959.]

84. [A translation of this article appears in VOPR. RAKETN. TEKHN., No 7, 1959, p 18.

88. Fayzullov, F. S.; Sobolev, N. N.; Kudryavtsev, Ye. M. DAN SSSR, No 127, 1959, p 541.

89. Losev, S. A.; Generalov, N. A.; Terebenina, L. B. OPTIKA I SPEKTROSKOPIYA, [Optics and Spectroscopy], No 8, 1960, p 570.

91. Biberman, L. M.; Norman, G. E. OPTIKA I SPEKTROSKOPIYA, No 8, 1960, p 433.

92. Biberman, L. M.; Norman, G. E.; Ul'yanov, K. N. OPTIKA I SPEKTROSKOPIYA, No 10, 1961, p 565.

94. Dronov, A. P.; Sviridov, A. G.; Sobolev, N. N. OPTIKA I SPEKTROSKOPIYA, No 12, 1962, p 677.

99. Biberman, L. M.; Vorob'yev, V. S.; Norman, G. E.; Yakubov, N. T. KOSMICH. ISSLED. [Space Research], Vol 2, No 3, 1964, p 441.

100. Belov, S. N.; Ogurtsov, N. N.; Podmoshenskiy, I. V. OPTIKA I SPEKTROSKOPIYA, Vol 25, No 5, 1968, p 684.

101. Krokhin, O. N. ZHTF, No 34, 1964, p 1325.

102. Basov, N. G.; Krokhin, O. N. ZHETF, No 46, 1964, p 171.

105. Anisimov, S. I.; Bonch-Bruyevich, A. M.; Yel'yashevich, M. A.; Imas, Ya. A.; Pavlenko, N. A.; Romanov, G. S. ZHTF, No 36, 1966, p 1273.

106. Afanas'yev, Yu. V.; Krol', V. M.; Krokhin, O. N.; Nemchinov, I. V. PMM [Applied Mathematics and Mechanics], No 30, 1966, p 1022.

107. Basov, N. G.; Boyko, V. A.; Dement'yev, V. A.; Krokhin, O. N.; Sklizkov, G. V. ZHETF, No 51, 1966, p 989.

109. Afanas'yev, Yu. V.; Krokhin, O. N. ZHETF, No 52, 1967, p 966.

110. Nemchinov, I. V. PMM, No 31, 1967, p 300.

111. Krol', V. M.; Nemchinov, I. V. PMTF, No 5, 1968, p 32.

112. Romanov, G. S.; Stepanov, K. L. ZHPS [Journal of Applied Spectroscopy?], No 8, 1968, p 783.

113. Krol', V. M. PMTF, No 4, 1968, p 18.

114. Vilenskaya, G. G.; Nemchinov, I. V. DAN SSSR. No 186, 1969, p 1048.

115. Afanas'yev, Yu. V.; Basov, N. G.; Krokhin, O. N.; Morachevskiy, N. V.; Sklizkov. ZHTF, No 39, 1969, p 894.

116. Vilenskaya, G. G.; Nemchinov, I. V. ZHPS, No 11, No 4, 1969.

117. Vilenskaya, G. G.; Nemchinov, I. V. PMTF, No 6, 1969.

118. Basov, N. G.; Krokhin, O. N.; Sklizkov, G. V. KVANTOVAYA ELEKTRONIKA. TRUDY FIAN SSSR [Quantum Electronics, Works of the Physics Institute of the USSR Academy of Sciences], No 52, 1970, p 171.

119. Nemchinov, I. V. PMM, Vol 34, No 4, 1970, p 706.

120. Gnoevoy, Ya. T.; Petrukhin, A.I.; Pleshanov, Yu. Ye.; Sulyayev, V. A. PIS'MA V ZHETF, Vol 11, No 9, 1970, p 440.

121. Anisimov, S. I.; Imas, Ya. A.; Romanov, G. S.; Khodyko, Yu. V. DEYSTVIYE IZLUCHENIYA BOL'SHOY MOSHCHNOSTI NA METALLY [Effect of High-Power Radiation on Metals], Moscow, Nauka, 1970.

122. Vilyunov, V. N.; Sidonskiy, O. B. FGV [expansion unknown], Vol 1, No 4, 1965, p 39.

123. Timov, V. M.; Fadeyenko, B. I.; Timov, N. S. DAN SSSR, Vol 180, No 5, 1968, p 1051.

124. Rusakov, M. M. PMTF, No 2, 1969.

125. [A translation of this article appears in VPR. RAKET. ETKHN., No 4, 1960.

127. Nemchinov, I. V.; Tsikulin, M. A. GEOMAGNETIZM I AERONOMIYA [Geomagnetism and Aeronomy], Vol 3, No 4, 1963, p 635.

129. Mandel'shtam, S. L.; Pashinin, P. P.; Prokhorov, A. M.; Rayzer, Yu. P.; Sukhodrev, N. K. ZHETF, No 49, 1965, p 127.

130. Rayzer, Yu. P. UFN, Vol 87, No 1, 1965, p 29.

131. [A translation of this article appears in UFN, No 72, 1960, p 521.

132. Ryabinin, Yu. N.; Tamm, I. I. FIZIKA VARYVA [Explosion Physics], No 5, 1956.

135. Novikov, N. N. PMTF, No 6, 1962.

136. Novikov, N. N. PMTF, No 1, 1963.

138. Zel'dovich, Ya. B.; Kompaneyets, A. S. TEORIYA DETONATSII [Theory of Detonation], Moscow, 1955.

139. Zagumenkov, A. S.; Timov, N. S.; Fadeyenko, Yu. N.; Chistyakov, V. P. PMTF, No 2, 1969, p 79.

140. Dubnov, L. V.; Khotina, L. D. FIZIKA GORENIYA I VZRYVA [Combustion and Explosion Physics], No 4, 1966, p 97.

141. Kartuzhanskiy, A. N.; Meyklyar, P. V. ZHETF, No 21, 1951, p 532.

142. Zatsepin, Yu. A. ZHNIPFIK [Journal of Scientific and Applied Photography and Cinematography], Vol 5, No 10, 1960, p 60.

143. Demidov, M. I.; Ogurtsova, N. N.; Podmoshenskiy, I. V.; Shelenina, V. M. ZHPS, No 3, 1968, p 9.

144. Ogurtsova, N. N.; Podmoshenskiy, I. V.; Demidov, M. I. OPTIKO-MEKHANICHESKAYA PROMYSHLENNOST' [Opticomedical Industry], No 1, 1960.

145. Grenishin, S. G.; Dubovik, A. S.; Yesin, R. A.; Ilyushin, G. P.; Kevlishvili, P. V.; Churbakov, A. I.; Shchepetkin, Yu. P. Z. NAUCHI. I PRIKL. FOTOGRAFII I KINEMATOGRAFII [Journal of Scientific and Applied Photography and Cinematography], Vol 12, No 5, 1967, p 344.

146. Dubovik, A. S. FOTOGRAFICHESKAYA REGISTRATSIYA BYSTROPROTEKAYUSHCHIKH PROTSESSOV [Photographic Recording of Fast Processes], Moscow, Nauka, 1964.

147. Kuznetsov, N. M. TERMODINAMICHESKIYE FUNKTSII I UDARNYYE ADIABATY VOZDUKHA PRI VYSOKIKH TEMPERATURAKH [Thermodynamic Functions and Shock Adiabats of the Air at High Temperatures], Moscow, Mashinostroyeniye, 1965.

148. Zaydel', A. N.; Shreyder, Ye. Ya. SPEKTROSKOPIYA VAKUUMNOGO UL'TRAFIOLETA [Vacuum Ultraviolet Spectroscopy], Moscow, Nauka, 1967.

149. Sobel'man, I. I. VVEDENIYE V TEORIYU ATOMNYKH SPEKTROV [Introduction to the Theory of Atomic Spectra], Moscow, 1963.

150. Zaydel', A. N.; Rayskiy, S. M.; Shreyder, Ye. Ya. TABLITSY SPEKTRAL'NYKH LINIY [Spectral Line Tables], Moscow, 1962.

152. D'yakov, S. P. ZHETF, No 27, 1954, p 288.

157. Biberman, L. M.; Ul'yanov, K. N. OPTIKA I SPEKTROSKOPIYA, Vol 16, No 3, 1964.

158. Kuznetsov, N. M. PMTF, No 2, 1967, p 141.

159. [Translation published by Mir Press, Moscow, 1967.]

164. Vanyukov, M. P.; Mak, A. A. UFN, No 66, 1958, p 301.

165. Kiselev, Yu. N.; Kristoforov, B. D. FIZIKA GORENIYA I VARYVA, Vol 10, No 1, 1974, p 116.

166. Volosevich, P. P.; Kurdyumov, S. P.; Popov, Yu. P. IZV. AN SSSR. MEKH. ZHIDK. I GAZA, No 1, 1968, p 67.

167. Voytenko, A. Ye.; Matochkin, Ye. P.; Fedulov, A. F. PTE [Experimental Instruments and Techniques], No 2, 1970, p 201.

168. Nemchinov, I. V. MEKHANIKA SPLOSHNOY SREDY I RODSTVENNYYE PROBLEMY ANALIZA [Mechanics of a Continuous Medium and Related Analysis Problems], Moscow, Nauka, 1972, p 337.

169. Bergel'son, V. I.; Nemchinov, I. V.; Novikova, V. V. FIZIKA GORENIYA I VARYVA, Vol 11, No 5, 1975, p 730.

170. Selivanov, V. V.; Shlyapintokh, I. Ya. ZHFKH, No 32, 1958, p 670.

171. Kay, D.; Laby, L. SPRAVOCHNIK FIZIKA-EKSPERIMENTATORA [Handbook for the Experimental Physicist], Moscow, IL, 1949.

172. Gubkin, K. Ye. RASPROSTRANENIYE VZRYVNYKH VOLN. MEKHANIKA V SSSR ZA 50 LET [Blast Wave Propagation, 50 Years of Mechanics in the USSR], Vol 2, Moscow, Nauka, 1970, p 269.

10845
CSO: 8144/1158

- END -